LBNL-41635

ERNEST ORLANDO LAWRENCE
BERKELEY NATIONAL LABORATORY

Ultrafast Transient Nonlinear Optical Processes in Semiconductors

D.S. Chemla

Materials Sciences Division

March 1998

To be published as
a chapter in
Nonlinear Optics
in Semiconductors,
R.K. Willardson and
A.C. Beers, Eds.,
Academic Press,
Chestnut Hill, MA, 1998

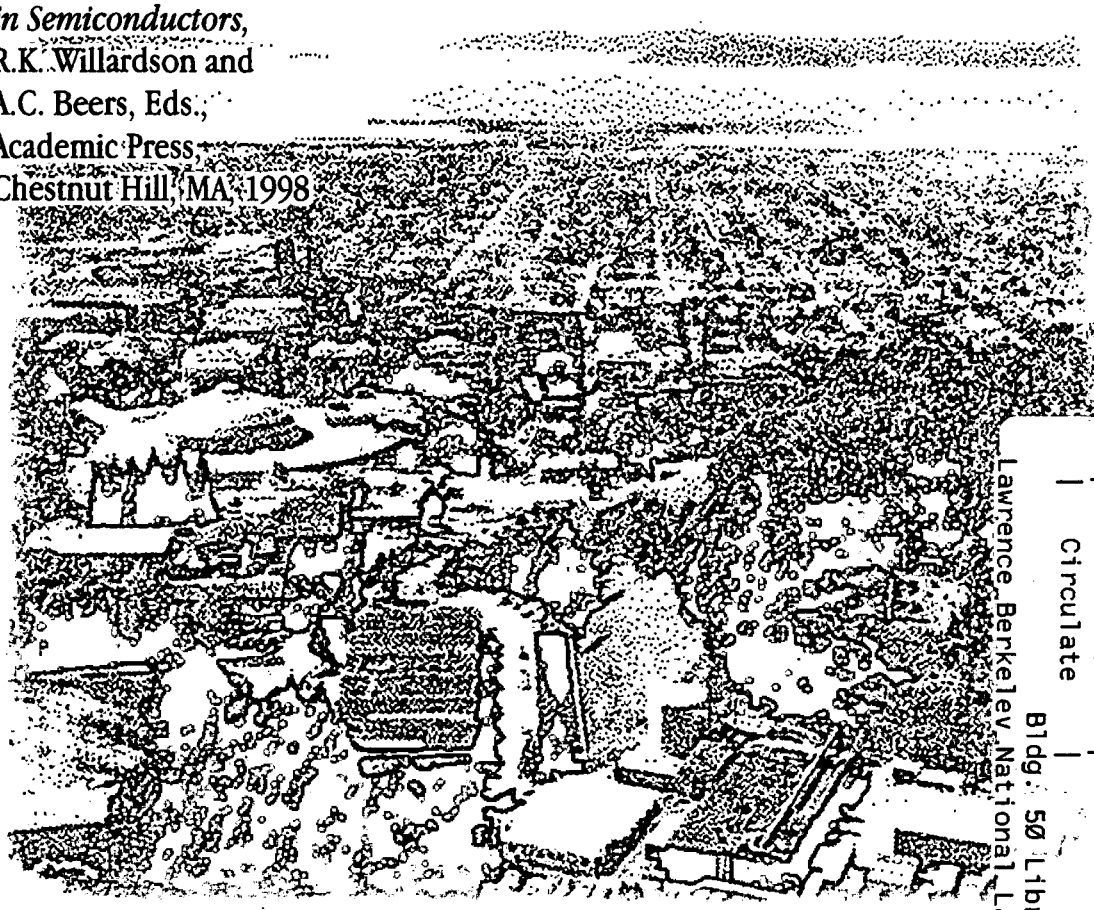

DISCLAIMER

LBNL-41635

Ultrafast Transient Nonlinear Optical Processes in Semiconductors

D.S. Chemla

Materials Sciences Division
Ernest Orlando Lawrence Berkeley National Laboratory
University of California
Berkeley, California 94720

March 1998

This work was supported by the Director, Office of Energy Research, Office of Basic Energy Sciences, Materials Sciences Division, of the U.S. Department of Energy under Contract No. DE-AC03-76SF00098.

Ultrafast Transient Nonlinear Optical Processes in Semiconductors

D. S. Chemla

Department of Physics, University of California at Berkeley

and

Materials Sciences Division, Lawrence Berkeley National Laboratory, Berkeley, CA 94720

(March 24, 1998)

in "Nonlinear Optics in Semiconductors"

R.K. Willardson and A.C. Beers, Academic Press

Table of Contents

I. INTRODUCTION

The electronic ground state of a perfect semiconductor is pretty boring. In these materials, electronic energy levels are well described by the Effective Mass Approximation; the electronic ground state is such that the valence bands are full, the conduction bands are empty and essentially nothing happens. Things become more interesting when this peaceful situation is disturbed, i. e., defects are present, lattice vibrations interact with the electrons, or an external perturbation is applied. In this chapter, we will mostly be concerned with the perturbations caused by an ultrashort laser pulse whose photon energy lies in the vicinity of the fundamental absorption edge. In that case, the material is raised from its ground state into an excited state, which can be described in terms of electronic excitations whose structure results from a delicate balance between quantum statistics and the Coulomb interaction. The fundamental quasi-particles, electrons (e) and holes (h), obey Fermi statistics. They can form more complex objects with an internal structure, such as excitons (X), biexcitons (X_2), polaritons (X-$h\nu$), Fano-resonances, dressed hole at the origin of Fermi edge singularities, e-h plasmas etc. These objects are essentially delocalized and long-lived. Obviously their nature and properties are very sensitive to the density and energy of the photons that create them. Despite the underlying Fermi statistics of the basic constituents e and h, some composite quasi-particles, X and X_2, can, in very specific low density regimes, exhibit a Bosonic behavior. A further critical dependence on the density stems from the fact that the strong and long range Coulomb force, that is responsible for the formation of these composite excitations, can be screened, in particular by e-h plasmas, thus changing their very nature. All these manybody mechanisms are modified in a non-trivial manner by quantum confinement in heterostructures or under high magnetic fields.

Just upon creation the excitations are coherent, their quantum mechanical phase being determined by that of the laser light that generates them. Very quickly, however, scattering within the electronic system and with the phonons starts to destroy that phase and the system evolves toward thermodynamic equilibrium, first among the electronic excitations,

and then later with the lattice. This fast and complicated kinetics impacts on fundamental issues related to coherence, dephasing, dissipation and memory, thus raising some interesting questions about the validity of approximations well-established in the quasi-static regime. The combination of extreme density dependence and ultrafast kinetics makes the behavior of electronic excitations in semiconductors and their heterostructures a fascinating topic at the frontier of condensed matter physics. Their creation or destruction is associated with interband and intraband polarization waves which, in turn, determine the optical properties of the material. The recent developments in ultrafast laser techniques have provided new tools, perfectly adapted to the study of semiconductor optics, thus opening new opportunities for investigating manybody effects in correlated quasi-particle systems in regimes previously inaccessible. A wealth of valuable and novel information on the physics that governs the electronic excitations of semiconductors has been obtained over the last decade, explaining the spectacular growth of the field of nonlinear spectroscopy of these materials.

Coherent nonlinear optical processes were first investigated in atomic and molecular systems using CW and long pulse lasers [1–3]. In these systems the energy levels are narrow, and usually well separated, so that experiments were well described by theoretical models involving only a few levels. In particular, in the case where one optical transition is nearly resonant with the exciting photons and all others are far away, the two-level-atom model very successfully accounts for most experimental results in the frequency domain [4], and the time domain [5]. Similar coherent nonlinear spectroscopy techniques in the nanosecond regime were applied to semiconductors for studying excitons [6,7] and biexcitons [8,9]. Here again, two or three level models were sufficient to explain the most salient results, giving more support to these phenomenological approaches. With the development of short pulsed lasers, picosecond time resolved experiments were performed on semiconductors and heterostructures [10,11]. Coherence and dephasing, however, continued to be discussed in terms of atomic systems concepts using formalism such as the two level atom model [12,13]. As the quality of the samples and the laser performances improved, experimental observations were found to be in qualitative contradiction with the "atomic" pictures. This has triggered a ma-

jor reconsideration of the theory of the dominant mechanisms governing ultrafast processes in semiconductors, which is still being improved. Recently several excellent review articles and books on light/semiconductor interactions have been published. However, they tend to concentrate on experimental [14] or theoretical [15–17] aspects of the subject. It is our opinion that the spectacular progress made in the field of ultrafast nonlinear spectroscopy of semiconductors is the result of the cross fertilization between experiment and theory. The parallel development of advanced ultrashort pulse laser sources and very sensitive data acquisition techniques on one hand, and formal theory and sophisticated numerical simulation on the other, have resulted in a new and extremely active area of condensed matter physics.

The purpose of this chapter is to give a comprehensive and balanced account of both experimental and theoretical advances, focusing on the most important physics and, as much as possible, giving an intuitive picture of the new phenomena that have been observed and explained. We shall attempt to give an organized presentation of a large body of work that is dispersed in the literature. However, because of the sheer volume of the publications in this active field, rather than giving a shallow review of many articles we prefer concentrating on the most relevant and fundamental work. In order to reach out to the Condensed Matter Physics community that is unaware of the recent advances, we will try to introduce as pedagogically as possible the basic concepts of nonlinear optical spectroscopy. For the specialists in atomic and molecular optics, we will present as progressively as possible some manybody concepts. Good interpretations of experiment often require sophisticated computational treatments in which one can lose track of the underlying physics. It turns out that it is possible to develop an intuitive model directly related to the correct theory, that captures the essential physics, although it misses some details. The model is deduced from the general kinetic equations by averaging over band or excitonic indices to define an "effective" interband polarization, which obeys a nonlinear Schrödinger equation. Each term of this equation has a simple and meaningful interpretation. We call it, and its generalizations, the "Effective Polarization Model". We shall use it every time an intuitive explanation can clarify the interpretation of experiments, keeping in mind that a true comparison with theory

can only be made through the full numerical treatment.

This chapter is organized as follows: In Section II we discuss the nature and properties of the electronic elementary excitations of semiconductors near the fundamental band gap. In Section III we examine the time scales of the scattering processes and their basic descriptions. In Section IV we review the nonlinear optical effect in which only virtual electron-hole pairs are excited, and use this example as an introduction to the interpretation and description of the physics governing the coherent regime in condensed matter. Having introduced the main ideas of manybody interactions in semiconductor optics, we turn to the processes involving excitation of real electron-hole pairs. Section V covers the fundamentals of processes that require accounting for 2-particle correlations, and some applications to electronic states in heterostructures are described in Section VI. In Section VII we discuss experiment and theory of processes involving 4-particle correlations. Section VIII is devoted to the very early time regime where memory effects and non-Markovian dynamics dominate. Finally, in Section IX, we give some concluding remarks and list a number relevant topics that are not covered in this chapter because of space, or because they are somehow less general.

II. NEAR BAND GAP EXCITATIONS

The semiconductors of interest in this review are direct gap Zinc Blende materials. The single particle states are well described by the Effective Mass Approximation (EMA). Close to the Γ point, the center of the Brillouin zone, four spin-degenerate bands contribute to the optical transitions. The conduction band, which originates from s-orbitals, has the $J = 1/2$ symmetry and is spin-degenerate, $J_z = \pm 1/2$. The upper valence band originates from p-orbitals and has a $J = 3/2$ character. It is split into the $J_z = \pm 3/2$ heavy hole (hh) and the $J_z = \pm 1/2$ light hole (lh) subbands which, in bulk materials, are degenerate at Γ but separate for $k \neq 0$, owing to their different curvature. The so-called spin-orbit split-off band, with $J = 1/2, J_z = \pm 1/2$ character, is considerably lower in energy. The optical transitions induced by $\sigma^{\pm}$-photons, which are in pure spin states, correspond to the

$\Delta J_z = \pm 1$ selection rule; they are sketched in Fig. (1). The sensitivity of the transitions to the photon polarization is often exploited in nonlinear optics to identify some pathways.

In heterostructures and/or in a magnetic field, the dimensionality of the electronic states is reduced by a potential that confines the particles in one or more directions [18]. Since this confinement depends on the mass, the *hh-lh* degeneracy is lifted, giving separate transitions to the conduction band. The particles are still free to move either in a plane (2D case) or along one axis (1D case). The band dispersion in the directions of free motion can be highly non-parabolic [18]. The degeneracy between the *hh* and the *lh* bands can also be lifted if a stress is applied to the sample, thus reducing the crystal symmetry.

In the description of optical properties of semiconductors, it is customary to introduce the joint density of states (DOS), $\mathcal{D}_{NI}(\omega)$, for the transitions at $\hbar\omega$ between the non-interacting particles of a valence band with energy dispersion $\epsilon_v(k)$, and a conduction band with energy dispersion $\epsilon_c(k)$. The general relation giving the density of states, $\mathcal{D}(\omega)$, in terms of the Green's function $G(k,k',\omega)$, is:

$$\mathcal{D}(\omega) = \Im m \left[\sum_{k,k'} G(k,k',\omega) \right] , \tag{1}$$

where

$$G(k,k',\omega) = \sum_n \frac{\phi_n(k)\phi_n^*(k')}{E_n - (\omega + i\eta)} , \tag{2}$$

and the $\phi_n(k)$ are the *e-h* eigen states of the system. In the simple case of non-interacting particles with parabolic band dispersion, these are plane waves. Because the bands form quasi-continua, the sum can be transformed into an integral, $\sum_k \rightarrow \int d\, k_d$, where the index $d = 3, 2, 1$ specifies the dimensionality, 3D, 2D and 1D, of the sample,

$$\mathcal{D}_{NI}^{(d)}(\omega) = 2\left(\frac{L}{2\pi}\right)^d A_d \left(\frac{2m}{\hbar^2}\right)^{d/2} (\hbar\omega - E_g)^{d/2-1}\, \Theta\left(\frac{\hbar\omega}{E_g} - 1\right) , \tag{3}$$

where, E_g is the band gap, m is the effective mass, $A_d = 1, 2\pi$ and 4π, and $\Theta(\hbar\omega/E_g - 1)$ is the Heaviside step function. For 1D, $\mathcal{D}_{NI}^{(1)}(\omega)$ has a singularity at the band edge, $\mathcal{D}_{NI}^{(1)}(\omega) \propto (\epsilon_c(k) - \epsilon_v(k) - \hbar\omega)^{-1/2}$. In 2D, $\mathcal{D}_{NI}^{(2)}(\omega)$ is a simple step function, and in 3D it has the usual $\mathcal{D}_{NI}^{(3)}(\omega) \propto (\epsilon_c(k) - \epsilon_v(k) - \hbar\omega)^{1/2}$ profile. For 0D the $\mathcal{D}_{NI}^{(0)}(\omega)$ is simply a series of δ-functions.

Although one can use these DOS for discussing single particle effects, for example as starting point for describing transport properties, this approach is very misleading in optics. It gives the impression that the Coulomb interaction is some kind of a refinement that is added *a posteriori* to improve an already pretty good description. This is completely wrong. The Coulomb interaction causes "zero order" effects that determine the very value of the optical band gap and simultaneously affect all optical transitions [19,20]. When such a transition occurs, the interaction of the particle promoted into the conduction band with those left in the valence bands is an integral part of the process. This "final state interaction" has profound effects on all optical properties.

To introduce the most salient features, let us consider the simple two-parabolic-band model of a semiconductor. The ground state, full valence band and empty conduction band, is denoted $|\emptyset>$. The simplest excited state or "exciton" has one electron removed from the valence band and one put in the conduction band. Rather than using the creation and destruction operators in the conduction and valence bands, $\hat{c}_k^\dagger$, $\hat{c}_k$, $\hat{v}_k^\dagger$ and $\hat{v}_k$, it is sometimes more convenient to work in the electron-hole representation, $\hat{c}_k^\dagger \rightarrow \hat{e}_k^\dagger$, $\hat{c}_k \rightarrow \hat{e}_k$, $\hat{v}_k^\dagger \rightarrow \hat{h}_{-k}$ and $\hat{v}_k \rightarrow \hat{h}_{-k}^\dagger$, with $\{\hat{e}_k^\dagger\,,\,\hat{e}_{k'}\} = \{\hat{h}_k^\dagger\,,\,\hat{h}_{k'}\} = \delta_{kk'}$, and all other $\{.,.\} \equiv 0$.

The operator creating an exciton with an electron at k_e and a hole at k_h is:

$$\hat{X}^\dagger(k_e,k_h) = \sum_{k_e,k_h} \phi(k_e,k_h)\,\hat{e}_{k_e}^\dagger \hat{h}_{k_h}^\dagger \tag{4}$$

where the amplitude $\phi(k_e,k_h)$ satisfies the k-space Schrödinger equation for an e-h pair interacting via the Coulomb potential. In the case of a photogenerated exciton, one can neglect the momentum of the photon so that the center of mass momentum is $K = 0$, and $k_e = -k_h = k$. Then the relative motion wavefunction satisfies the k-space Wannier equation,

$$\left(E_g - E + \frac{\hbar^2}{2m}k^2\right)\phi_\alpha(k) - \sum_{k'} V(k-k')\phi_\alpha(k') = 0\,, \tag{5}$$

where the Greek index, α, labels the internal motion quantum number and runs over the bound and unbound states. Eq. (5) is just the Fourier transform of the r-space hydrogen

problem. It appears naturally in crystals where, because of Bloch's theorem, it is usual to work in k-space. It shows explicitly that in k-space the Coulomb interaction, $\sum_{k'} V(k-k')\phi_\alpha(k')$, couples states at different k. The solutions of Eq. (5) form a complete basis and satisfy the closure relation,

$$\sum_k \phi_\alpha(k)\ \phi^*_{\alpha'}(k) = \delta_{\alpha\alpha'}\,.$$

Using these eigen-functions in Eq. (1) and (2) gives $\mathcal{D}_X(\omega)$, the DOS for the Coulomb interacting and optically active pair states:

$$\mathcal{D}_X(\omega) = \sum_n |\phi_\alpha(r=0)|^2\ \delta(\omega - E_n)\,. \tag{6}$$

Where $r = r_e - r_h$ is the e-h relative coordinate. For non-interacting particles where $V(k) \rightarrow 0$, the $\phi_\alpha(k)$ are plane waves with $\phi_\alpha(r=0) = 1$, and one recovers the result of Eq. (3), $\mathcal{D}_{NI}(\omega) = \sum_k \delta\left(\epsilon_c(k) - \epsilon_v(k) - \hbar\omega\right)$.

When the Coulomb interaction is accounted for, only the s-like pair states with $\phi_{nS}(r=0) \neq 0$ contribute to the optical transitions. Eq. (3) includes the bound and unbound states, and therefore accounts for the contribution of the resonances as well as the Sommerfeld enhanced continuum. It implies the famous Elliott formula for the linear absorption [21], which for the 3D case is written as:

$$\alpha^{3D}(\omega) = \alpha_0^{3D}\frac{\hbar\omega}{R_y}\left[\sum_{n=1}^{\infty}\frac{4\pi}{n^3}\,\delta\left(\Delta\Omega + \frac{1}{n^2}\right) + \Theta(\Delta\Omega)\frac{\pi e^{\pi/\sqrt{\Delta\Omega}}}{\sinh(\pi/\sqrt{\Delta\Omega})}\right], \tag{7}$$

with

$$\alpha_0^{3D} = \frac{2|\mu_{cv}|^2}{\hbar n_0 c\, a_0^3}, \qquad \text{and} \qquad \Delta\Omega = \frac{\hbar\omega - E_g}{R_y}$$

measures the photon excess energy in units of the exciton Rydberg R_y. Here μ_{cv} is the inter-band transition dipole matrix element, which can be considered as independent of k with an excellent accuracy; a_0 is the exciton Bohr radius and n_o is the background refractive index. Similar expressions for 2D and 1D can be found in many text books. One significant implication of the Elliot formula is that the absorption remains well above the non-interacting particle result, $\alpha_{NI} \propto \Theta(\Delta\Omega)\sqrt{\Delta\Omega}$, even far away from the gap (for $\Delta\Omega \approx 50$, α^{3D} is still

about ten percent above α_{NI}). It turns out that an analytical expression for the real part of the dielectric function, and hence for the refractive index, can be derived as well [22]. In Fig. (2) the solid lines give the experimental low temperature, $T = 5K$, absorption and refractive index spectra of a high quality $1\mu m$ thick $GaAs$ sample. The sample is antireflection coated on each side and glued on a Sapphire substrate. Stress due to different thermal expansion lifts the *lh-hh* degeneracy. One can distinguish clearly in the $\alpha(\omega)$ spectrum the two exciton peaks and the onset of the continuum. The small bump at the threshold of the latter is likely due to the $2S$ resonance. All these features have a "dispersive" correspondent in the refractive index spectra. On the scale of Fig. (2), the non-interacting particle absorption would barely be visible. The dotted lines show a fit to the analytical expressions [21,22]. Although the main features are accurately reproduced, some details that are smoothed out in the experimental curves are more apparent on the theoretical ones.

Strictly speaking, as soon as a second pair is created one should account for the interaction between the four particles. Intuitively, however, one expects that, as long as the distance between the two pairs is much larger than a_o, the above results should not be affected too much. In order to be more quantitative, let us compute the commutation rule of the exciton operator. One finds, as a function of the number operators for electrons, $\hat{n}_e(k) = \hat{e}_k^\dagger \hat{e}_k$, and holes, $\hat{n}_h(k) = \hat{h}_{-k}^\dagger \hat{h}_{-k}$:

$$[\hat{X}_\alpha^\dagger\,,\,\hat{X}_\alpha] = \sum_k |\phi_\alpha(k)|^2\,(1 - \hat{n}_e(k) - \hat{n}_h(k))\;, \tag{8}$$

in which we recognize a form of the Pauli principle. We need the expectation values of $\hat{n}_e(k)$ and $\hat{n}_h(k)$ in the exciton state $|X_\alpha> = \hat{X}_\alpha^\dagger|\emptyset>$. It is easy to show that

$$n_e^{(\alpha)}(k) = <X_\alpha|\hat{n}_e(k)|X_\alpha> = n_h^{(\alpha)}(k) = <X_\alpha|\hat{n}_h(k)|X_\alpha> = |\phi_\alpha(k)|^2\,, \tag{9}$$

so that,

$$\left(1 - n_e^{(\alpha)}(k) - n_h^{(\alpha)}(k)\right) = (1 - 2|\phi_\alpha(k)|^2). \tag{10}$$

Hence from the point of view of quantum statistics, creating one exciton is equivalent to creating a "very-special" distribution of electrons and holes: $|\phi_\alpha(k)|^2$. This result implies

that the generation of excitons prevents the subsequent generation of other excitons, a behavior of Fermions and not of Bosons.

Quite often it is found in the literature that excitons behave as Bosons, because they are made of an electron and a hole with opposite spin. This is wrong; at most one can consider that excitons are non-ideal "composite" Bosons with underlying Fermi statistics reflecting that of their constituents. Creating an exciton uses some states of the pool of Fermionic states of the crystal and produces Pauli blocking. This effect is called excitonic "Phase Space Filling" (PSF) in the literature. The magnitude of the exciton Pauli blocking can be estimated by noting that for the bound states $\phi_\alpha(k) \simeq 0$ for $k \gg a_0^{-1}$, for example, $\phi_{1S}(k) = 8\sqrt{(\pi a_o^3)}/[1+(ka_o)^2]^2$. Therefore, returning in r-space to express the result intuitively, once an exciton is created a small volume of semiconductor $\simeq a_0^3$ can no longer sustain other excitons. Since the center of mass momentum vanishes, $K \equiv 0$, the "location" of this "excluded volume" is not known; nevertheless the net effect of creating an exciton is to decrease the absorption of the sample. The exact value of the "excluded volume" has to be calculated from more precise manybody theory considerations [23]. The approximately Bosonic behavior of excitons can only be observed in the low density regime $N \times a_o^3 \ll 1$. Let us note for future reference that, for the same reasons, a plasma with e and h distributions, $n_e(k)$ and $n_h(k)$, also causes a PSF due to the overlap between these distributions and $\phi_\alpha(k)$.

As the density increases, excitons begin to interact and one expects, in analogy with the hydrogen problem, that two pairs would bind to form an excitonic molecule or biexciton X_2. Theoretical considerations show that the singlet state is indeed bound for all values of the electron/hole mass ratio, whereas the triplet state is unbound, i. e., X-X. Biexcitons can be created directly by a two-photon transition, or via relaxation and binding in an exciton population. Therefore, they are active in coherent processes involving two or more photons. The bound singlet state, X_2, requires two photons of opposite polarization to be excited. This is achieved either by two distinct laser beams, one σ^+ and one σ^-, or by use of linearly polarized beams. For future reference let us note that the four polarization configurations that are two-photon active are often called co-circular ($\sigma^\pm/\sigma^\pm$), counter-

circular ($\sigma^{\pm}/\sigma^{\mp}$), linear parallel ($\|$-polarized) and linear perpendicular ($\perp$-polarized). Bound biexcitons have been observed in bulk large gap semiconductors, II-VI and I-VII, but not directly in III-V semiconductors because, in these materials, their binding energy is very small, $\leq 1meV$. In quantum confined systems, heterostructures and/or under large magnetic fields, the biexciton binding energy is enhanced and, as discussed in Section VII, they play an important role in nonlinear coherent processes.

In quantum confined systems a potential, either modulation of the band gap in heterostructures or cyclotron energy in magnetic fields, quantizes the e and h motion in some directions. Let L_j be the effective confinement length in directions $\vec{x}_j$. Then the corresponding components of the momentum can only take quantized values, $k_j \approx n_j(2\pi/L_j)$ and the particles acquire confinement energies $E_{e,h}(n_j) \approx \sum_{n_j}(\hbar k_j)^2/(2m_{e,h})$. Usually, because of the symmetry of the envelope functions, the strongest optical transitions occur between e and h subbands with the same index n_j. They have onsets at $\hbar\omega = E_g + E_e(n_j) + E_h(n_j)$ followed by continua associated with the free motion in the unconfined directions. Therefore, one expects to see an excitonic structure at each one of these thresholds. This is the case with, however, an interesting twist for the high energy transitions. Their excitons overlap in energy with the lower energy continua, and are coupled to them by the Coulomb interaction [24,25]. The true eigen-states, $|\psi(\epsilon)>$, are superpositions of the (n_j)-excitons and the $(n_l < n_j)$-continua. This is the recipe for a quantum interference that produces highly asymmetric "Fano" resonances [26]. Let us consider for simplicity the case of a single discrete state, $|X>$, coupled to a featureless continuum, $|C(\epsilon)>$, and let V be the coupling constant. Then, even in the absence of any other dissipation mechanism, the Fano resonances acquire a linewidth $\Gamma = \pi V^2$ and a transition dipole moment,

$$|\mu_{\psi(\epsilon)g}|^2 \propto \frac{(q-\Delta\omega)^2}{\Delta\omega^2+1}\,, \tag{11}$$

where $\Delta\omega = (\epsilon - \hbar\omega)/\Gamma$, and $q = |\mu_{Xg}/\mu_{Cg}|^2/\pi V$ is the Fano parameter that measures the ratio of dipole moment of the discrete state and the continuum. The transition probability, $\propto |\mu_{\psi(\epsilon)g}|^2$, vanishes for $\Delta\omega = q$ and has a maximum at $\Delta\omega = -q^{-1}$, thus giving the

very asymmetric profile to the absorption spectrum. Fano resonances have been observed in heterostructures and in bulk semiconductors in magnetic fields [24,25]. They do not correspond to bound states and should be considered as "structured continua". An example of Lorentian excitons and Fano resonances observed in the absorption spectrum of $GaAs$ at a magnetic field of $B = 12T$ for the two polarizations σ^+ and σ^- is shown in Fig.(3).

The case where a large density of carriers is already present in the sample is also very interesting. In that case, the common wisdom would say that the Coulomb interaction is screened and that one should recover the non-interacting particle results. Again, this is far from being the case. To illustrate what occurs in the presence of carriers, let us consider the optical transitions in modulation-doped quantum well (QW) or quantum wire structures. In these heterostructures, dopants are introduced in the large gap material during the growth. The dopant nuclei remain locked in that material, but the carriers move to the lowest gap in the structure where they form extremely high mobility electron or hole gases. To discuss a specific situation, let us assume an n-doped QW structure where electrons form a 2D electron gas, and therefore fill the conduction band up to a Fermi energy E_F. Because of final state occupation in the non-interacting particle picture one expects that the transitions vary as $\propto \mathcal{D}^{(2)}_{NI}(\omega) \times [1 - n_e(\omega)]$. Therefore, at low temperature the absorption profile should vanish around E_g, have a threshold around E_F, and recover its usual profile above E_F, i. e., exhibit the Burstein shift. This is not at all what is observed; in fact close to E_F the absorption exhibits a strong spectral peak called a Fermi Edge Singularity (FES) [27,28]. An example of FES is shown in Fig. (4), where the absorption spectra of an undoped and a modulation-doped $GaAs/AlGaAs$-QW structure are compared [29]. At low temperature, the FES produces a spectral feature as strong as that of the excitons! The FES originates from Coulomb mediated static and dynamic manybody effects. The physics behind the FES is that in an absorption process the photoexcited hole interacts not only with its photoexcited electron companion, but with the electrons of the entire Fermi sea [30,31]. Furthermore, the dynamic Coulomb effects result in a complicated reaction of the Fermi sea at the sudden appearance of the photoexcited hole. Electrons *inside* the Fermi sea,

with momentum $q_e < k_F$, interact with the photo-hole and scatter to states of momentum $p_e > k_F$, while the photo-hole recoils from k_h to $k'_h = k_h + q_e - p_e$. We have to introduce this heavy notation to distinguish between the e and h photo-generated in the interband optical transitions, from those created in the conduction band by intraband transitions that are due to the dynamic readjustment of the Fermi sea. It turns out that this readjustment cannot be described by a perturbative approach. The first order perturbation amplitude for the scattering described above is $\propto V_s/\Delta\epsilon$, where V_s is the screened e-h interaction and $\Delta\epsilon = \epsilon_c(p_e) - \epsilon_c(q_e) + (m_e/m_h)[\epsilon_v(k'_h) - \epsilon_v(k_h)]$. Close to E_F, $\Delta\epsilon$ can be vanishingly small and the number of scattered particles can become very large. The combination of an infinitely large number of processes of vanishing energy leads to a breakdown of the perturbation expansion! A number of approximations, very often used for treating manybody effects, "rigid Fermi sea approximation" or energy independent Coulomb interaction, etc., fail completely and lead to unphysical results. In fact, the dynamic readjustment of the Fermi sea gives an energy dependent e-h interaction. Recently a non-perturbative approach was developed for the case of a hole with an infinite mass. It has been shown that the final state wavefunction is a coherent superposition of all the Fermi sea excited states [32–34]. In the case where the h has an infinite mass, the absorption profile exhibits a power law divergence, [35]

$$\alpha(\omega) \propto |\frac{\xi_0}{\omega - \Omega_T}|^\beta \Theta(\omega - \Omega_T)\,, \tag{12}$$

were Ω_T is the threshold transition, ξ_0 is a typical conduction bandwidth and β is a function of the screening charges in the immediate vicinity of the hole [36]. Finite h mass raises the difficult question of the h-recoil. A more complete treatment shows this produces two thresholds, one at $\approx E_g + (1 + m_e/m_h)E_F$ for the vertical transitions, whereas the indirect transitions start at $\approx E_g + E_F$, with creation of conduction band e-h pairs and plasmons for conservation of momentum. The singularity is smeared over an energy range of the order of the hole band width and is, therefore, changed into a peak [37,38]. This leads to the broad spectral feature seen in Fig. (4). The theory is not yet finalized, due to formidable difficulties, such as the nonlocal e-h interaction that the valence band dispersion and the

conservation of the total momentum impose.

This concludes the brief review of the dominant elementary excitations that are involved in near band gap optical processes. In the next section we consider the time scales of their dynamics.

III. TIME SCALES AND DYNAMICAL TRENDS

When discussing coherent processes, it is important to compare the time scales of the optical excitation with those of the "fast" and "slow" electronic degrees of freedom that interact with it. For the light field, $E(t) = \mathcal{E}(t)\exp(-i\omega t) + c.c.$, one can distinguish the duration of the optical cycle, $T = 2\pi/\omega$, of the carrier wave from the characteristics of the pulse envelope $\mathcal{E}(t)$. For excitation close to the band gap of common semiconductors, the period of the optical cycles, $T \approx 2\pi\hbar/E_g$, is in the 2fs $\rightarrow$ 3fs range. Modern ultrashort pulsed lasers deliver 5fs $\rightarrow$ 1ps pulses. It is customary to assume that the optical field drives interband e-h charge fluctuations that can follow the carrier wave, and to make the so called "slow varying envelope" approximation for discussing light/semiconductor interactions. This separates the fast variations of the material parameters at frequency ω, from the slow variations that follow $\mathcal{E}(t)$. For example, in the case of the polarization, one assumes the ansatz: $P(t) = \mathrm{P}(t)\exp(-i\omega t) + c.c.$. The problem is further simplified by the Rotating Wave Approximation (RWA), that retains only the resonant or quasi-resonant terms of the equations of motion. Although these approximations may be legitimate for the longer 100fs $\rightarrow$ 1ps pulses, for the shorter ones, containing less than ten cycles, they may be problematic.

The general theoretical approach for describing optical processes in semiconductors is to try to solve the kinetic equations of the Density Matrix. For the off-diagonal elements and the diagonal elements, i. e., the polarization amplitudes p_k and the occupation numbers $n_e(k)$ and $n_h(k)$ respectively, the kinetic equations take the form;

$$\frac{\partial}{\partial t}p_k = \frac{\partial}{\partial t}p_k|_{coh} + \frac{\partial}{\partial t}p_k|_{scatt} \tag{13}$$

and

$$\frac{\partial}{\partial t} n_{e,h} = \frac{\partial}{\partial t} n_{e,h}|_{coh} + \frac{\partial}{\partial t} n_{e,h}|_{scatt} \tag{14}$$

The coherent parts of Eq.(13) and (14) are derived from the Heisenberg equations and are discussed in Section IV and V. In this section, we analyze the scattering terms. The nature of the electronic species that are excited, and the time scales over which they can maintain well defined phases, depend on $\hbar\omega$ relative to the band gap. It is clear from the previous section that one can roughly distinguish three excitation regimes: well below the lowest energy resonances, around the resonances and well above them.

In the first case, the excitation energy $\hbar\omega$ falls in the transparency range of the material. During excitation, the quantum state of the sample can be described as a linear superposition of excited states, i. e., only "virtual" excitations are generated. If we define a typical detuning as: $\Delta\omega = \Omega_{eh} - \omega$, the uncertainty principle tells us that the "lifetime" of the virtual excitation is $\tau \approx (\Delta\omega)^{-1}$. During that lifetime, the virtual excitations possess all the properties of real ones; they, however, do not participate in the dissipation processes (or they would become real) and they disappear over a time of the order of τ once the excitation ceases. This is a true coherent regime where the virtual excitations are completely driven by the light field, and they are described by Eq. (13) and (14) with the last term set equal to zero. The corresponding nonlinearities are small, but they are extremely fast. Both properties stem from the fact that $\Delta\omega$ is large. This case is covered in Section IV.

In the two other cases, the photons generate real *e-h* pairs, whose quantum mechanical phase is well defined only initially. These *e-h* pairs can participate in coherent processes over a time scale of the order of a dephasing time, T_2, that is determined by the scattering rates, Γ_i; $T_2 = [\sum_i \Gamma_i]^{-1}$. It is clear that these differ widely depending on whether the *e-h* pairs form bound states and/or are strongly correlated, or have a significant relative kinetic energy. Relaxation affects more strongly the high energy carriers, but even for these it is not an instantaneous process. In the few fs following excitation, manybody interactions start to take place, destroying the *e-h* quantum mechanical phase coherence, and creating "real carriers". A semiconductor, as any quantum mechanical system, is described by a

Schrödinger equation that is local in time. Therefore, strictly speaking, the knowledge of the Hamiltonian and the present state is enough to determine the future evolution. In practice, however, the semiconductor is such a complex manybody system that this ideal program cannot be achieved. It is customary to divide the full system into a sub-system that is analyzed and a thermal "reservoir" of all the other degrees of freedom on which we have only partial information, for example, respectively, the interband transitions and the phonons and other carriers. Then, one can distinguish two stages in the dynamics of the sub-system: the long term behavior occurring when scattering processes have randomized the degrees of freedom, which is well described by Boltzmann Kinetics, and the behavior at very early time where it is necessary to follow up the uncompleted scattering processes in the sub-system/reservoir interaction. This stage of the dynamics is highly non-classical; the uncertainty principle tells us that the energy of each *e-h* pair is not well defined, populations and polarization, i.e., diagonal and off-diagonal elements of the density matrix, are strongly coupled, and the lattice and the photo-plasma are just starting to react. In that regime, the dynamics of the polarization and k-dependent occupation numbers must be described by Quantum Kinetics, with non-Markovian statistics and memory structures. A comprehensive review of the current theory [17] of that early stage of relaxation is beyond the scope of this chapter. It is, however, useful to consider a very simple model for introducing the main concepts and discussing the essential physics [15]. In this model, the sub-system is a harmonic oscillator, $\hat{x}$, coupled to a bath of other harmonic oscillators, $\hat{A}_\nu$. The Hamiltonian is,

$$\hat{H} = \hbar\omega\, \hat{x}^\dagger \hat{x} + \sum_\nu \hbar\Omega_\nu\, \hat{A}_\nu^\dagger \hat{A}_\nu + \sum_\nu g_\nu (\hat{x}^\dagger \hat{A}_\nu + \hat{A}_\nu^\dagger \hat{x})\,. \tag{15}$$

The Heisenberg equations of motion for $\hat{x}$ and $\hat{A}_\nu$ are,

$$\frac{d}{dt}\hat{x} = -i\hbar\omega\, \hat{x} - i\sum_\nu g_\nu \hat{A}_\nu\,, \qquad \text{and} \qquad \frac{d}{dt}\hat{A}_\nu = -i\hbar\Omega_\nu\, \hat{A}_\nu - i g_\nu \hat{x}\,.$$

The last equation can be integrated formally, $\hat{A}_\nu(t) = -ig_\nu \int_{-\infty}^{t} dt' \hat{x}(t') \exp[-i\Omega_\nu(t-t')]$, assuming $\hat{A}_\nu(-\infty) = 0$, and put back in the first one, which takes the form,

$$\frac{d}{dt}\hat{x} = -i\hbar\omega\,\hat{x} + \int_{-\infty}^{t} dt'\Gamma(t-t')\hat{x}(t')\,, \tag{16}$$

where we have introduced the memory kernel: $\Gamma(t-t') = i\hbar\sum_\nu g_\nu \exp[-i\Omega_\nu(t-t')]$, characterizing how long the sub-system remembers its past. Sub-systems with an ultrashort memory, $\Gamma(t-t') = \gamma\delta(t-t')$, are called Markovian, and their relaxation can be described by a single dephasing time $T_2 = \gamma^{-1}$. In our oversimplified model, the Markovian regime is obtained by making a number of simplifying approximations: i) the reservoir is assumed to have a dense and featureless continuous spectrum with density of states $\mathcal{D}(\omega)$, ii) the coupling is assumed to be weak, $g_\nu \ll \Omega_\nu$, so that one can develop the equations of motion to first order in g_ν, which is furthermore taken as a constant $g_\nu \approx \tilde{g}$ and, more importantly, iii) all the transient effects are neglected by extending the integrals to $t \to +\infty$, thus introducing energy conserving δ-functions, $\lim_{t\to+\infty}\left[g_\nu \int_{-\infty}^{t} dt'\hat{x}(t')\exp[-i\Omega_\nu(t-t')]\right] \to i\pi\tilde{g}\hat{x}(t)\delta(\Omega_\nu-\omega)$, giving $\gamma \approx 2\pi\hbar\tilde{g}^2\mathcal{D}(\omega)$. This procedure is equivalent to calculating the scattering rates using Fermi's golden rule.

This almost trivial example illustrates how memory effects manifest themselves in general: at time t' some dynamical variable of the sub-system interacts with the reservoir and drives it; the degrees of freedom of the reservoir then evolve according to their own eigen energies, in turn, at a later time t, the reservoir interacts with the subsystem, carrying information about the dyanamical variables of the sub-system at time t' as well as its own dynamics between t' and t. Depending on the nature of the sub-system and of the reservoir, the kinetic equations can be more or less complicated to write and solve, but the behavior of the simple example sketched above is generic. In general, because of the very large number of degrees of freedom of the reservoir, interferences are the rule between t and t' and information is lost (from the point of view of the sub-system). That "scrambling" is not instantaneous and often it is possible to define a correlation time, τ_c, that characterizes the memory kernel, i. e. $\Gamma(t) \neq 0$ for $t < \tau_c$ and $\Gamma(t) \to 0$ for $t \gg \tau_c$. For $t - t' < \tau_c$ the scattering integrals must be calculated explicitly. It is clear that they have an oscillatory behavior with frequencies related to the natural frequencies of the reservoir Ω_ν. These

oscillations translate the wave nature of the elementary excitations and the finite duration of their "collisions". Let us note that because t is small, energy conservation is not strict in the scattering events, but is limited by the time/energy uncertainty relations. It is also worth noting that the time domain memory kernel corresponds by Fourier transform , $\mathcal{F}.\mathcal{T}.$, to energy dependent scattering rates, $\mathcal{F}.\mathcal{T}.[\int \Gamma(t-t')\hat{x}(t')dt] \rightarrow \Gamma(\omega)\hat{x}(\omega)$, in the frequency domain. To apply the line of thoughts sketched above to realistic situations, one has to turn to much more powerful theoretical techniques and more sophisticated treatments [39–46,16].

The main dephasing mechanisms in semiconductors are the electron/phonon and the electron/electron interactions. Most of the direct gap semiconductors are at least partially ionic, and the dominant coupling with the phonons is due to the Frölich LO-phonon/carrier interaction. The time scale of the initial non-Markovian regime can be estimated by noting that the time it takes a lattice or a plasma to react to a perturbation is of the order of one period of their natural oscillation [45]. For example, in the case of $GaAs$, the LO-phonon period is $T_{LO} = 2\pi/\Omega_{LO} = 115$fs, and for a plasma of density of $n_{eh} = 10^{18}\text{cm}^{-3}$ in the same material $T_{pl} = 2\pi/\Omega_{pl} \approx 100$fs.

The non-Markovian regime in phonon scattering of photocarriers generated by ultrashort pulses was recently analyzed, revealing some features specific to the early time domain [39,40]. These carriers are not classical; each one is spread over a large portion of k-space by the uncertainty principle. This spread must be accounted for in each scattering event. At an early stage of the relaxation, p_k and $n_{e,h}(k)$ are coupled and cannot be analyzed independently. This "polarization scattering" is discussed in Section IV. Collisions are "incomplete" in the sense that carriers do not lose or gain *exactly* one phonon because their energy is not well defined. Consequently, the collision integrals exhibit a "memory behavior"; for example, in the case of electrons they have the following structure,

$$\frac{\partial}{\partial t} n_e|_{scatt} \propto \int_{-\infty}^{t} dt'[1-n_e(k,t')]n_e(k-q,t') \qquad (17)$$
$$[N_{LO}(q,t')\cos[\xi_-(t-t')] + (N_{LO}(q,t')+1)\cos[\xi_+(t-t')]] \ ,$$

with $\xi_\pm = (\epsilon_e(k) - \epsilon_e(k-q) \pm \Omega_{LO})$, plus terms that account for polarization scattering,

[39,40]. Here N_{LO} is the LO-phonon occupation number. Note the oscillatory functions of time under the integral; they describe the "incompleted" scattering events. It is interesting to note that because the dispersion of LO-phonons is negligible, these lattice vibrations form a "single mode reservoir" whose frequency explicitly appears in Eq. (17). For the reasons evoked above, in the Markovian limit, $t \longrightarrow \infty$, the oscillatory functions of Eq. (17) transform into energy conserving δ-functions and the collision integrals take a more familiar form,

$$\begin{aligned} \frac{\partial}{\partial t} n_e|_{scatt} \propto & \, 2\pi\delta(\xi_-)[1 - n_e(k,t)]n_e(k-q,t)N_{LO}(q,t) \\ & + 2\pi\delta(\xi_+)[1 - n_e(k,t)]n_e(k-q,t)[N_{LO}(q,t)+1]\,, \end{aligned} \tag{18}$$

with phonon emission and absorption terms multiplying the Pauli blocking factors. In particular, this implies that in the non-Markovian regime the rates of scattering-in and scattering-out of one state are modified as compared to the Boltzmann case. In the latter they are two Lorentzians (broadened δ-functions) with opposite sign and separated by $\hbar\Omega_{LO}$. In the non-Markovian case, Fig.(5), the region of k-space involved in the scattering is only defined with an accuracy $\hbar/(t-t')$; i. e., a much wider region of phase space is accessible than for the exchange of exactly one phonon, resulting in a very broad scattering-in rate and a slightly reduced scattering-out rate.

In the long time regime, the steady state scattering rate is given by the Fermi golden rule [14]:

$$\Gamma^{(LO)} = \Gamma_0^{(LO)} \left(\frac{\hbar\Omega_{LO}}{\epsilon_{e,h}(k)}\right)^{1/2} \left[N_{LO}\sinh^{-1}\left(\frac{\epsilon_{e,h}(k)}{\hbar\Omega_{LO}}\right) + [N_{LO}+1]\sinh^{-1}\left(\frac{\epsilon_{e,h}(k)}{\hbar\Omega_{LO}} - 1\right)\right], \tag{19}$$

where,

$$\Gamma_0^{(LO)} = \frac{e^2}{4\pi\hbar^2}\left(\epsilon_\infty^{-1} - \epsilon_0^{-1}\right)\sqrt{(2m_{(e,h)}\hbar\Omega_{LO})}\,.$$

Here ϵ_∞ and ϵ_0 are the material optical and static dielectric constants respectively, and $m_{(e,h)}$ is the e- or h-effective mass. There is evidently a threshold for the emission of LO-phonons at energy $\epsilon_{e,h}(k) \approx E_G + \hbar\Omega_{LO}$, and no threshold for the absorption. The time scale for the establishment of the steady state regime is given by $\Gamma_0^{(LO)} \approx (125\text{fs})^{-1}$ in the case of a moderately ionic compound like $GaAs$. We should mention that the deformation

potential scattering couples the lattice to carriers in all materials, purely covalent or ionic. Acoustic phonon interactions result in much slower scattering rates. The phonon scattering rates for excitons are usually calculated independently for the electron and the hole with a form factor that accounts for their relative motion [47]. The steady state dephasing rate of excitons can be estimated from their spectral linewidth. At low temperature, it is limited by the defects in the sample. In high quality materials, the exciton dephasing time is in the range $0.5ps < T_2 < 10ps$. As the temperature increases, phonon scattering shortens T_2. It is found experimentally [11], and theoretically substantiated, that the exciton linewidth varies approximately linearly with the density of thermal LO-phonons, $\Gamma_X \approx \Gamma_0 + \Gamma_{ph} \times N_{LO}(T)$, resulting in dephasing times $T_2 \approx 100\text{fs} - 200\text{fs}$ at room temperature.

Dephasing through carrier-carrier scattering is much more difficult to describe. In the case of interaction with phonons, the lattice is the thermal reservoir and the electronic degrees of freedom are distinct from those of the reservoir. Carrier-carrier scattering proceeds from the Coulomb interaction, the very force that determines the nature of the elementary excitations. In a sense the "sub-system" is its own "reservoir". The screened Coulomb potential, $V_s(r,t)$, itself is a retarded function with its own kinetics. In particular, screening is not instantaneous; it builds up over a time scale $\approx T_{pl}$, and for shorter times is essentially unscreened, $V_s(r, t \approx 0) \rightarrow V(r)$ [45]. Carrier-carrier scattering is often described in terms of the semiclassical Boltzmann Kinetics [48,49]. On the very short time scale, this formalism is plagued by a number of problems related to the fact that it conserves exactly the kinetic energy, is local in time and thus violates the uncertainty principle. On that time scale carrier-carrier scattering has to be described by Coulomb Quantum Kinetics (CQK). As for phonons, CQK involves collective effects, and a number of features discussed above in the case of phonons remain valid. For example, the carrier energy is not well defined, and this broadening can be larger than the typical energy transfer in 2-particle collisions which, therefore, are "incomplete" [46]. As opposed to LO-phonons, however, an electron gas has a gapless spectrum that cannot be characterized by well defined and discrete frequencies. Therefore, in general carrier-carrier scattering tends to broaden significantly and quickly any

distribution of electrons or holes. CQK expresses scattering in terms of transient scattering integrals with a memory structure. These have exactly the same structure for e and h [17],

$$\frac{\partial}{\partial t}n_i(k,t)|_{scatt} \propto \sum_j \int_{-\infty}^{t} dt' \int dq \int dk' \, |V(q)|^2 \cos[\frac{1}{\hbar}\Delta\epsilon(t-t')] \qquad (20)$$
$$[n_i(k,t')n_j(k',t')[1-n_i(k-q,t')][1-n_j(k+q,t')]$$
$$-n_i(k-q,t')n_j(k'+q,t')[1-n_i(k,t')][1-n_j(k,t')]] \ ,$$

here $i,j \rightarrow e,h$, $V(q)$ is the unscreened Coulomb potential and $\Delta\epsilon = \epsilon_i^{(0)}(k) + \epsilon_j^{(0)}(k') - \epsilon_i^{(0)}(k-q) - \epsilon_j^{(0)}(k'+q)$, where the $\epsilon_i^{(0)}(k)$ are the bare energies, see Section IV. The transient scattering integrals satisfy the Pauli principle as seen from the scattering in and out terms, and conserve the number of carriers and the total polarization. Conservation of the kinetic energy, however, is not strict, as expressed by the terms $\propto \cos\Delta\epsilon(t-t')$. As a result a carrier distribution injected in the band spreads very quickly over a portion of k-space much larger than predicted by Boltzmann Kinetics. The associated broadening tends to attenuate the visibility of the phonon sidebands. Since, in the early time $n_k \approx |p_k|^2 \approx |E|^2$ the initial scattering rates scale as the excitation intensity. An example of the time evolution of a distribution of electrons generated in 20fs calculated with CQK formalism is shown in Fig. (6). One can clearly see a considerable broadening of the distribution, even during carrier injection. Current CQK calculations, however, have an infinite memory depth; the transient scattering integrals can have an unstable evolution at long time, leading to overshoots in the carrier distributions. These theories are, therefore, only reliable for describing the early time behavior, whereas Boltzmann Kinetics theory is valid in the other limit of long times. Making the link between the two time scales still represents a formidable theoretical challenge.

It is worth noting that a very different description of early time dephasing has been proposed [50]. Because, immediately upon creation, a photoplasma is still immobile, one can consider that its effect is to create a random potential that is associated with an inhomogenous broadening and thus leads to a dephasing mechanism. The phase decay is obtained by averaging over the disordered potential, giving, in bulk materials, a non exponential decay for the polarization, $|p_k(t)| \propto \exp(t/\tau)^3$, with $\tau^{-3} \propto R_y^3 \, (na_o^3) \, (ka_o)$. The cubic time dependence

is related to the dimensionality of the system; in 2D it becomes a quadratic dependence. By analogy with atomic physics, dephasing due to interaction between carriers is sometimes described as a source of "collisional broadening" and the effect of electrons and/or holes on a linewidth is written as $\gamma = \gamma_0 + \gamma_e n_e + \gamma_h n_h + ...$. Although intuitively attractive, this generalization can be misleading, especially in the context of coherent processes. Putting, without precaution, this expression in Eq.(13) can lead to severe contradictions. To see this more clearly, let us consider the case of a polarization component, $p_k = < \hat{e}_k \hat{h}_k >$. The product $\gamma p_k = (\gamma_0 + \gamma_e n_e + \gamma_h n_h) p_k$, contains terms of the form $< \hat{e}^\dagger_{k'} \hat{e}_{k'} >< \hat{e}_k \hat{h}_k >$ and $< \hat{h}^\dagger_{k'} \hat{h}_{k'} >< \hat{e}_k \hat{h}_k >$, which, in fact, originate from the uncontrolled factorization of the 4-particle operator products, $\hat{e}^\dagger_{k'} \hat{e}_{k'} \hat{e}_k \hat{h}_k$ and $\hat{h}^\dagger_{k'} \hat{h}_{k'} \hat{e}_k \hat{h}_k$. The coherence of these quantities must be accounted for by the equation of motion of the corresponding 4-particle correlation-functions, which are coupled among themselves and with that of the density matrix. Since *e-h* pairs, just upon generation, have a well defined phase, the distinction between coherent and incoherent carrier-carrier interactions is a nontrivial matter that must be considered very carefully for each case, see Section VII. For example, when carriers form a Fermi sea in a sample, the Laundau theory of Fermi Liquids predicts that the lifetime of quasi-particles with excess energy $\delta\epsilon$ varies as $\tau \propto (E_F/\delta\epsilon)^2$ and, therefore, becomes infinite on the Fermi surface. Evidently this has important consequences for all coherent optical processes. Nevertheless, it is true in general that the presence of a large number of carriers, photogenerated or not, reduces significantly the period of phase coherence.

In summary, following the excitation of a semiconductor by an ultrashort laser pulse, one can distinguish the following time sequences. Initially, during the first few optical cycles, *e-h* pairs oscillate coherently between the valence and conduction bands; then typically in a few tens of fs, manybody interactions start to destroy the phase coherence. As *e*, *h* and nuclei start to move, a number of processes begin to be "turned on", the Coulomb potential, which is initially bare, starts to be screened [46], and the lattice begins to react to the appearance of charges [39,40]. During this transient period the non-Markovian dynamics are described by Quantum Kinetics. Although the carriers start to relax, their distribution cannot be de-

scribed by Fermi functions and a "temperature" cannot be defined. As scattering processes become effective, the coherence continues to decay, and is completely lost after several tens of femtoseconds when the quasi-particle scattering rates have reached a regime where the occupation numbers follow Fermi-Dirac statistics and the system can be described by Boltzmann Kinetics. Early in that regime there is still no equilibrium among different carrier species or between the carriers and the lattice, but carrier-phonon and carrier-carrier scattering recover their usual behavior. Eventually the carriers equilibrate first among themselves and later with the lattice before finally recombining.

IV. A PURELY COHERENT PROCESS INVOLVING ONLY VIRTUAL ELECTRON-HOLE PAIRS: THE EXCITONIC OPTICAL STARK EFFECT

A true coherent state of a semiconductor is realized when the material is excited well below its optical transition energy threshold by a coherent laser field. Then only virtual excitations are generated. They do not participate in dissipation and their phase is determined by that of the laser. Such situations can also be realized in atomic systems, where it is well known that the laser field induces the so called Optical Stark Effect (OSE), whereby the k-atomic level experiences a shift in energy,

$$\delta\epsilon(k) \propto \frac{|\mu_k \cdot E|^2}{\Delta\epsilon(k)} \tag{21}$$

where μ_k is the transition dipole moment and $\Delta\epsilon(k) = \hbar(\Omega_{kg} - \omega)$ is the laser detuning [51]. The Rabi frequency, $|\mu_k \cdot E|$, measures the atom/EM-field coupling. An apparently similar effect was observed in semiconductor QW structures excited in their transparency range. Ultrashort pulse pump/probe experiments revealed, indeed, that the exciton resonances experience a shift that follows instantaneously the laser pulses, Fig. (7), with a magnitude inversely proportional to the detuning, and proportional to the laser intensity, in agreement with Eq. (21) [52,53]. In these experiments the small changes in sample transmission seen by a weak probe laser and induced by a strong pump laser are measured. In the small signal

regime, the differential transmission spectrum (DTS), $\Delta T/T = [T(I_p) - T(I_p = 0)]/T(I_p = 0)$, reproduces faithfully the changes in the absorption spectrum of the sample, $\alpha(\omega)$, since $\Delta T/T \approx -\Delta\alpha(\omega) \times l$. A number of reports confirmed these early observations and provided more detailed information on the excitonic-OSE [54–57]. The most interesting aspects of the excitonic-OSE, however, relate to its interpretation [58,59]. Because of its importance as an introduction to the physics that governs light/semiconductor interactions, it is worth discussing the fundamental issues. Furthermore, the excitonic-OSE provides us with a very natural way of introducing the theoretical basis for the coherent part of the kinetic equations, i. e., the first part of Eq. (13) and (14).

One approach for describing the excitonic-OSE could be to start from the quasi-continuum of valence and conduction band states, and apply to each transition at k the atomic picture. Considering for simplicity the two-parabolic-band model, the levels at the bottom of the conduction band and at the top of the valence band are repelled more than the higher levels because of their smaller detuning $\Delta\epsilon(k)$. Hence the curvature of the band is modified by the laser field, and the effective masses are renormalized by the light! Since excitons are made of the $(k \leq a_o^{-1})$-states, the "new" excitons would be constructed from these dressed single particle states. This approach gives the priority to the single particle/EM-field interaction over the Coulomb interaction between particles, but as shown in Section-II, this is not justified. The alternative approach is to treat the excitons as eigen states of the crystal, and apply to them the atomic picture. In that case, the priority is given to the Coulomb interaction and not to the interaction with the EM-field. The charges, however, react to the total field, whatever its origin, the laser or other charge oscillations in the medium. This lengthy discussion is aimed at demonstrating that one must treat the Coulomb interaction and the interaction with the EM-field on the same footing. This is true for *any* light/semiconductor interaction, and causes some theoretical difficulties.

Let us apply this program to the two-parabolic-band model. The basic Hamiltonian of the electronic system is,

$$\hat{H}_{el} = \sum_k \epsilon_c(k)\,\hat{c}_k^\dagger \hat{c}_k + \epsilon_v(k)\,\hat{v}_k^\dagger \hat{v}_k \tag{22}$$

$$+\frac{1}{2}\sum_{k,k',q\neq 0} V_q\,[\,\hat{c}_{k+q}^\dagger \hat{c}_{k'-q}^\dagger \hat{c}_{k'}\hat{c}_k + \hat{v}_{k+q}^\dagger \hat{v}_{k'-q}^\dagger \hat{v}_{k'}\hat{v}_k - 2\,\hat{c}_{k+q}^\dagger \hat{v}_{k'-q}^\dagger \hat{v}_{k'}\hat{c}_k\,],$$

where the first line describes the dispersion in the conduction and valence bands, and the second line the intraband and interband Coulomb interaction. For the purely coherent excitonic-OSE we do not need to consider dissipation, i. e., we can put $\partial p_k/\partial t|_{scatt} \equiv 0$ in Eq. (13) and, therefore, as a starting point we do not have to explicitly involve electron-phonon and carrier-carrier scattering. The light/matter interaction is treated in the semi-classical dipole approximation and the rotating wave approximation with the interaction Hamiltonian:

$$\hat{H}_I = -\sum_k \left[\mu_{cv,k} E(t) \hat{c}_k^\dagger \hat{v}_k + \mu_{cv,k}^* E(t)^* \hat{v}_k^\dagger \hat{c}_k\right]. \tag{23}$$

The total Hamiltonian, $\hat{H}_{tot} = \hat{H}_{el} + \hat{H}_I$, has no known solutions, and approximations are necessary at this point. The general approach for describing optical properties of a system is to determine the expectation value of operators such as the Polarization $\hat{P}$ through the Density matrix operator $\hat{n}$ by: $P = Tr(\hat{n}\hat{P})$ [2,3]. In the two-parabolic-band model the matrix elements of $\hat{n}$ are the expectation values of 2-particle operators:

$$n_{cc,k}(t) = <\hat{c}_k^\dagger \hat{c}_k> \qquad n_{cv,k}(t) = p_k(t) = <\hat{c}_k \hat{v}_k^\dagger> \tag{24}$$

$$n_{cv,k}(t) = p_k^\dagger(t) = <\hat{c}_k^\dagger \hat{v}_k> \qquad n_{vv,k}(t) = <\hat{v}_k^\dagger \hat{v}_k> .$$

The normal procedure for getting the equation of motion of $\hat{n}$ is to write the Heisenberg equations for the 2-particle operators using $\hat{H}_{Tot}$, to apply the fundamental anti-commutation rules and then to take the expectation values. Because $\hat{H}_{Tot}$ contains 4-particle operators, these appear in the 2-particle operator equation of motion, so that one has to write the Heisenberg equations for the 4-particle operators. These in turn contain 6-particle operators, leading to an infinite hierarchy of coupled equations. This behavior is a fundamental problem of manybody systems that can find many embodiments in various formalisms (Feynman Diagrams, Green's Functions etc.), in all cases, when an exact solution is not available,

one has to decide on a way to truncate this development. The simplest approach, beyond the independent particle model, is to factorize the expectation values of the 4-particle operators into products of expectation values of 2-particle operators, i. e., performing the Random Phase Approximation. This is equivalent to the time dependent Hartree-Fock treatment [60]. At this HF/RPA level, correlation between four or more particles are neglected, and we will see in Section VI schemes for accounting for them.

With all these approximations and considering only vertical transitions because the photon momentum is negligible, the density matrix breaks into 2×2 blocks,

$$\hat{n}(t) = \sum_k \hat{n}_k(t) = \sum_k \begin{bmatrix} n_c(k) & p_k \\ p_k^* & n_v(k) \end{bmatrix} . \tag{25}$$

It obeys the Liouville equation of motion, without the usual relaxation term, $\frac{\partial}{\partial t}\hat{n}_k(t)|_{scatt}$,

$$i\hbar \frac{\partial}{\partial t} \hat{n}_k(t) = [\, \hat{H}_k(t) \,,\, \hat{n}_k(t) \,] \,, \tag{26}$$

and the effective HF/RPA Hamiltonian

$$\hat{H}_k(t) = \begin{bmatrix} \epsilon_c(k) & 0 \\ 0 & \epsilon_v(k) \end{bmatrix} + \begin{bmatrix} 0 & -\mu_k E(t) \\ -\mu_k^* E^*(t) & 0 \end{bmatrix} - \sum_{k'} V_{k,k'}\, \hat{n}_{k'}(t) \,. \tag{27}$$

Eq. (27) immediately shows that the Coulomb interaction renormalizes, at the same level, the energies and the coupling to the EM-field as measured by the Rabi frequency,

$$\epsilon_i(k) \rightarrow \epsilon_i(k) - \sum_{k'} V_{k,k'}\, n_i(k') \,, \tag{28}$$

$$\mu_k E(t) \rightarrow \Delta_k = \mu_k E(t) + \sum_{k'} V_{k,k'}\, p_{k'} \,. \tag{29}$$

Eq. (28) expresses a renormalization of the single particle energies caused by the virtual populations, it is reminescent of the "Band Gap Renormalization" (BGR) which is often considered in a different context for incoherent electrically injected carriers or thermalized photocarriers. Coherent populations also cause a BGR and, since in that regime the polarizations have not dephased, the transient BGR, Eq. (28), is accompanied by a similar

transient renormalization of the Rabi frequency, Eq. (29). This equation simply expresses that carriers experience the "total" field, laser plus Coulomb coupling to other dipoles. The Liouville Eq. (26) then becomes,

$$i\hbar \frac{\partial}{\partial t} p_k = [\epsilon_c(k) - \epsilon_v(k) - \hbar\omega]p_k + [n_{cc}(k) - n_{vv}(k)]\Delta_k \tag{30}$$

$$i\hbar \frac{\partial}{\partial t} n_{cc}(k) = -i\hbar \frac{\partial}{\partial t} n_{vv}(k) = [p_k \Delta_k^* - p_k^* \Delta_k]\,. \tag{31}$$

These equations have two constants of motion,

$$n_{cc}(k) + n_{vv}(k) = 1 \qquad 4|p_k|^2 + [n_{cc}(k) - n_{vv}(k)]^2 = 1\,, \tag{32}$$

which simply express that, since there is no dissipation, the populations of optically coupled levels and the modulus of the Bloch vector are constant.

Considering excitation by a monochromatic field, $\partial/\partial t \rightarrow 0$, and transforming to the electron-hole representation, $n_{cc}(k) = n_e(k) = n_k$ and $n_{vv}(k) = 1 - n_h(k) = 1 - n_k$, we get, $(\epsilon_k - \hbar\omega)p_k - (1-2n_k)\Delta_k = 0$ and $\Im m(p_k^* \Delta_k) = 0$ where $\epsilon_k = \epsilon_c(k) - \epsilon_v(k)$. The last equation expresses that there is no absorption. It is worth noting that in the small excitation regime, the conservation of the Bloch vector modulus implies: $n_k \approx |p_k|^2$. The eigenvalues of $\hat{H}_k$ gives the dispersion of the "dressed" bands,

$$\epsilon^{\pm}(k) = \frac{1}{2}\left[\epsilon_c(k) + \epsilon_v(k) \pm [(\epsilon_c(k) - \epsilon_v(k))^2 + 4|\Delta_k|^2]^{1/2}\right]\,.$$

As mentioned before, the curvature of these "dressed" bands is different from that of the unexcited semiconductor. This can be viewed as an "electronic polaron" effect whereby the e and h drag with them the cloud of short-lived ($\tau \approx \hbar/(\epsilon_k - \hbar\omega)$) virtual e-h pairs, hence becoming heavier [61].

The Hamiltonian $H = \sum_k \hat{H}_k$ can be diagonalized by a canonical transformation $\hat{U}_k$. In the new basis the density matrix, $\hat{U}_k \hat{n}_k \hat{U}_k^{\dagger}$, has only one non-zero matrix element equal to 1, in the ground "condensed" state. The solutions are:

$$n_k = \frac{1}{2}\left[1 - \frac{(\epsilon_k - \hbar\omega)}{[(\epsilon_k - \hbar\omega)^2 + 4|\Delta_k|^2]^{1/2}}\right]\,, \quad \text{and} \quad p_k = \frac{\Delta_k}{[(\epsilon_k - \hbar\omega)^2 + 4|\Delta_k|^2]^{1/2}}\,, \tag{33}$$

and the "gap" equation:

$$\Delta_k = \mu_k E + \sum_{k'} \frac{V_{kk'}\Delta_{k'}}{[(\epsilon_{k'} - \hbar\omega)^2 + 4|\Delta_{k'}|^2]^{1/2}} \,. \tag{34}$$

The approach sketched in the previous paragraph is a mean field theory of the laser excited semiconductor, where p_k and n_k are the order parameters. They play respectively the same role as the pair amplitude and the mean occupation number in the BCS theory of superconductors. Indeed Eq. (33) and (34) are *formally* identical to the BCS equations describing superconductivity [62], and to those describing the Bose condensation of excitons [63,64], with two modifications: i) the chemical potential is replaced by the photon energy, and ii) the gap equation contains an extra term, the Rabi frequency. The first change expresses that each virtual exciton is created by a photon, the second that the condensation is not spontaneous, but induced by the EM field. In the same spirit it is worth noting that Eq. (27) is the analog of Anderson's "pseudo spin Hamiltonian" in superconductivity theory.

In order to describe pump and probe experiments, one has to consider that the applied field is comprised of two parts, the strong pump field, $E(t)$, and the weak probe field, $\delta E(t)$. The former gives rise to a renormalized semiconductor "ground state", described by Eqs. (33, 34), while the linear response to $\delta E(t)$ yields the corresponding renormalized "excitation spectrum", which is blue shifted and thus exhibits the OSE. The theory also predicts a small nonlinear and coherent gain below the pump central frequency which involves processes of high order in the applied field [58,59]. All these results stress the profound effects that the Coulomb interaction has on the optical properties of semiconductors. The physics of these materials excited by a laser field is more closely related to that of condensed manybody systems than to that of laser excited atoms. Another description of the excitonic-OSE has been proposed [65,66]. Although starting from a different point of view, it yields results that are equivalent to those of Ref. [58,59] when the biexciton contribution does not play an important role.

Linearizing Eqs. (31) and (30) with respect to $\delta E(t)$, and considering only the effects of the leading 1S-resonance to get analytical results [58,59], one finds that the exciton peak is

shifted by

$$\delta E_{1s} \propto \frac{|\mu E_p|^2}{(E_{1s} - \hbar\omega_p)} \times \frac{|\phi_{1S}(r=0)|^2}{N_s^{PSF}}, \tag{35}$$

where N_s^{PSF} is the saturation density due to excitonic-PSF mentioned in Section II. The first fraction in Eq. (35) reproduces the atomic results, Eq. (21); the second gives the changes due to the excitonic structure.

The dependence of the OSE-shift on dipole matrix element was confirmed by comparing the shifts experienced by *hh*-X and *lh*-X in the same measurement [53]. Its dependence on the exciton relative motion wavefunction was studied by distorting $\phi_{1S}(r = 0)$ using an electrostatic field applied perpendicular to the plane of the QW. A strong reduction of the excitonic-OSE has been observed as $|\phi_{1S}(r = 0)|^2$ decreases, in agreement with theory [56,57]. A more complete treatment, using the Coulomb Green's functions for solving the formalism of Ref. [58], reveals that the condensation of virtual excitons is distributed over all the bound and unbound states [67]. The relative occupation is a sensitive function of the detuning and pulse duration. Interestingly, it is related to the *real* part of the susceptibility in contrast with the cases where real excitons are generated and where the occupation is related to the imaginary part of the susceptibility [68].

Numerical calculations based on the theory of Refs. [58,59] predicted that in 2D and for pump detunings of about $10R_y$, low-intensity nonresonant excitation should produce a pure Stark shift of the 1S exciton without any loss of oscillator strength, while in 3D the oscillator strength increases slightly with pump intensity [71–74]. The physical origin of this behavior is that the Stark shift of the band gap is always larger than that of the 1S-exciton because of the larger spatial extent of scattering states. This corresponds to an effective increase in the 1S-exciton binding energy and, thus, in its oscillator strength, which can overcome the decrease due to phase space filling by the virtual *e-h* pairs. An example of DTS at $\Delta t = 0$ seen in a QW sample excited $50meV$ below the 1S *hh*-X, for a low pump excitation, $\approx 30MWcm^{-2}$, is shown as a solid line in Fig. (8). In the case of a pure shift, the DTS should have exactly the same lineshape as the derivative of the linear absorption $\partial\alpha(\omega)/\partial\omega$, which is shown as a

dashed line in the figure. Indeed the two lineshapes are identical. In addition, the integral of the DTS around to the resonance is zero, as it should be for pure shift. As the pump intensity is increased, the DTS profile becomes indicative of both a shift and broadening. This is due to the finite bandwidth of ultrashort pulses whose Fourier components have different detuning and amplitude, leading to an "inhomogeneous broadening" of the absorption spectrum, which increases with intensity [71,72]. An alternative interpretation of that broadening is that, for ultrashort pulse excitation at small detuning, the effective masses of the "dressed" bands experience a significant and time dependent variation. For the "slow" degrees of freedom, such as an e orbiting an h in a bound state, the time dependent masses induce a strong dephasing. Very recently, the coherent nonlinear gain below the pump frequency has been observed [75]

The OSE was also observed in modulation-doped samples, where excitons are not present, and the absorption edge exhibits a FES. In ultrashort pulse experiments carried out under the same conditions as for undoped samples, together with the blue shift there was observed a small, but significant, optical gain just below the FES and a much smaller reduction in the optical absorption strength [29]. The FES-OSE is much more complicated to treat, because the reaction of the whole Fermi sea must be accounted for. The low lying excitations of the Fermi sea are slow; they cannot adjust adiabatically to the rapid effective mass changes induced by the virtual interband transitions. The combination of the reduced "electronic polaron" enhancement of the effective masses and the time dependence of gap E_g explains, qualitatively, the small gain and the changes in the FES absorption [61,76,77].

It is worth noting how much the formalism and the interpretation of the experiments discussed above are different from that of atomic systems. Having introduced the main manybody concepts, we can now proceed to the case where real carriers are created.

V. FUNDAMENTALS OF TWO-PARTICLE CORRELATION EFFECTS INVOLVING REAL ELECTRON-HOLE PAIRS

In this section we discuss the fundamental mechanisms that are responsible for nonlinear optical processes in semiconductors when real *e-h* pairs are created.

The first experiments performed with ultrashort pulse excitation at, or slightly above, exciton resonances were concerned with the effects that a gas of excitons or an *e-h* plasma have on the excitonic absorption, in bulk [78,79] and in QW structures [11,80–83]. The loss of exciton oscillator strength in the presence of an *e-h* plasma, seen in the bulk, was first attributed to screening. It was the interpretation of pump/probe experiments performed on quasi-2D QW structures, where the effects of screening are reduced, that helped identify Pauli blocking of exciton transitions as important [84,23]. Interestingly, it was found that the reduction of oscillator strength occurred as the absolute energy of the exciton remained constant in 3D [78,79,13], whereas in 2D it was accompanied by a non negligible blue shift [80,82]. Furthermore, the relative magnitude of these effects depended strongly on the nature of the excited species, exciton gas or *e-h* plasma, and on their temperature, T, resulting in complicated dynamics. The *e-h* pairs appeared to be more effective than an exciton gas in reducing the band edge absorption at low temperature, but less effective at high temperature. Although a comprehensive theory was not available at that time, the constant value of the exciton energy in 3D was explained as near perfect cancellation of Pauli blocking (hard core repulsion) and screening [78,85]. In 2D, since screening is strongly reduced, this compensation does not occur and the Pauli blue shift dominates [84,23].

Analytical results for the change in the exciton oscillator strength, f_α, in the leading order in the density, N, were obtained in reasonably good agreement with experiments:

$$\frac{\Delta f_\alpha}{f_\alpha} = -\frac{N}{N_s}. \tag{36}$$

Here $N_s^{-1} = (N_s^{PSF})^{-1} + (N_s^{EXCH})^{-1}$, where N_s^{PSF} accounts for the PSF of the states out of which excitons are made and N_s^{EXCH} accounts for the change in the exciton relative

motion wavefunction due to screening. It follows from Eq.(10) that $(N_s^{PSF})^{-1} = \sum_k [n_e(k) + n_h(k)]\phi_\alpha(k)/\phi_\alpha(r=0)$. For an exciton gas, $n_e(k) = n_h(k) \propto |\phi_\alpha(k)|^2$ and $(N_s^{PSF})^{-1} \propto$ the exciton volume ($4\pi a_o^3/3$ for $n = 1S$ in bulk and $2\pi a_o^2 L_z$ in QW). For the *e-h* plasma N_s^{PSF} depends on the temperature, through the overlap between the plasma distribution, $n_e(k)$ and $n_h(k)$, and $\phi_\alpha(k)$ [84,23]. At low temperature, the carriers occupy the band minima and efficiently block the transitions at $k < a_0^{-1}$; at high temperature, they spread out, the overlap decreases and $N_S^{-1} \propto R_y/k_BT$. For the same reasons, N_s^{EXCH} follows similar trends.

The ultrafast evolution between these different regimes is shown in Fig. (9). Here the DTS spectra of a 10nm *GaAs* QW structure excited about 20meV above the exciton resonances are presented as the pump probe time delay Δt is varied from -100fs to 200fs by 50fs steps [81]. At early time delay one sees a spectral hole around $1.513eV$ that follows approximately the pump spectrum, and a more complex DTS signal at the exciton resonances around $1.498eV$ indicative of broadening and loss of oscillator strength. The spectral hole is due to the PSF induced in the continuum states by the nonthermal distributions of photocarriers generated by the pump. As shown in the inset of Fig. (9) for another experiment, the spectral hole is always shifted as compared to the pump spectrum. The lineshape of the spectral hole and its location relative to that of the pump are discussed below. The signal at the exciton peaks is due to a combination of collisional broadening (see Section VII) and coherent excitation of the resonances. As Δt increases, the spectral hole in the continuum moves down in energy and smooths out until $\Delta t \approx 200$fs, where it has acquired an exponential profile reminiscent of a Maxwell-Boltzmann distribution. This is interpreted as due to the cooling down and thermalization of the photo-plasma. Simultaneously, the signal at the excitons increases because PSF and screening increases with the overlap of the plasma distribution with the excitons wavefunctions $\phi_\alpha(k)$.

For small time delays, the spectral hole is always seen shifted with respect to the laser spectrum, as detailed in Fig. (10) [86]. This very interesting coherent effect was investigated experimentally [86,87] and theoretically [67,88]. The mechanisms responsible for the FES, discussed in Section I, generalized to a nonequilibrium population [86–88], give a qualitative

understanding of the observations. The quasi-instantaneous *e-h* distributions created by ultrashort laser pulses have two edges that are not sharp, since they follow the laser pulse spectrum. Immediately upon their creation, however, the carriers are coherent, and thus can participate in FES-like processes. Manybody theories have been developed to describe these mechanisms [88]; for an intuitive discussion let us neglect the valence band dispersion and assume that *e-e* interactions do not perturb significantly the *h*-Fermi sea interaction. We can then consider that the ultrashort laser pulses create a nonthermal electron distribution $n_e(\epsilon - \epsilon_0, t)$ centered at energy ϵ_0, that one can describe as the sum of two parts: $n_e(\epsilon - \epsilon_0, t) = n_{ce}(\epsilon, t) - n_{ch}(\epsilon, t)$, a negatively charged distribution of conduction band electrons, *ce*, $n_{ce}(\epsilon, t) = \Theta(\epsilon - \epsilon_0) + \Theta(\epsilon_0 - \epsilon) \times n_e(\epsilon - \epsilon_0, t)$ and a positively charged distribution of conduction band holes, *ch*, $n_{ch}(\epsilon, t) = \Theta(\epsilon - \epsilon_0) \times [1 - n_e(\epsilon - \epsilon_0, t)]$. These two distributions have a step-like Fermi-profile, and one can apply to them the static FES theory [30,35], i) as long as the non thermal distribution remains coherent, and ii) with opposite sign for the *cb-e* and the *cb-h* distributions, i. e., at the high energy, ϵ_2, and low energy, ϵ_1 edges. As for the case of the static FES, the singularities are smeared out because of processes neglected in this oversimplified discussion and appear as resonances. Altogether, the dominant physics is that the absorption is enhanced close to ϵ_2 because of the *attraction* between the *cb-e*-Fermi sea and the photogenerated valence hole, whereas it is reduced close to ϵ_1 because of the *repulsion* between the *cb-h*-Fermi sea and the valence hole. Let us note that, in the same spirit, excitonic effects at the edges of nonthermal Gaussian distributions were obtained in the in theory of pump/probe DTS involving a transient *e-h* population, Ref. [67].

Similar considerations show that the same resonant features occur in the emission process. The dynamic FES at both edges of the non-thermal distribution lead to absorption enhancement and emission reduction i. e., to a blue shift of the spectral lineshapes of the absorption and emission spectra, as compared to that of the pump laser pulses. A crucial point on which all these arguments is based is that of the coherence of the non-thermal distribution; the energy shift lasts only as long as the coherence is maintained. This issue was investigated by a comparative spectro-temporal analysis of the time sequence for generation of non thermal

distributions in pump/probe and self-diffraction four wave mixing (FWM) experiments [87].

The self diffraction FWM technique is aimed at measuring the simplest non-trivial coherent emission. Two laser pulses, $E_1(t)$ and $E_2(t)$, separated by a time delay, $\Delta t = t_2 - t_1$, and propagating in the directions $\vec{k}_2$ and $\vec{k}_1$, interfere via some nonlinearity in a sample. They generate several nonlinear polarization waves that contain one contribution, $P_s(t, \Delta t)$, emitting photons in the background-free direction $\vec{k}_s = 2\vec{k}_2 - \vec{k}_1$. The excitation configuration is exactly the same as for pump/probe measurements although, in the latter case, it is the change in the transmission of the $\vec{k}_1$ pulses that is measured. It is important to emphasize on the different time sequences for the generation of the first order polarization, $p^{(1)}$, second order population, $n^{(2)}$ and third order polarization, $p^{(3)}$ in the two experiments. For FWM: $p^{(1)}(\vec{k}_1) \propto E(\vec{k}_1)$, $n^{(2)}(\vec{k}_2 - \vec{k}_1) \propto \Im m[p^{(1)}(\vec{k}_1)^* E(\vec{k}_2)]$, and $p^{(3)}(\vec{k}_s) \propto E(\vec{k}_2) n^{(2)}(\vec{k}_2 - \vec{k}_1)$, whereas for pump/probe $p^{(1)}(\vec{k}_2) \propto E(\vec{k}_2)$, $n^{(2)}(\vec{k} = 0) \propto \Im m[p^{(1)}(\vec{k}_2)^* E(\vec{k}_2)]$ and $p^{(3)}(\vec{k}_1) \propto E(\vec{k}_1) n^{(2)}(\vec{k} = 0)$. Our convention for positive delay, $\Delta t = t_2 - t_1 > 0$, refers to the usual one for the polarization decay of a two level atom. The dynamical FES is expected to occur on a time scale where incoherent screening starts to become effective. In the experiments of Ref. [87] the FWM and pump/probe power spectra measured vs. Δt show a shift of the instantaneous frequency immediately after the nonthermal second order distributions, $n^{(2)}(\vec{k}_2 - \vec{k}_1)$ and $n^{(2)}(\vec{k} = 0)$ respectively, are created, i. e., for the opposite time sequences between the pulses in direction $\vec{k}_2$ and $\vec{k}_1$. This demonstrates that the blue shift associated with the dynamical FES does not depend on the particular time ordering of the pulse sequence: it is only related to the coherent part of the manybody interaction, i. e., as long as the $n^{(2)}$'s are coherent. Importantly, the disappearance of the blue shift is still seen well after the *conventional* relaxation time T_2 [89,90], clearly indicating that some correlation in the *e-h* system survives for rather long times. In fact, the experiments show that the loss of coherence in a dense medium is far too complex to be described by a single parameter such as T_2 [87], as we discuss in Section VIII.

The first investigations directly testing the relaxation time T_2 of the excitonic polarization were performed by degenerate FWM. In the case of a homogeneously broadened two level

atom the FWM-signal is emitted immediately after the second pulse and corresponds to "Free Polarization Decay" [5]. For inhomogeneously broadened atomic lines, the FWM-signal is delayed by Δt after the second pulse and corresponds to a "Photon Echo" [4]. FWM techniques have been applied extensively to atomic and molecular systems. In the two level atom case of Free Polarization Decay, $P_s(t, \Delta t)$, is zero for $\Delta t < 0$ and exhibits a simple exponential decay for $\Delta t > 0$. For this reason, the easiest and most commonly used measurement technique for atomic-like systems, is to time-integrate the FWM signal, with a slow detector, as Δt is varied to determine the so called "Time Integrated" FWM (TI-FWM),

$$S_{TI}(\Delta t) \propto \int_{-\infty}^{+\infty} dt \, |P_s(t, \Delta t)|^2 . \tag{37}$$

For a two level atom, $S_{TI}(\Delta t)$, reproduces, as a function of Δt the same temporal behavior as $|P_s(t, \Delta t)|^2$ vs. t at any fixed Δt. Because of the historical background of atomic and molecular physics, and the simplicity of the two level atome results [5], the early ultrashort pulse investigations of FWM in semiconductors concentrated on the dephasing of resonances and were analyzed using that model [12,13,91]. It was deduced from the decay of S_{TI} vs. Δt that the exciton dephasing time was in the ps time scale. These experiments were extended to study the effects of temperature, density of exciton gases and e-h plamas on the exciton dephasing time [92,93]. Again, early analyses were performed according to atomic models as sketched in Section III, and we will revisit this issue in Section VII.

A qualitative difference with the ideas commonly accepted in coherent spectroscopy was observed when very high quality heterostructures, with homogeneously broadened exciton resonances, were probed with $\approx$ 100fs pulses [94]. As shown in Fig. (11), TI-FWM experiments revealed a very strong $S_{TI}(\Delta t)$ signal for $\Delta t < 0$, extending at least as far as 20 times the laser pulse duration before $\Delta t = 0$. As seen on the figure temperature dependence study demonstrated that the rise time of $S_{TI}^{-} \equiv S_{TI}(\Delta t < 0)$ is exactly half the decay time of the "regular" signal $S_{TI}^{+} \equiv S_{TI}(\Delta t > 0)$. This direct contradiction with the atomic theories, which always predict that $S_{TI}^{-} \equiv 0$ identically [5], forced a re-evaluation of the analysis of

coherent processes in semiconductors. As shown below, the Coulomb interaction induces nonlinearities that are a behavior qualitatively different from that of two level atoms and are responsible for the non-zero value of S_{TI}^{-}.

The two-parabolic band model formalism described in Section III, with the addition, in Eq. (26), of phenomenological relaxation and dephasing times describing the interaction with phonons, gives a good starting point for discussion [95]. It is instructive to write the coupled equations satisfied by the density matrix elements. For the off-diagonal and diagonal terms, Eq.(30) and Eq.(31) in the e-h representation, $n_e(k) = n_c(k)$, $n_h(k) = 1 - n_v(k)$, we have respectively;

$$\begin{aligned} i\hbar \frac{\partial}{\partial t} p_k \; + \; [i\hbar\gamma - (E_g + \frac{\hbar^2 k^2}{2m})]p_k + \sum_{k'} V_{k,k'}\, p_{k'} = \\ - [1 - n_e(k) - n_h(k)]\mu_k E(t) \\ + \sum_{k'} V_{k,k'} \left[p_{k'}(n_e(k) + n_h(k)) - p_k(n_e(k') + n_h(k'))\right]. \end{aligned} \tag{38}$$

and

$$\hbar(\frac{\partial}{\partial t} + \Gamma_e) n_e(k) = \hbar(\frac{\partial}{\partial t} + \Gamma_h) n_h(k) = 2\Im m \left(p_k(\mu E(t) + \sum_{k'} V_{k,k'} p_{k'})^* \right). \tag{39}$$

These equations deserve several comments. First, we should note that in Eq.(38) we have identified the "observed" band gap E_g with the energy difference $\epsilon_c(k=0) - \epsilon_v(k=0) + \sum_{k'} V_{k,k'}$. Thus, within the very restrictive HF/RPA discussed in Section III, this indicates that the gap energy includes the Coulomb interaction of the full valence band electrons, $n_h(k) = 0$ and $n_e(k) = 0$. The sources of nonlinearity in Eq. (38) and (39) are due to the excited photocarriers, $n_h(k) \neq 0$ and $n_e(k) \neq 0$, but their origin stems from the same potential $V_{k,k'}$ that determines the gap. Hence, our remark in Section II: The Coulomb interaction causes "zero" order effects; this is, in fact, a general result substantiated by much more thorough theoretical treatments [19,20]. If the right hand side of Eq. (38) is put equal to zero and the steady state is assumed ($\partial p_k/\partial t \rightarrow 0$), one recovers the k-space exciton Wannier equation, Eq. (5), so that Eq. (38) includes all the "excitonic" effects. If $V_{k,k'}$ is put equal to zero in Eq. (38) and (39), one recovers the Optical Bloch equations for

the independent two level atom model of the "atomic" picture.

The nonlinear source term on the right hand side of Eq. (38) is comprised of two parts. The first one expresses the reduction of the Rabi frequency because of Pauli Blocking, and it is active for all material systems made of Fermions, atoms, molecules or solids. It appears as a coupling between electric field $E(t)$, and the populations $n_e(k)$, and $n_v(k)$. The second term expresses the Coulomb coupling between polarization p_k and populations $n_e(k')$ and $n_h(k')$. This term is new; it appears only in condensed matter. Because of the consistent treatment of the self-energy and vertex corrections, it vanishes for $k = k'$, avoiding unphysical divergences and translating the fact that a plane wave does not interact with itself. Finally, Eq.(39) expresses that the populations are generated by the *total* field, Δ_k of Eq.(29). In this chapter, we shall call the HF/RPA Coulomb nonlinearities, the Bare Coulomb Interaction (BCI). The set of coupled equations, Eq. (38) and Eq. (39), are called the Semiconductor Bloch Equations (SBE). Over the last decade the SBE have been applied very successfully to explain a number of nonlinear optical processes in semiconductors [72,60,15,96]. In the k-space representation, numerical solutions of the SBE, with a complete description of the energy band structure, have been applied successfully to realistic materials and heterostructures [96]. They have also been investigated in the r-space representation [97,98], where interesting spatio-temporal aspects of the polarization dynamics are better expressed [99].

Coming back to the experimental results of Ref. [94], let us see how they can be explained by the SBE. The processes responsible for the FWM signal in the direction k_s are at least third order in the field. They can originate from one of the two nonlinear sources of Eq.(38). For ultrashort pulses, the polarization and population components rise with the fields and then decay exponentially. Thus the PSF source $\propto [n_e(k)+n_v(k)]\mu_k E(t)$ generates the FWM signal only for the sequence where the field $E(\vec{k}_2)$ overlaps with the second order population $n^{(2)}(\vec{k}_2-\vec{k}_1)$, i. e., for $\Delta t > 0$. On the contrary, the Coulomb source $\propto V_{k,k'}p_k[n_e(k)+n_v(k)]$ is non-zero for both $\Delta t < 0$ and $\Delta t > 0$. Furthermore, since in the $\chi^{(3)}$-regime $n^{(2)}(\vec{k}_2-\vec{k}_1) \propto \Im m[p^{(1)}(\vec{k}_1)^* E(\vec{k}_2)]$, the rise time of S_{TI}^- is twice as fast as the decay time of S_{TI}^+. Therefore,

in the experiments of Ref. [94], the observation of S_{TI}^{-} and the value of its rise time are a direct manifestation of Coulomb mediated manybody effects.

The SBE suggest further interesting aspects of FWM. Since the PSF due to Pauli blocking is instantaneous, but the polarization needs to build up to make a significant contribution, the "Time Resolved" FWM signal (TR-FWM), measuring the "absolute time" dependence of the polarizarion $P_s(t, \Delta t)$, at fixed Δt,

$$S_{TR}(t, \Delta t) \propto |P_s(t, \Delta t)|^2 , \tag{40}$$

is expected to be highly non-exponential and is comprised of two contributions, one instantaneous, due to PSF, and one delayed due to Coulomb manybody effects. This was indeed observed, leading to novel features of coherent wave mixing not seen in atomic systems [100–102]. These effects can be significant, as shown in Fig. (12). In high quality materials at low temperature the TR-FWM signal is very substantially delayed and even appears as a pulse well separated from exciting lasers pulses. At high temperature, as the excitation density is increased, excitons are ionized, generating free carriers that screen the Coulomb interaction and, hence, modify the relative contributions of the two sources of nonlinearities. A careful study and analysis of TR-FWM experiments in $GaAs$ QWs at room temperature gave an accurate measure of the relative strength of PSF and BCI as a function of the photocarrier density [101]. In Fig. (13), the ratio of the BCI/PSF contributions is plotted versus $N_{eh}\pi a_{QW}^2$, the number of photogenerated carrier per QW-exciton area. The plot exhibits a remarkably sharp transition from a BCI dominated regime for $N_{eh} \times \pi a_{QW}^2 < 1$, to a PSF dominated one for $N_{eh} \times \pi a_{QW}^2 > 1$, quite evocative of a phase transition.

It is interesting to express the SBE in the exciton basis. Since the wavefunctions of the bound and unbound states, $\phi_\alpha(r)$, form a complete basis, any function of r and t, $f(r,t)$, can be written as:

$$f(r,t) = \sum_\alpha f_\alpha(t)\phi_\alpha(r) \quad \text{with} \quad f_\alpha(t) = \int dr f(r,t)\phi_\alpha(r) , \tag{41}$$

and the polarization is expressed as:

$$P = \sum_k \mu_k^* p_k = \sum_\alpha p_\alpha \phi_\alpha(r=0)\,. \tag{42}$$

Applying Eq. (41) to the diagonal and off-diagonal elements of the density matrix yields,

$$\begin{aligned} i\hbar \frac{\partial}{\partial t} p_\alpha \; &= \; \hbar[\Omega_\alpha - i\gamma_\alpha]p_\alpha - \phi_\alpha^*(r=0)\mu E(t) \\ &+ [n_{e;\alpha} + n_{h;\alpha}]\mu E(t) + \sum_{\beta\gamma} V_{\alpha\beta\gamma}[p_\beta(n_{e;\gamma} + n_{h;\gamma}) - p_\gamma(n_{e;\beta} + n_{h;\beta})]\,, \end{aligned} \tag{43}$$

and

$$\hbar(\frac{\partial}{\partial t} + \Gamma_{(e,h)})n_{(e,h);\alpha} = -2\Im m\left(\mu E(t)p_\alpha^* + \sum_{\beta\gamma} V_{\alpha\beta\gamma}p_\beta p_\gamma^*\right)\,, \tag{44}$$

where

$$V_{\alpha\beta\gamma} = \int dr'\, dr V(r')\phi_\alpha^*(r)\phi_\beta(r')\phi_\gamma(r-r')$$

is the *nonlocal* Coulomb coupling between excitons. If we restrict ourselves to the linear regime, Eq.(43) and (44) are similar to that of a two level atom with the substitution $\mu \rightarrow \mu\phi_\alpha^*(r=0)$. Since the polarization is obtained by multiplying the polarization amplitudes by $\phi_\alpha(r=0)$, in the early days of the study of excitons it was commonly accepted that the only effect of BCI was the excitonic enhancement of the oscillator strength, $|\mu|^2 \rightarrow |\mu|^2|\phi_\alpha(r=0)|^2$, consistent with Elliott's formula, Eq. (7). Obviously, in the nonlinear regime excitons are sensitive to both PSF and BCI. It is worth noting some aspects of the nonlocal BCI between excitons: i) it is active even when only one *e-h* pair is excited, but is distributed over several exciton states, as in the case of ultrashort pulse excitation; ii) it vanishes exactly for $\alpha = \beta = \gamma$, showing that a single exciton does not interact with itself. It is also interesting to note that the first nonlinear polarization, $P^{(3)} \propto \chi^{(3)}$, contains a PSF term $\propto |\mu|^4|\phi_\alpha(r=0)|^2$, and BCI terms $\propto |\mu|^4|\phi_\alpha(r=0)|^3$, and $\propto |\mu|^4|\phi_\alpha(r=0)|^4$, showing that the exciton internal structure does not affect the two sources of HF/RPA nonlinearity in the same way.

A useful and intuitive model can be deduced from Eq.(43) and (44). Assume that, in the case of ultrashort pulse excitation with a significant linewidth, one can replace the polarization, Eq. (42), by an "average" $\mathcal{P}$, so that the sums in Eq. (43) and (44) are written

as averaged as well. Assuming, furthermore, that excitation is low enough that one can take $n_i(k) \approx |p_k|^2$, $\mathcal{P}$ is found to satisfy the nonlinear Schrödinger equation:

$$[i\frac{\partial}{\partial t} + i\gamma - \Omega_0]\mathcal{P}(t) = -\mu \cdot \mathbf{E}(1 - \frac{|\mathcal{P}(t)|^2}{\mathcal{P}_s^2}) + \mathcal{V}\mathcal{P}(t)|\mathcal{P}(t)|^2 \tag{45}$$

where $\mathcal{P}_s$ is a saturation parameter, and $\mathcal{V}$ an effective Coulomb coupling [95,103]. We call this approximation the "effective polarization model" (EPM). $\mathcal{P}$ behaves like a harmonic oscillator driven by two source terms. These express the dual character of laser excited semiconductors. The first source term translates the "atomic" character of the optical transitions and has its origin in the Pauli Blocking saturable electron-photon coupling. The second is a Coulomb mediated self-interaction, which has the same form as that of the order parameter in the Ginzburg-Landau theory of superconductivity, and has its origin in the electron-electron manybody coupling. Eq. (45) captures the essential physics of the light/semiconductor interaction at the HF/RPA level and it was found very useful for intuitively explaining a number of experiments [95,103,101]. In the following sections, we will use the EPM and its generalization to discuss the physics behind a number of interesting observations. This is very convenient for giving an intuitive picture. However, for accurate simulation of experiments it is necessary to use the full numerical solutions of the SBE, including the actual band structure and spin selection rules of each particular sample.

VI. APPLICATIONS: SPECTROSCOPY AND DYNAMICS OF ELECTRONIC STATES IN HETEROSTRUCTURES

Modern optoelectronics makes extensive use of semiconductor heterostructures, and very often electronic and photonic devices operate in conditions of high density and high field. A generic question of this field of research is to understand and control the electronic states and their dynamics in these artificial structures. In that respect, time resolved nonlinear optical spectroscopy has proven to be a very powerful tool, much more versatile than the conventional techniques such as photoluminescence. The interpretation of many important

experiments with ultrafast dynamics requires a correct description of the interplay between PSF and BCI. This section reviews some of them.

A first example is the Quantum Beats (QB) observed in TI-FWM when the *lh*-X and *hh*-X of a QW-structure are simultaneously excited by ultrashort pulses [104–107]. As shown in Fig.(14), when the central frequency of the excitation is tuned between the two excitons, both $S_{TI}^{+}(\Delta t)$ and $S_{TI}^{-}(\Delta t)$ exhibit a strong modulation in time. The period is related to the *lh*-X/*hh*-X energy splitting, $\epsilon_{lh} - \epsilon_{hh} = \hbar\Omega_{lh-hh}$, by $T_{QB} \approx 2\pi/\Omega_{lh-hh}$. If the beat period is in agreement with an atomic-like 3 level system (3LS) model [106], the large $S_{TI}^{-}(\Delta t)$ indicates that BCI is active as well. The FWM is also found to be very sensitive to the polarization of the laser pulses. The combination of a large $S_{TI}^{-}(\Delta t)$ and polarization selectivity indicates that one must include both the Coulomb interaction and an adequate band structure for explaining the data. The polarization selection, alone, can be accounted for by phenomenological atomic-like models with six levels reproducing the near band edge spin-symmetry of Fig. (1) [108]. The correct interpretation is given by the SBE formalism with the full six spin-degenerate bands Luttinger Hamiltonian [96]. We will analyze more in detail the important question of FWM polarization selection rules in Section VII. For the moment, we satisfy ourselves with a qualitative discussion.

Using the band structure sketched in Fig. (1) we see that it is possible to build up four exciton manifolds for the transitions $hh \rightarrow e$ and $lh \rightarrow e$ excited by photons with polarization $\sigma^{\pm}$. Introducing the mixed band-spin indices $\nu = (hh, \pm), (lh, \pm)$, a straightforward generalization of the EPM is,

$$[i\frac{\partial}{\partial t} + i\gamma_\nu - \Omega_\nu]\mathcal{P}_\nu(t) = -\mu_\nu \cdot \mathbf{E}(1 - \sum_{\nu'} \frac{|\mathcal{P}_{\nu'}(t)|^2}{\mathcal{P}_{s,\nu\nu'}^2}) + \mathcal{P}_\nu(t) \sum_{\nu'} \mathcal{V}_{\nu\nu'}|\mathcal{P}_{\nu'}(t)|^2 \qquad (46)$$

where the PSF due to excitons sharing a common band is characterized by the saturation parameter $\mathcal{P}_{s,\nu\nu'}$, and the BCI coupling between two exciton species by the parameter $\mathcal{V}_{\nu\nu'}$. It turns out that at the HF/RPA level the BCI is diagonal with respect to the different bands due to the orthogonality of the different spin states in the conduction and valence bands. Thus for FWM in a linear parallel polarization configuration (with all photons $\|$-polarized),

the four exciton species are excited. They are quantum mechanically coupled by PSF, and BCI coupling is active within each spin manifold. Thus the oscillations in the FWM signal are true Quantum Beats. Conversely, in the co-circular $\sigma^{\pm}/\sigma^{\pm}$ polarization configurations, the spin polarized lh-$X^{\pm}$ and hh-$X^{\pm}$ do not share a conduction band, and they are not BCI-coupled. Thus, in these polarization configurations any beat seen in $S_{TI}(\Delta t)$ originates from a Polarization Interference (PI), unless processes beyond the SBE are active. As we will see in Section VII the coupling between lh-$X^{\pm}$ and hh-$X^{\pm}$ is, in fact, a signature of four-particle interaction processes not accounted for at the HF/RPA level. Finally, in the cross-linear case, ($\perp$-polarization configuration), we will show in Section VII that among the processes beyond the SBE, only the exciton-exciton exchange is active and thus the FWM signal is weaker, whereas for the σ^{-}/σ^{+}-polarization one does not expect to see a FWM signal at any order [109].

These investigations triggered several experiments aimed at distinguishing the QB within a single multi-level quantum mechanical system from the interference in the emission of independent two level atoms [110,111]. This latter can be considered as the simplest case of inhomogeneous broadening and, in TR-FWM experiments, the rephasing of the different emission frequencies has the same time dependence as for a Photon Echo. Therefore, the maxima of the spectrally resolved FWM signal,

$$S_{PS}(\omega, \Delta t) \propto |P_s(\omega, \Delta t)|^2 , \tag{47}$$

vary as $\mathrm{Max}[S_{TR}(t, \Delta t)] \approx 2\Delta t + 4\pi n/\Omega_{lh-hh}$. The QB, on the contrary, follow the same time dependence as free polarization decay, i. e., $\mathrm{Max}[S_{TR}(t, \Delta t)] \approx \Delta t + 2\pi n/\Omega_{lh-hh}$. This was verified in an elegant experiment [110] by comparing the TR-FWM from two QW samples. One consisted of only one type of QW and thus exhibited hh-X/lh-X QB, whereas the other sample had two types of QW electronically separated, with distinct exciton transitions, and gave only PI. A comparison of the $S_{TI}(\Delta t)$ in the two cases is shown in Fig.(15) [110], where the two slopes are easily distinguished. The different time behavior of QB and PI has its counterpart in the frequency domain [111]. The component of $S_{PS}(\omega, \Delta t)$ at a given

frequency ω_s shows oscillation as Δt is varied. By scanning ω_s across the resonances, it is found that the oscillation pattern remains unchanged for QB, but for PI it experiences a π-shift and the signal amplitude vanishes exactly at the center of the two resonances.

An important aspect of QB is related to the uncertainty principle. As for any quantum mechanical effect in a single system, the frequency shift during a QB cannot be instantaneous and must satisfy $\Delta E \times \Delta t \geq \hbar$. This was actually measured in experiments where both the amplitude and the phase of the FWM signal were determined [112–114]. Fig. (16) shows the "time-energy" picture of QB obtained under conditions where the spectral weights of the *hh*-X and *lh*-X contributions were equalized, Fig. (16a). The QB appear beautifully in the interferometric first order auto-correlation, (AC-FWM),

$$S_{AC}(\tau, \Delta t) \propto \int_{-\infty}^{+\infty} du \, |P_s(u, \Delta t) + P_s(\tau - u, \Delta t)|^2 \,, \tag{48}$$

Fig. (16b), with a 230fs beat period corresponding to the *hh*-X/*lh*-X splitting seen in the spectrally resolved FWM. The phase of the FWM signal relative to the laser, Fig. (16c), shows that the emission starts approximately in coincidence with the laser, which in this case coincides with the *lh*-X. Then, around 120fs, it experiences an abrupt π-shift when it moves suddenly to the *hh*-X, where it remains until the next beat. The π-shift does not occur instantaneously, but takes about 50fs to be completed. The QB "duration" is more precisely determined in Fig. (16d), where a set of fringes at the center of the AC-FWM is compared to a set of fringes close to the first node. One can actually count the number of fringes it takes to complete the π-shift. The frequency modulation is very fast, $\Delta E \times \Delta t = (1.4 \pm 0.1)\hbar$, yet still above the fundamental quantum limit. QB were also observed and investigated in other systems including magneto-excitons [115,116], excitons localized by interface roughness in QW-structures [117], and unbound *e-h* continua states [118].

Ultrafast nonlinear optical spectroscopy has also found useful applications in the study of electronic transport in coupled-layer heterostructures, such as resonant tunneling of electronic wave-packets in double-QW systems, and Bloch Oscillations in superlattices.

A double QW system that consists of two QW's with thickness $L_z > L_z'$, separated by

a very thin large-gap barrier layer, can sustain tunneling of e wave-packet between the two QW's when the conduction subband energy levels in the two QW's are brought in coincidence, say by application of an electrostatic field. The electronic levels of the combined QW-system are, approximately, the symmetric and antisymmetric combinations of the isolated QW-levels, and are separated by $\hbar\delta\Omega_{s,as}$. For properly chosen $L_z > L_z'$ the hole levels are not coupled and remain localized in each QW. An electronic wave-packet prepared in one QW will oscillate between the two QW's with a period $\tau_{osc} = 2\pi/\delta\Omega_{s,as}$. The electron motion can be detected by probing the interband transition between the hole localized in one QW and the combined electronic levels, because when the electron is in the same QW as the hole that transition is blocked by PSF. This program was actually performed in pump/probe and FWM experiments [119]. Fig. (17) presents the DTS spectra measured on a heterostructure that consisted of double QW within a pin-diode, the resonance condition was achieved by applying a reverse bias to the pin-diode. The DTS shows periodic oscillation with period $\tau_{osc} \approx 1.3ps$ close to the nominal value corresponding to $\hbar\delta\Omega_{s,as} = 3.2\,meV$ [119]. The amplitude of the oscillations depends on the bias voltage, translating the proximity to resonance. Clearly, these are damped, showing that the electronic wave-packet loses its coherence as it moves back and forth between the two QW's. Although the electron motion is well described by the single particle model sketched above, it is necessary to take into account BCI between electron and hole [120] to reproduce the experimental interband transition energy [121].

Since the early days of solid state physics it was argued that, because of the k-space periodicity of the energy dispersion of carriers in a crystal, an electron subject to a constant electric field, F, would perform an oscillatory motion both in r-space and in k-space [122,123]. Such dynamics, called Bloch Oscillations (BO), were never observed in bulk crystals because, to execute one BO, the electron would have to reach the edge of the Brillouin zone, thus gaining an energy on the order of the band width, i.e., a few eV, without experiencing any scattering, as the analysis of Ref. [122,123] assumed. A much more favorable situation for observing BO is provided by semiconductor superlattices (SL). Here one works with the

envelope-wavefunctions, the SL-period d, and SL-minibands rather than with the Bloch-wavefunction, the lattice period and the energy bands. This change of scale brings, among other things, the BO period, $\tau_{BO} = h/eFd$ in the ps range. In the presence of a static electric field, the absorption spectrum of SL exhibits the so called Wannier-Stark ladder (WSL) structure, [124,125]. It consists of evenly spaced transitions, $E_N = E_0 + N\Delta E$, with $N = 0, \pm 1, \pm 2, ...$, whre $\Delta E = h/\tau_{BO} = eFd$, between the SL-electronic states and a hole state that is localized owing to the large mass of the holes. Again excitonic effects strongly modify the interband transition energies and must be properly accounted for [126] . In a certain sense, the WSL structure is the frequency domain manifestation of the BO [127]. Nevertheless, the direct observation of BO in the time domain remained a challenge until ultrafast time-resolved nonlinear optical spectroscopy techniques were exploited. The idea is rather similar to that discussed in the previous paragraph. An ultrashort pulse whose spectra covers several WSL transitions would create an electronic wave-packet that would oscillate with the period τ_{BO}. This charge oscillation should be observable in a FWM experiment since it would modulate the interband polarization. A clear signature of the BO, that distinguishes them from other oscillations, such as *lh*-X/*hh*-X QB, is that their period $\tau_{BO} = h/eFd$ depends on the applied field and is, therefore, tunable. This scenario was indeed applied, using SL located in the intrinsic region of a p-i-n heterostructure [128–131]. An example of BO observed through TI-FWM is shown in Figure (18). The field dependence of the period is clearly seen. Strictly speaking, however, it is not clear that the features seen in the TI-FWM correspond directly to an oscillation of the center of mass of the electronic wave-packet, as a symmetric breathing mode of the envelope wavefunction also could modulate the TI-FWM signal as well. Recently, an elegant experiment [132] was able to actually directly measure the spatial amplitude of the electronic wave-packet. The experiment is based on the observation that as the wave-packet oscillates it creates a field that superimposes itself on the constant applied field F, thus modulating the spectrally resolved FWM whose maxima experience shifts as Δt is varied. The magnitude of the oscillating dipole, and hence the amplitude of the center of mass motion, are directly related to these shifts. The center of

mass of the wave-packet executes damped sinusoidal oscillations as shown in Fig. (19). The amplitude is macroscopic, $\approx$ 14nm for the first oscillation, and follows, quite closely, the theory [132].

VII. FUNDAMENTALS OF FOUR-PARTICLE CORRELATION EFFECTS INVOLVING REAL ELECTRON-HOLE PAIRS

So far we have been able to describe the main observations by accounting for Pauli Blocking and 2-particle correlation at the HF/RPA level. As mentioned in the introduction, coherent nonlinear optical processes involving bound biexcitons have been extensively investigated in bulk semiconductors in the nanosecond regime [8,9]. Obviously, processes involving two excitons require a description accounting for 4-particle correlations, at least. Effects associated with bound states of biexcitons are easily identified in II-VI and I-VII semiconductors, because their binding energy, $\Delta E_{X_2} = \hbar(\Omega_{X_2} - 2\Omega_X)$, is large enough that the two-photon biexciton resonances, $2\omega \approx \Omega_{X_2}$, are well separated from the one-photon exciton resonances, $\omega \approx \Omega_X$. In III-V materials, biexcitons have a very small binding energy $\Delta E_{X_2} < 1meV$, and were not expected to play an important role in nonlinear optics. In quantum confined structures, although $\Delta E_{X_2} \approx 1 - 3meV$ is enhanced [133], it remains of the order of the exciton linewidth in these inhomogenously broadened systems. Thus it came rather as a surprise when oscillations at a frequency different from the *lh*-X/*hh*-X splitting were observed in *GaAs/AlGaAs* QW structures through pump/probe [134] and FWM [135] experiments. An example of the exciton/biexciton oscillations seen in pump/probe experiments [134] is shown in Fig. (20). The origin of these new features was correctly identified as due to the bound biexciton contribution, which appears in coherent processes because a two-photon transition (one σ^- from the probe and one σ^+ from the pump) directly connects the ground state to a X_2-state, no matter what the inhomogeneous broadening is. Phenomenological 5-level models including the ground state $|g>$, the two $X^{\pm}$ excitons, a bound biexciton and unbound exciton pairs, and accounting for inhomogeneous broaden-

ing, were proposed to interpret the data [136]. More systematic studies [137–139] using 3-pulse FWM in a number of polarization configurations were able to separate the quantum beats between *lh*-$X^{\pm}$ and *hh*-$X^{\pm}$ from those between these excitons and their bound $(lh\text{-}X^{\pm})_2$ and $(hh\text{-}X^{\pm})_2$ states. Again, the FWM signals measured in these experiments have a very clear polarization selectivity: strong FWM signal for $\|$-polarization, weak signal for $\perp$-polarization and co-circular $\sigma^{\pm}/\sigma^{\pm}$-polarization and almost vanishing signal for counter-circular $\sigma^{\pm}/\sigma^{\mp}$-polarization [137,139,140]. Interestingly it was found that the phase of the *lh*-$X^{\pm}$-*hh*-$X^{\pm}$ quantum beats seen in $\perp$-polarization configuration exhibit a clear π-shift as compared to those seen in $\|$-polarization. Describing qualitatively the overall line shapes of these experiments required the extension of the phenomenological models to ten levels!

The correct interpretation of these experiments requires formalisms able to handle n-particle correlations, including many obviously important mechanisms such as screening, which are not described by the HF/RPA of the SBE [16,141–151]. In the continuum of almost free *e-h* pairs, one could use non-equilibrium Green's functions and a second Born approximation with a satisfactory accuracy. However, in the domain of highly correlated *e-h* pairs, the Coulomb interaction must be accounted for consistently to arbitrary order. Several theoretical approaches have been proposed for achieving this goal. The first one was developed in the context of molecular systems and, because of this, has received little attention from the "semiconductor community", although it is absolutely general [141–145]. A formalism that naturally extends the density matrix approach of the SBE and is able to account for high order correlation is called the Dynamic Controlled Truncation Scheme (DCTS) [146]. Other formalisms that proceed through diagrammatic techniques [148], or through the development of correlation functions in the basis of n-exciton eigenstates, have been proposed recently [149]. We will base our discussion on the DCTS because it allows us to maintain the continuity with the previous sections.

The DCTS consists of: i) writing the Heisenberg equations of motion for all relevant products of operators, ii) applying the fundamental Fermion anticommutation rules, and iii) taking the expectation values. This results in an infinite hierarchy of equations of mo-

tion coupling the n-particle and the $(n+m)$-particle correlation functions. The consistent truncation scheme is based on the fact that in nonlinear optics one is usually interested in a development in powers of the interaction Hamiltonian, Eq. (23), so that the electric field $E(t)$ is the natural expansion parameter. When one wishes to describe the effects up to $E(t)^n$, the system of coupled equations is truncated at this power and the terms $O\left(E(t)^{n'>n}\right)$ are neglected. This results in a closed system of equations that, in principle, can be solved exactly.

The 4-particle correlation functions that appear in the development of the kinetic equations beyond the 2-particle correlation functions, Eq. (24), have the form [146],

$$\mathrm{N}^{\mathrm{e-e}} = \langle \hat{e}_1^\dagger \hat{e}_2^\dagger \hat{e}_3 \hat{e}_4 \rangle \qquad \mathrm{N}^{\mathrm{h-h}} = \langle \hat{h}_1^\dagger \hat{h}_2^\dagger \hat{h}_3 \hat{h}_4 \rangle \qquad \text{and} \qquad \mathrm{N}^{\mathrm{X}} = \langle \hat{e}_1^\dagger \hat{h}_2^\dagger \hat{h}_3 \hat{e}_4 \rangle \tag{49}$$

or

$$\mathrm{P}^{\mathrm{e_3h_4}}_{(\mathrm{e_1e_2})} = \langle \hat{e}_1^\dagger \hat{e}_2 \hat{e}_3 \hat{h}_4 \rangle \qquad \mathrm{P}^{\mathrm{e_3h_4}}_{(\mathrm{h_1h_2})} = \langle \hat{h}_1^\dagger \hat{h}_2 \hat{e}_3 \hat{h}_4 \rangle \qquad \text{and} \qquad \mathrm{B}^{\mathrm{h_1e_2h_3e_4}} = \langle \hat{h}_1 \hat{e}_2 \hat{h}_3 \hat{e}_4 \rangle \,, \tag{50}$$

and similar ones obtained by permutation of the indices or Hermitian conjugation of the e and h operators. Here, to simplify the notation, we have lumped all the quantum numbers that distinguish particles in a single index. The 4-particle correlation functions represent coherent processes with a very intuitive interpretation. Those appearing in Eq. (49) can be interpreted respectively as: an e-density/density correlation, an h-density/density correlation and an X-occupation, whereas those in Eq. (50) represent an e-screened 1pair-emission, an h-screened 1pair-emission and a 2pair-emission. It is worth noting that they correspond to coherent processes, in contrast to the products of 2-particle correlation functions that are deduced from them by applying a RPA and thus destroying the phase relation between the terms of the products. For example, the 4-operator product appearing in $\mathrm{P}^{\mathrm{e_3h_4}}_{(\mathrm{e_1e_2})}$, $\hat{e}_1^\dagger \hat{e}_2 \hat{e}_3 \hat{h}_4$, represents the single process in which an e-h pair (e_3, h_4) and an electron (e_2) are destroyed while an electron (e_1) is created. Hence, our interpretation of $\mathrm{P}^{\mathrm{e_3h_4}}_{(\mathrm{e_1e_2})}$ as a e-screened 1pair-emission, i. e., (e_3, h_4)-recombination acompanied by the $e_2 \rightarrow e_1$ scattering. The intuitive picture carried by Eq. (49) and (50) relates nicely to mechanisms that are usually considered

in a more heuristic description of light/matter interaction; the DCTS formalism, however, is completely consistent.

It is clear that, as the order of the development increases, the number of correlation functions to consider becomes quickly unmanageable. It turns out, however, that it is possible to develop a systematic procedure for identifying all those that contribute at a given order [147]. In the limit of third order processes, $\chi^{(3)}$-truncation, a number of factorization-summation relations valid $O\left(E(t)^{n>3}\right)$ can be demonstrated. They take forms like: $(\mathrm{P}^{\mathrm{h_3h_4}}_{(\mathrm{e_1h_2})})^* = \langle \hat{e}_1^\dagger \hat{h}_2^\dagger \hat{h}_3^\dagger \hat{h}_4 \rangle = \sum_{e_j} \langle \hat{e}_1^\dagger \hat{h}_2^\dagger \hat{h}_3^\dagger \hat{e}_j \rangle \times \langle \hat{e}_j \hat{h}_4 \rangle + O\left(E(t)^5\right)$, showing that many coherent 4-particle processes can be expressed in terms of only two types of correlation functions: the 1pair-transition, $\mathrm{P^{eh}} = \langle \hat{e}\hat{h} \rangle$, the 2pair-transition, $\mathrm{B^{heh'e'}}$, and their complex conjugates [151]. A physically meaningful expression for the exciton-exciton correlation function $\mathrm{B^{heh'e'}}$ appears naturally when operator products that have already been factorized in the SBE approximation are subtracted from the bare 4-particle correlation function (with proper sign changes due to Fermi operator commutation rules). Then $\mathrm{B^{heh'e'}}$ takes the following form: $\mathrm{B^{ehe'h'}} = \langle \hat{e}\hat{h}\hat{e}'\hat{h}' \rangle - \langle \hat{e}\hat{h} \rangle \langle \hat{e}'\hat{h}' \rangle + \langle \hat{e}\hat{h}' \rangle \langle \hat{e}'\hat{h} \rangle$ [151], and has an straightforward interpretation. It characterizes the deviation from the HF/RPA meanfield theory. This underlying physics make the coupled equations of motion of $\mathrm{P^{eh}}$ and $\mathrm{B^{heh'e'}}$ much more transparent since they can be written in such a way that the first term in $\partial \mathrm{P^{eh}}/\partial t|_{coh}$ exactly reproduces the SBE. This procedure shows that the DCTS includes, of course, the HF/RPA meanfield formalism [151], furthermore, it is very useful in practice, since it identifies the processes that are, or are not included in the SBE.

Discussing the details of the theory is beyond the scope of this chapter. Therefore, to get an insight into the mechanisms relevant for the experiments mentioned in the previous paragraph, we will use a generalization of the EPM, Eq. (45) and (46), which, as we have seen, gives a good intuitive picture of the physics. The model proceeds along the same lines as EPM. If we consider only the $hh \rightarrow e$ transition, we have to account for the two spin manifolds and introduce two effective polarizations, $\mathcal{P}^{\pm}$, respectively associated with the absorption of $\sigma^{\pm}$ photons, and, in addition, an "effective 4-particle correlation function" $\mathcal{B}$,

which represents a two-photon (one σ^+ and one σ^-) bound biexciton transition. With these ingredients one can derive from the full kinetic equations the coupled system;

$$[i\frac{\partial}{\partial t} + i\gamma - \Omega_X]\mathcal{P}^{\pm}(t) = -\mu \cdot \mathbf{E}(1 - \frac{|\mathcal{P}^{\pm}(t)|^2}{\mathcal{P}_s^2}) + \mathcal{V}\mathcal{P}^{\pm}(t)\,|\mathcal{P}^{\pm}(t)|^2 \tag{51}$$
$$+\mathcal{V}_{XX}^{exch}\mathcal{P}^{\pm}(t)\,|\mathcal{P}^{\pm}(t)|^2 - \mathcal{V}_{XX}^{Screen}\,\mathcal{P}^{\pm}(t)[\,|\mathcal{P}^{\pm}(t)|^2 + |\mathcal{P}^{\mp}(t)|^2]$$
$$+\mathcal{V}_{XX_2}\mathcal{B}(t)\mathcal{P}^{\pm}(t)^*$$

and

$$[i\frac{\partial}{\partial t} + i\Gamma - \Omega_{X_2}]\mathcal{B}(t) = \mathcal{P}(t)^-\,\mathcal{P}(t)^+\,. \tag{52}$$

In Eq. (51), $\mathcal{V}$ is the effective BCI coupling and, therefore, the first line reproduces the SBE-approximation Eq. (45). All the other terms in Eq. (51) and (52) originate from correlation effects beyond HF/RPA; $\mathcal{V}_{XX}^{Screen}$ is the effective parameter describing excitonic screening, $\mathcal{V}_{XX}^{exch}$ is the corresponding exchange term and $\mathcal{V}_{XX_2}$ accounts for the exciton-biexciton interaction. It is worth noting that the excitonic screening couples the two exciton spin-manifolds and explains the coupling between $\mathcal{P}(t)^-$ and $\mathcal{P}(t)^+$, whereas the excitonic exchange term has the same form as the BCI and can be lumped with it. The effective 4-particle correlation function, $\mathcal{B}(t)$, is driven by a product of two effective polarizations, $\mathcal{P}(t)^- \times \mathcal{P}(t)^+$. The model readily explains how processes not included in the SBE affect FWM experiments and govern their polarization selectivity [150,151]. In the $\chi^{(3)}$ limit, i. e., $O\,(E(t)^5)$ solution, the polarizations in the RHS of Eq. (51) and (52) are the linear polarizations $\mathcal{P}^{(1)\pm}(t) \propto E(t)$. In the configuration $\sigma^{\pm}/\sigma^{\pm}$, either $\mathcal{P}(t)^-$ or $\mathcal{P}(t)^+$ is zero, the RHS of Eq. (52) vanishes and bound biexcitons are not created. All the other terms contribute at the same level and Eq. (51) has the same form as the SBE approximation, Eq. (45). In the $\|$-polarization configuration the RHS of both Eq. (51) and (52) are nonzero; therefore bound biexcitons are created. The oscillations at frequency $2\Omega_X - \Omega_{X_2}$ arise naturally, $\mathcal{P}(t)^-$ is coupled to $\mathcal{P}(t)^+$ through $\mathcal{V}_{XX}^{Screen}$ and the FWM signal is large. Finally, in the $\perp$-polarization configuration the coefficient of $\mathcal{V}_{XX}^{Screen}$ vanishes and the exciton-biexciton interaction contribution is dominant, but the signal is weaker.

Other, apparently simple processes, also imply correlation beyond more than two particles. This is the case, for example, for the dephasing induced by the presence of other charged carriers or other excitons. In Section V, we mentioned that early FWM experiments, where e, h or X populations were intentionally photogenerated, were satisfactorily described by using empirical density-dependent scattering rates, $\gamma = \gamma_0 + \gamma_i n_i$, with $i = e, h, \text{or} X$ in analogy with the concept of collisional broadening of atomic physics [12,13,91]. It is easy to convince one's self that such density dependent scattering rates imply processes beyond the third order. As mentioned in Section III, when introducing a density broadening parameter in the kinetic equations, Eq. (13) and (14), terms of the form $\gamma_e n_{e,h} \times p_k$, appear, and since $n_e \approx n_h \approx |p_k|^2 + |p_k|^4 + O(E^5)$ and $p_k = O(E)$ they contain contributions $O(E^5)$.

Recently, the effects of collisional broadening have been re-examined carefully, their consequences on the FWM emission were clarified and they were baptized "excitation induced dephasing" (EID) [152,153]. It was found that even at low excitation densities, the exciton resonances experience a significant broadening. This is shown in Fig. (21), where the pump/probe DTS, measured near the X-resonances of a $0.2\mu m$ $GaAs$ sample kept at low temperature, is presented. In that experiment the pump generated $N_X^{Coh} \approx 3 \times 10^{15} cm^{-3}$ excitons. The DTS is very well interpreted as the difference between Lorentzian resonances with the same strength, but slightly different widths. FWM experiments, using a pre-pulse to introduce a controlled amount of excitons, N_X^{Incoh}, long enough before the arrival of pump and probe pluses on the sample to be incoherent with the excitons involved in the FWM, confirmed the earlier results. Moreover they have shown that, as $N_X^{Incoh} \approx 6 \times 10^{14} cm^{-3} \rightarrow 5 \times 10^{15} cm^{-3}$, the FWM efficiency was reduced by a factor ≈ 6, while the ratio $S_{FWM}^{\parallel}/S_{FWM}^{\perp}$ varied from $10 \rightarrow 5$. All these changes were found to be independent of the spin of the incoherent excitons created by the pre-pulses. Obviously the Coulomb coupling between the two sub-systems of excitons is responsible for the observations.

Since screening in its various forms is not included in the SBE, a description of EID requires using formalisms such as the DCTS. In fact, up to $O\left(E(t)^5\right)$, the discussion of

the previous paragraphs gives a pretty good idea of the mechanisms involved. The exciton screening, i. e. the term $\propto \mathcal{V}_{XX}^{Screen}$, introduces the channel that couples the X^+ and X^- populations, and the ratio $S_{FWM}^{\parallel}/S_{FWM}^{\perp} \gg 1$ follows from Eq. (51). At the $O\left(E(t)^3\right)$ level, exciton screening does not affect the dephasing, and one has to look for an explanation beyond that order. A full and consistent theory of wave mixing experiments, including a correct description of screening, is such a formidable task that it has not yet been attempted.

In the experiments of Ref. [152,153], because the two exciton populations are completely incoherent and the densities are rather small, it is possible to use a less general scheme to explain the main trends [154]. An effect of screening by the incoherent excitons is to renormalize the transition energies between the conduction and valence bands, Eq. (28). In the conditions considered here, the self-energies, $\Sigma_{c,v}$, can be estimated within the second Born approximation, in which all terms up to $O\left(E(t)^2\right)$ are included in the screened potential [85]. The real and imaginary part of $\Sigma_{c,v}$ describe respectively a shift and a broadening of the single particle levels. The exciton energy is very robust, however, because of the cancellation between band shift and binding energy, (see Section V), and only the broadening remains. By developing the corresponding parameter to the first order in the density, $\gamma = \gamma_0 + \gamma_X(N_X^{Incoh} + N_X^{Coh})$, the heuristic approach of Ref. [12,13,91] is recovered and justified [154]. In the context of the experiments of Ref. [152,153], this introduces in the SBE the desired X^+ and X^- coupling, as in the DCTS, and accounts for the observed broadening of the exciton resonances. In a certain sense, EID provides new source terms for the nonlinear polarization whose effects appear in many nonlinear optical processes. This is indeed the case, and the coherent transients associated with the EID due to exciton-continuum scattering have been observed in $GaAs$ by 15fs short pulse FWM experiments that excite the resonances as well as e-h pairs in the continuum [155].

It was expected that the bound biexciton states would make a noticeable contribution in processes where two-photon transitions are active, and it was rather implicit that the continuum of unbound exciton-pairs would play a minor role. Surprisingly, this is not the case. Recently, it was found that correlations in the continuum of X-X scattering states can

have important, and even dominant, effects in regimes of distorted excitons at low density, [156–158]. A magnetic field $\vec{B} \parallel \vec{z}$, applied to a semiconductor, confines electrons and holes in the $(\vec{x},\vec{y})$-plane, inducing a 3D to 1D transition for the density of states, and strongly modifying the internal structure of the excitons. They experience a shrinkage, $\propto \sqrt{(|B|)}$, in the $(\vec{x},\vec{y})$-plane and $\propto \mathrm{Ln}(|B|) \parallel \vec{z}$. The magnetic confinement is expected to have significant effects at fields $|B| \gg B_c$ where B_c is the field strength at which the cyclotron radius equals a_0, the (B=0)-excitonic Bohr radius [159–161]. For semiconductors, that regime can easily be explored, for example in $GaAs$ $B_c \approx 3.4$T, with the further practical advantage of an adjustable confinement while studying the same volume in a single sample. This continuous tuning of the manybody interactions governing the nonlinear optical response provides a perfect laboratory for studying manybody interaction processes. Fig. (22) shows the experimental TI-FWM for different magnetic field strengths up to $B = 10T \approx 3B_c$, in an optically thin ($0.25\mu m$), high quality $GaAs$ layer, with homogeneously broadened lh-X and hh-X excitons ($\gamma \approx 0.4$meV), which are visible because of mechanical strain [162]. The measurement was performed with co-circular polarization σ^-/σ^- to minimize the effect of bound biexcitons. The signal at $B = 0T$ shows an exponential decay superimposed on oscillations for $\Delta t > 0$, with a dephasing time $T_2 \approx 1.5ps$ and oscillation period corresponding to the lh-X/hh-X splitting. For $\Delta t < 0$, the signal is much smaller and its rise time is $\sim$ 300fs. As B is increased, the $\Delta t > 0$ signal, S^+_{TI}, changes only slightly, whereas the $\Delta t < 0$ signal, S^-_{TI}, changes drastically. Its magnitude increases significantly relative to S^+_{TI}, and above $B \approx B_c$ the rise time lengthens to 3ps while the profile becomes highly non-exponential with an unususal positive curvature. As the density is lowered to $N \approx 5 \times 10^{14} cm^{-3}$, i. e., at an average exciton-exciton separation as large as $d \approx 10a_0$, S^-_{TI} can be seen as far as $\Delta t \approx -10ps$, i. e., 100 times the pulse duration! Furthermore, it was confirmed that the oscillations are quantum beats and not polarization interference, by inspection of the slope of the peak of the TR-FWM vs. Δt [110] and, more importantly, because it was found in the spectrally resolved FWM signal $S_{PS}(\omega, \Delta t)$ that the lh-X and the hh-X significantly exchange oscillator strength as Δt is varied. In fact, that exchange can be so strong that

$S_{PS}(\omega, \Delta t)$ could be completely dominated by the *lh*. This is in contradiction to the SBE, which predict a *lh*-X contribution about an order of magnitude smaller than that of the *hh*-X, and constant relative contributions of the *lh*-X and *hh*-X to the signal. Again, these observations require accounting for 4-particle correlations to be explained.

Before showing the result of full numerical simulation of the experiment within the DCTS formalism, let us again use the extension of the EPM to gain an intuitive insight into the physics. In general, $\mathcal{B}$ encompasses both bound biexcitonic states and unbound biexciton states. In the σ^-/σ^- configuration, the former are not active and only the X-X scattering states need to be considered. In that case, it is easily found that $\mathcal{P}$ and $\mathcal{B}$ obey the coupled equation system,

$$[i\frac{\partial}{\partial t} + i\gamma - \Omega_X]\mathcal{P}(t) = -\mu \cdot \mathbf{E}(1 - \frac{|\mathcal{P}(t)|^2}{\mathcal{P}_s^2}) + \mathcal{V}_{eff}\mathcal{P}(t)|\mathcal{P}(t)|^2 + \mathcal{V}_{XX_2}\mathcal{B}(t)\mathcal{P}(t)^* \qquad (53)$$

and

$$[i\frac{\partial}{\partial t} + i\Gamma - 2\Omega_X]\mathcal{B}(t) = \mathcal{P}(t)^2 \qquad (54)$$

where now, $\mathcal{B}$ accounts only for the X-X scattering states, which are modeled as a single resonance at $2\Omega_X$, and $\mathcal{V}_{eff}$ lumps all the exciton-exciton interactions active in the σ^-/σ^- configuration. One recognizes the EMP model of the SBE, Eq. (45), in the left hand side and first two terms of the RHS of Eq. (53). Eq. (54) can be formally integrated and put in Eq. (53), giving a third source term

$$\propto \mathcal{P}(t)^* \int_{-\infty}^{t} dt' \mathcal{P}(t')^2 e^{-(i2\Omega_X + \Gamma)(t-t')},$$

due to exciton-exciton correlation (XXC). This new term is obviously of the same order as the PB and BCI contributions; however, it has a completely different, non-Markovian, time dependence , i. e., it grows first as the integral of the square of the polarization before exhibiting an exponential decay. The origin of that "coherent" memory is easy to interpret. Clearly, for a third order signal in the direction $2\vec{k}_2 - \vec{k}_1$, $\mathcal{P}(t)^*$ is generated by $E(\vec{k}_1)$, whereas the integral over $\mathcal{P}(t')^2$ comes from $E(\vec{k}_2)$. Therefore, when the $\vec{k}_2$-pulse arrives

first, at $\Delta t < 0$ it generates a 4-particle correlation $\propto \mathcal{P}(t')^2$ which, because it corresponds to a two-photon transition, cannot emit light and builds up as $\int_{\Delta t}^{t} dt' ...$, until the $\vec{k}_1$-pulse arrives and triggers the emission of the FWM signal. The TI-FWM response of Eq. (53) and (54) can be easily calculated. An example is shown in Fig. (23) for values of the parameters chosen to reproduce the experiment of Ref. [156], and displaying the separate contributions arising from the PB, BCI, and XXC. Of course, only the general features are reproduced by this simple model and many details, such as the *lh*-X/*hh*-X beats, are not included. Nevertheless, one sees that the large S_{TI}^{-} is reproduced and that it has the long duration and non-exponential profile with the positive curvature for small $\Delta t < 0$ that is observed experimentally.

The results of the full numerical calculation of the coupled equations of motion of P^{eh} and $\mathrm{B}^{\mathrm{ehe'h'}}$, including the correct band structure and the magnetic field, are shown in Fig. (24) [158]. The solid curve is the TI-FWM, which shows the slow rise time of S_{TI}^{-}. There are strong beats in the theoretical S_{TI}^{-} which are not seen as clearly in the experimental data. Their attenuation in the experiment is most likely due to exciton-density correlations which contribute beyond the coherent limit. The dashed curve is the result of the calculation without XXC. Here we see that the signal without XXC has a much faster rise time for $\Delta t < 0$. Furthermore, the XXC contribution completely dominates the FWM; for $\Delta t < 0$ the signal without XXC is three orders of magnitude smaller than the signal with XXC, and even for $\Delta t > 0$ it is still an order of magnitude smaller. The theoretical spectrally resolved FWM signal calculated for different Δt recovers the enhancement of the *lh*-X signal and the exchange of oscillator strength between the *lh*-X and *hh*-X with Δt. These quantum beats, not predicted by the HF/RPA, are due to the strong coupling between the *lh*-X and the *hh*-X in the 4-particle correlation functions, due to the distorsion of their relative-motion wavefunction and to their large mass difference. Looking for an intuitive explanation for the enhancement of the XXC by the magnetic field, it is worth noting that the 4-particle correlation function $\mathrm{B}^{\mathrm{ehe'h'}}$, which includes all the X-X interactions, contains the X-X multipole interaction in the long-wavelength limit (very low density). Clearly, in high magnetic fields

excitons are squeezed in the $(\vec{x},\vec{y})$-plane and develop large quadrupole moments that allow them to interact via a long range quadrupole-quadrupole interaction.

At this point it is useful to comment on the reason why the exciton-exciton correlation function $B^{ehe'h'}$ naturally appears in the description of effects that are beyond the HF/RPA level of the SBE. As mentioned in Sections IV and V, at that level of approximation one obtains a mean field theory where the order parameters are the pair amplitude, P^{eh}, and the electron and hole occupation numbers, n_e and n_h. It is thus natural that the effects not included in that theory involve the exciton-exciton correlation function: $B^{ehe'h'} = \langle\hat{e}\hat{h}\hat{e}'\hat{h}'\rangle - \langle\hat{e}\hat{h}\rangle\langle\hat{e}'\hat{h}'\rangle - \langle\hat{e}\hat{h}'\rangle\langle\hat{e}'\hat{h}\rangle$, since it measures the difference between the bare 4-particle correlation function, $\langle\hat{e}\hat{h}\hat{e}'\hat{h}'\rangle$, and the two products of two-particle correlation functions, $\langle\hat{e}\hat{h}\rangle\langle\hat{e}'\hat{h}'\rangle$ and $\langle\hat{e}\hat{h}'\rangle\langle\hat{e}'\hat{h}\rangle$, derived from it in the HF/RPA factorization. In the experiments described above, the time delays that are probed are short compared to the mean free time for X-X scattering. Thus, not enough scattering events happen over the time span of one experiment for each X to interact with a substantial fraction of its neighbors, i.e., for the HF/RPA mean-field conditions to be established. These experiments, therefore, access the new regime where the fluctuations in X-X scattering induce large fluctuations of the HF/RPA mean-field order parameters. We will come back on the generality of that comment in our conclusion.

This is not the end of the story. Nonlinear optical effects are extremely sensitive to the interactions between elementary excitations. They provide direct information on processes that are inaccessible to other spectroscopic techniques. Therefore, it is most likely that investigations of high order manybody effects through nonlinear optical spectroscopy are going to be an important direction of research in condensed matter physics. Already in the experiments described above there are indications that mechanisms beyond $\chi^{(3)}$ are active [156], and recently there have been reports of unambiguous observation of $\chi^{(5)}$ and $\chi^{(7)}$ processes [163]. Although the general framework for describing these effects exists in principle, the detailed theory is far from being developed, and one can anticipate surprises.

VIII. DYNAMICS IN THE QUANTUM KINETICS REGIME

We have seen in Section III that the most non-classical dynamics regime occurs at very early times after *e-h* pairs are created. The time scale of that regime is determined by the period of the elementary excitations, plasmons and phonons for semiconductors. Therefore, in the first few tens of femtoseconds after excitation, one expects to see new features in the nonlinear optical response of these materials. These can be used for investigating this poorly understood thermodynamic regime. This is the topic of this section; we shall discuss in turn the effects of carrier-carrier scattering and those of carrier-phonon scattering.

Evidence for non-Markovian behavior was found in experiments where both the amplitude and the phase of FWM signal were measured [112–114]. Through a combination of interferometric, time resolved, and frequency resolved measurements, a "time-energy" picture of the process was developed. An example of such a study is shown in Fig. (25). The *GaAs* QW sample is weakly excited, $N \approx 3 \times 10^9 cm^{-2}$, just below the *hh*-X resonance. The left curve gives the logarithm of $S_{TI}(\Delta t)$; the arrows mark the Δt at which the spectrally resolved signal, $S_{PS}(\omega, \Delta t)$ shown in the central panel and $\Delta\Phi(t)$, the phase (relative to that of the reference laser) shown in the right panels, were obtained. For comparison the laser spectrum is despicted as a dotted line in the $\Delta t = 0$ graph of $S_{PS}(\omega, \Delta t)$. For $\Delta t = -80$fs, the emission spectrum is essentially at the *hh*-X, and $\Delta\Phi(t)$ shows an almost linear slope corresponding to a constant emission frequency, $\Delta\Phi(t) = (\omega - \omega_\ell)t = 0$. For $\Delta t = 0$, $S_{TI}(\Delta t)$ has an asymmetric profile with a low energy tail extending well into the laser spectrum, indicating that the instantaneous frequency of the emission is chirped. Correspondingly, $\Delta\Phi(t)$ exhibits a linear part first, but after about 250fs the slope changes and after 350fs it flattens. At $\Delta t = 160$fs, $S_{PS}(\omega, \Delta t)$ has two separate contributions, one close to the *hh*-X and the other approximately following the laser spectrum. $\Delta\Phi(t)$ takes a more pronounced S-shape, indicating that the emission is first centered at the laser, $\omega \approx \omega_\ell$, then shifts at the hh-X, $\omega \approx \Omega_{hh}$, and then moves back again to the laser, $\omega \approx \omega_\ell$.

The experiments were modeled by a SBE theory, with screening treated in the static

single plasmon pole approximation and with dephasing accounted for by a constant rate. The calculated $S_{TI}(\Delta t)$ (dashed curves) are unable to account for the lineshape. A "frequency dependent" rate, $\Gamma(\omega)$, would give better agreement and would correspond to a memory kernel, $\Gamma(t-t')$ as seen in Section III. The phase dynamic within one ultrashort pulse is governed by events occurring within a few optical cycles; during such short times the elementary excitations only experience a few "collisions", thus the phase cannot randomize and memory effects become apparent. Although the discrepancies between experiments and the SBE theory were traced back to the approximations used, the exact origin of the mechanisms at work in $\partial p_k/\partial t|_{scatt}$ were not precisely identified in Ref. [114].

More recently, experiments have been specifically designed to investigate the non-Markovian regime, and theoretical simulations have been developed to interpret them. In the work of Ref. [164], the authors argued that, since the Liouville Eq. (26) relates $\hat{n}$ and $\partial\hat{n}/\partial t$, the simultaneous determination of both the DTS $(\Delta T/T)$, and its derivative with respect to Δt, $\delta(\text{DTS}) = \partial(\Delta T/T)/\partial\Delta t$ vs. ω, and Δt would put very strict restrictions on any theory invoked to explain the data [164]. Their experiments were performed on $GaAs$ using a pump/probe technique, with independently adjustable pump and probe durations $30 \rightarrow 100$fs. In experiments with rather long, ($\geq$ 70fs) pulses and moderate density, the DTS exhibits a spectral hole slightly red-shifted relative to the pump spectrum, in agreement with previous reports, see Fig. (9) and (10) [81,86]. When pulses much shorter than the natural time scales, T_{LO} and T_{pl}, are used, no spectral hole is seen in the DTS, which is featureless and extends from below the pump central frequency all the way to the exciton edge. More importantly, for very short Δt smaller than the pump duration, the δ(DTS) shows a uniform positive growth shifted toward the exciton, that reverses and changes sign immediately at the end of the pump pulse, Fig. (26a) [164]. This is indicative of generation in the medium, during the pump pulse, of a polarization out of phase with the probe field, over a broad range of energy below the pump, and of a sudden change in phase when the pump pulse ends.

Interpretation of the experiments were attempted by calculating the DTS and δ(DTS)

using a four-band version of the SBE within the Boltzmann Kinetics relaxation time approximation. The first attempts, consistent with Boltzmann Kinetics, considered only dephasing and assumed no population relaxation. It was possible to qualitatively reproduce the DTS lineshape with a value $T_2 \approx 200$fs that agrees with the time scale seen experimentally. The calculated δ(DTS), however, presents qualitative discrepancies with experiments, Fig. (26b). It can reproduce neither the shift towards the band-edge during carrier generation, nor the negative δ(DTS) seen close to the laser center frequency immediately after the pump pulse is over Fig. (26a). By including a population relaxation towards a Maxwell-Boltzmann distribution with the same instantaneous number of carriers and total energy as that generated by the pump pulse, it was possible to get better agreement with the experiments, see Fig. (26c). However, this occurs only for unphysical population relaxation times much shorter than the dephasing time, $\tilde{T}_1 \sim 36\text{fs} \ll T_2$ and, furthermore, too short to be compatible with theories based on Boltzmann Kinetics [48,49]. Any attempts to salvage Boltzmann Kinetics by using more complicated models for dephasing, such as EID, [154] failed to remove the unphysical results: i) $T_2 \gg \tilde{T}_1$, and ii) $\tilde{T}_1 \ll 2\pi/\Omega_{LO}$ and $\ll 2\pi/\Omega_{pl}$. The features observed are, however, consistent with Quantum Kinetics theories, see Fig. (6). In the experiments of Ref. [164], both electrons and holes are generated, thus complicating the interpretation.

An elegant technique allowing one to follow the evolution of the electrons alone was implemented in Ref. [165]. In these pump/probe experiments, the $\approx$ 130fs pump excites the $hh \rightarrow e$ and $lh \rightarrow e$ transition, but the $\approx$ 30fs probe was tuned to the spin-orbit split-off transition. In the case of $GaAs$, the spin-orbit splitting is large enough, $\approx 340meV$, that no holes are excited by the pump at that transition, and the probe measures only the effects of the electrons. Although very small spectral holes are seen in the DTS at the $hh \rightarrow e$ and $lh \rightarrow e$ thresholds for very early time delay, in that case, again, the DTS is immediately very broad and becomes featureless even before the end of the pump pulse [165]. The DTS line shape and its evolution vs Δt are very similar to those reported in Ref. [164]. They were calculated from the SBE with Coulomb Quantum Kinetic scattering terms of the type of Eq.(20). The agreement with the experiment is remarkable; most of the features observed experimentally

are qualitatively reproduced, including the overall lineshape and the disappearance of the spectral holes for $\Delta t \geq 80$fs. As mentioned in Section III, because the excitation spectrum of a plasma is gapless, carrier-carrier scattering tends to produce broad and featureless distributions. Furthermore, the experiments and theories discussed above show that in the Quantum Kinetics regime, carrier-carrier interactions almost instantaneously scatter the carriers out of the energy window in which they were created, resulting in a distribution much broader than that of the pulse that generates them, and even broader than that predicted by Boltzmann Kinetics [41,42,44–46].

The other scattering processes that can produce memory effects are due to the carrier-phonon interaction. We have seen that in polar semiconductors this interaction is dominated by LO-phonon scattering, which has a well defined and single frequency and form a "single mode reservoir" as mentioned in Section III. Very strong coupling of the exciton to LO-phonons was observed in II-VI nanocrystals [166–168]. In these systems, however, the electronic excitations form discrete levels because of quantum confinement in all directions and the interaction with vibrations can be analyzed as for molecules [167,168]. For structures of higher dimensionality, the electronic levels form bands and LO-phonon scattering results in intraband transitions normally associated with irreversible processes and dissipation.

Non-Markovian effects due to LO-phonon intraband transitions were observed recently in FWM experiments, where bulk $GaAs$ is resonantly excited by $\approx$ 14fs pulses, much shorter than the LO-phonon period. As shown in Fig. (27), the TI-FWM signal, $S_{TI}(\Delta t)$, presents a strong oscillatory modulation superimposed on the usual exponential decay. The period, $\approx$ 98fs, corresponds to the separation between two conduction band states coupled by one LO-phonon, i. e., $(1 + m_e/m_h)\Omega_{LO}$ [169,170]. The amplitude of the oscillations decreases when the excitation density increases. Surprisingly, these features are not reflected in the spectrally resolved signal, $S_{PS}(\omega, \Delta t)$, which at each Δt consists of a single line without phonon sidebands [169,170]. This implies that the electrons excited by the first pulse interact with the LO-phonons, which in turn affect, at a later time, electrons involved in the transitions of the second pulse, i. e., the kind of memory of the electron sub-system

interacting with the LO-phonon thermal bath that we discussed in Section III. An analysis based on a SBE description of the FWM, but with a $\partial p_k/\partial t|_{scatt}$ described by Quantum Kinetics scattering integrals for the interaction for the electron and phonon sub-systems [171,172], equivalent to that of Ref. [39], see Eq. (17), was able to explain quite nicely the data [169,170]. In particular, the period of the oscillation was related to beats of interband transitions whose electronic states are coupled by an LO-phonon.

Phonon oscillations are also expected to appear in the DTS of pump/probe experiments. In the early investigations, where rather large excitation densities were used [173,174], the DTS was dominated by carrier/carrier scattering and phonon replicas were not observed. With the improvement of the laser and detection techniques the topic has been successfully revisited recently [175,176]. Using a combination of low excitation density, $\approx 8 \times 10^{14} cm^{-3}$, ultrashort probe pulses, $\approx$ 25fs, and circular polarization selection rules to detect only the carriers generated in the $hh \rightarrow e$ transition, several phonon replicas were observed in $GaAs$ [176]. Broad features are seen at very short Δt ($\leq$ 80fs), due to the energy uncertainty relation; but over times of the order of the LO-phonon period the phonon replica start to appear superimposed on a broad background. Their width narrows and become of the order of that of the laser at later times. In fact, it seems that the successive replica appear one after the other and are roughly separated in time by an LO-phonon period. This indicates a succession of quantum interferences whose time scale is related to the internal period of the "thermal reservoir", as discussed in Section III. It turns out that an analytical solution for the electron-phonon Quantum Kinetic equation for a one dimensional system was found recently [177]. Using this model to calculate the scattering integrals of a SBE description of the pump-probe experiments, theoretical DTS in remarkable agreement with the experimental ones were obtained [176].

To finish this section we want to discuss some important and recent developments. In the previous paragraphs we have seen that what is usually called an "irreversible" process is, in fact, a quantum mechanical interaction with an oscillatory behavior that couples a degree of freedom of a sub-system to the numerous ones of a thermal reservoir. The process becomes

really "irreversible" only after several oscillations. Therefore, it should be possible to *reverse or enhance*, after it has already started, an interaction process that would become irreversible if the sub-system and the reservoir were left to themselves. Following this argument and the narrative of the previous paragraphs, such a situation could be implemented by replacing one of the pulses of a canonical FWM configuration by a pair of pulses whose relative phase is properly chosen. This has been demonstrated in a recent FWM experiment [178], where two phase-locked pulses, 1 and 1′, propagating in the direction $\vec{k}_1$ and separated by the time delay $\Delta t_{11'} = t_1 - t_{1'}$, interact with a pulse propagating along $\vec{k}_2$ delayed by $\Delta t_{21'} = t_2 - t_{1'}$ in a $GaAs$ sample at $T = 77$K. The FWM signal is detected, as usual, in the direction $2\vec{k}_2 - \vec{k}_1$, so that in the $\chi^{(3)}$-regime the pair of phase-locked pulses enter linearly polarized. The 15fs pulses are tuned to the band gap; they are all linearly polarized and have approximately the same intensity. The relative phase between pulse-1 and pulse-1′ is defined to better than 0.1fs. If only one $\vec{k}_1$-pulse is present, this is the same experiment as in Ref. [169] and the same results are reproduced. With the pair of phase-locked pulses, the $S_{TI}(\Delta t_{21'})$ shown in Fig. (28), exhibits remarkable features as $\Delta t_{11'}$ is varied over a range corresponding approximately to one optical cycle. Depending on the time delay between the phase-locked pulses, the phonon oscillation can disappear completely (for example around $\Delta t_{11'} = -43.64$fs) or can be very pronounced (for example around $\Delta t_{11'} = -42.38$fs). The detailed theory of these experiments is not yet available, but model calculations, able to reproduce the main trends, confirm this interpretation [178]. These experimental results clearly demonstrate that it is indeed possible exploit the techniques of ultrafast nonlinear optics to manipulate the so called "irreversible" scattering processes.

The Quantum Kinetics regime is still poorly understood. In particular, there are still outstanding questions about how to connect Quantum Kinetics and Boltzmann Kinetics theories. Currently, our interpretations are based on a SBE description of $\partial p_k/\partial t|_{coh}$, augmented by $\partial p_k/\partial t|_{scatt}$ calculated using scattering integrals that rely on mechanisms beyond the HF/RPA level of the SBE. One may look for a more consistent formalism, which may be derived from a treatment such as the DCTS that is, in principle, exact. Nevertheless,

ultrashort pulse time-resolved experiments are now able to explore regimes that were not previously accessible and will continue to provide novel information on the very short-time dynamics of manybody interactions.

IX. CONCLUSION

As we conclude this chapter, it may be useful to reflect on the recent developments in the area of time-resolved nonlinear optical spectroscopy of semiconductors that we have just reviewed, and to compare them to parallel advances in other areas of condensed matter physics. In general one can say that observing and describing manybody effects has been a driving force for this whole field of physics. However, in most of the other sub-fields (quantum transport, superconductivity, quantum Hall effect etc.) researchers are interested in understanding how degrees of freedom lock together as the energy scale is lowered. Correspondingly, they concentrate on the low energy elementary excitations and the "long time" scales. In that regime, one can probe the formation of "order parameters" and the establishment of mean-fields. Several aspects of time-resolved nonlinear optical spectroscopy of semiconductors can be contrasted with this approach. Firstly, optical processes with photon energies close to the band gap of semiconductors correspond to the creation of elementary excitations whose dynamics evolve significantly on short time and short length scales. Therefore, what can be explored with ultrafast optical techniques is the new regime where the fluctuations of the "order parameters" become important and the mean-field pictures break down. Secondly, it is clear that the manybody mechanisms that are responsible for the formation of the quasi-particles seen in the linear regime, are also responsible for the interaction among these quasi-particles that are seen in the nonlinear regime. However, what was discovered in the last decade is that these various interactions have specific dynamics with specific time scales, and that they are strongly and differently affected by quantum confinement. Thus, as already noted, time-resolved nonlinear optical spectroscopy in quantum confined systems provides information on manybody interactions that is inaccessible to

conventional spectroscopic techniques. Finally, electronic states in semiconductors are well described by the effective mass and mean field approximations, and their basic physics is well understood. Thus, they constitute an almost ideal ground for testing advanced many-body theories. This, combined with important experimental advances, has placed the field of time-resolved nonlinear optical spectroscopy of semiconductors in an exceptional situation. By exploiting ultrafast time-resolved techniques under quantum confinement, it has been possible to design experiments for investigating manybody processes, in almost perfect samples, with an unprecedented flexibility and sensibility. This has provided theorists with a wealth of reliable and novel experimental data that motivated them to develop very refined descriptions of subtle phenomena and enormously further our understanding of manybody systems. It is not a big stretch of imagination to predict that the same approach will be applied soon to other outstanding problems of condensed matter physics.

In this chapter we have tried to give an overview of the spectacular recent progresses made in the time-resolved spectroscopy of semiconductors. Because of space restrictions we had to concentrate on the conceptual and fundamental aspects of the subject and leave apart a number of interesting areas. Concerning the material systems, we have not covered the II-VI and I-VII compounds, mostly because the fundamental physics is quite similar to that of the III-V's, the main differences being due to the magnitude of some parameters such as the electron-phonon coupling or the binding energies of the exciton complexes. This, nevertheless, can affect significantly the carrier relaxation and correlation [179–181]. The magnetic-semiconductors present, in addition, some extremely important and exciting spin-related effects, that form a separate topic in their own right [182–184]. The III-V nitride family promises to have a great impact in photonics and electronics in the next decade. Although the material quality has greatly improved recently, more progress must be made in defect control, but there is no doubt that the III-V nitrides will soon attract much attention in the area of nonlinear spectroscopy. In terms of elementary excitations, magneto-excitons in quantum well structures [185–189] and magnetically induced Fano resonances [190,191] have complex and very interesting ultrafast dynamics which we have not reviewed. Finally

we have also left aside a number of applications, for example the generation and utilization of THz radiation from heterostuctures excited by ultrashort laser pulses [192] or the dynamics of micro-cavities where the number of photon modes interacting with the e-h pairs can be controlled [193]. Covering all these topics would have required at least doubling the size of the chapter.

ACKNOWLEDGMENTS

It is a pleasure to acknowledge many very fruitful discussions with S. Schmitt-Rink, W. Schäfer, S. Mukamel, I. Perakis, L. Sham, M. Wegener and A. Stahl. We would like also to thank D.-H. Lee for his critical comments of the manuscript. This work was supported by the Director, Office of Energy Research, Office of Basic Energy Sciences, Division of Material Sciences of the U.S. Department of Energy, under Contract No. DE-AC03-76SF00098.

REFERENCES

[1] M. D. Levenson, "*Introduction to Nonlinear Laser Spectroscopy*", Academic Press, N.Y. (1982).

[2] R.Y. Shen, "*Principles of Nonlinear Optics*" Wiley-Interscience Pub. (1984).

[3] S. Mukamel, "*Principles of Nonlinear Optical Spectroscopy*", Oxford, NY (1995).

[4] L. Allen, J. H. Eberly, "*Optical Resonance and Two Level Atoms*", Dover Pub. Co. NY, (1987).

[5] T. Yajima, and Yoichi Taira, J. Phys. Soc. Jpn. **47**, 1620 (1979).

[6] S. D. Kramer, F. G. Parsons, N. Bloembergen, Phys. Rev. B **9**, 1853 (1974).

[7] S. D. Kramer, F. G. Parsons, N. Bloembergen, Phys. Rev. B **14**, 4654 (1976).

[8] A. Maruani and D.S. Chemla, Phys. Rev. B**23**, 841 (1981).

[9] D.S. Chemla and A. Maruani Rep. Prog. Quant. Electr. **8**, 2 (1982).

[10] J. Hegarty, M.D. Sturge, C. Weisbuch, A.C. Gossard, W. Wiegmann, Phys. Rev. Lett. **47**, 995 (1982).

[11] D.S. Chemla, D.A.B. Miller, P.W. Smith, A.C. Gossard, W. Wiegmann, IEEE J.QE-**20**, 265 (1984).

[12] L. Schultheis, M.D. Sturge, J. Hegarty, Appl. Phys. Lett. **47**, 995 (1985).

[13] L. Schultheis, J. Kuhl, A. Honold, C.W. Tu, Phys. Rev. Lett. **57** 1635 (1986), and **57** 1797 (1986).

[14] J. Shah, "*Ultrafast Spectroscopy of Semiconductors and Semiconductor Nanostructures*", Springer Solid State Sciences **115**, Springer Berlin, (1996).

[15] H. Haug and S. W. Koch, "*Quantum theory of the optical and electronic properties of semiconductors*", 2nd edition, World Scientific, Singapore, (1993).

[16] R. Binder, S.W. Koch, "*Nonequilibrium Semiconductor Dynamics,*" Prog. Quant. Electron. **19**, No. 4/5 (1995).

[17] H. Haug and A.-P. Jauho "*Quantum Kinetics in Transport and Optics of Semiconductors*", Springer Series in Solid State Sciences **123** Springer, Berlin (1996).

[18] G. Bastard "*Wave Mechanics Applied to Semiconductor Heterostructures*", Les Editions de Physiques, Les Ulis, Cedex France (1988).

[19] M. S. Hybertsen, S. G. Louie, Phys. Rev. Lett. **55**, 1418 (1985), and Phys. Rev. B **34**, 5390 (1986).

[20] For a recent review see S. G. Louie, "*First-Principles Theory of Electron Excitation Energies in Solids, Surfaces, and Defects,*" in Topics in *Computational Materials Science*, Ed. C. Y. Fong, World Scientific, Singapore, (1997).

[21] R. J. Elliott, Phys. Rev. **108**, 1384 (1957)

[22] C. Tanguy, Phys. Rev. Lett. **75**, 4090 (1995).

[23] S. Schmitt-Rink, D.S Chemla, D.A.B. Miller, Adv. in Phys. **38**, 89 (1989).

[24] S. Glutsch, U. Siegner, M.-A. Mycek, D. S. Chemla, Phys. Rev. B **50**, 17009 (1994).

[25] S. Glutsch, D. S. Chemla, F. Bechstedt, Phys. Rev. B **51**, 16885 (1995).

[26] U. Fano, Phys. Rev. **124**, 1866 (1961).

[27] M. S. Skolnick, J. M. Rorison, K. J. Nash, D. J. Mowbray, P. R. Tapster, S. J. Bass, and A. D. Pitt, Phys. Rev. Lett **58**, 2130 (1987).

[28] Livescu,, D.A.B. Miller, D.S. Chemla, M. Ramaswamy, T.Y. Chang, N. Sauer, A.C. Gossard, J.H. English, IEEE, J. Quan. Electr. **24** 1677, (1988).

[29] I. Brener, W. H. Knox, and W. Schäfer, Phys. Rev. B **51**, 2005 (1995).

[30] G.D. Mahan, Phys. Rev. **153**, 882 (1967).

[31] G. D. Mahan in *Fermi Surface Effects*, J. Kondo and A. Yoshimori Eds. (Springer, Berlin), **41** (1988).

[32] I. E. Perakis and Y.-C. Chang, Phys. Rev. B **44**, 5877 (1991).

[33] I. E. Perakis and Y.-C. Chang, Phys. Rev. B **43**, 12556 (1991).

[34] I. E. Perakis and Y.-C. Chang, Phys. Rev. B **47**, 6573 (1993).

[35] P. Nozieres and C.T. De Dominicis Phys. Rev. **178**, 1097 (1969).

[36] J.J. Hopfield, Comments Solid State Phys. **2**, 40 (1969).

[37] J. Gavoret, P. Nozieres, B. Roulet, and M. Combescot, J. Phys. (Paris), **30**, 987 (1969).

[38] T. Uenoyama and L. J. Sham, Phys. Rev. Lett. **65**, 1048 (1990).

[39] A. Kuznetsov, Phys. Rev. B **44**, 8721 (1991).

[40] A. Kuznetsov, Phys. Rev. B **44**, 13381 (1991).

[41] K. El Sayed, H. Haug, Phys. Stat. Sol. (b) **173**, 189 (1992).

[42] K. El Sayed, T. Wicht, H. Haug, L. Bányai, Z. Phys. B. **86** 345 (1992).

[43] M. Hartmann, W. Schäfer, Phys. Stat. Sol. (b) **173**, 165 (1992).

[44] D.B. Tran Thoi and H. Haug, Z. Phys. **B91**, 199 (1993).

[45] K. El Sayed, S. Schuster, H. Haug, F. Herzel and F. Henneberger Phys. Rev. B **49**, 7337 (1994-I).

[46] K. El Sayed, L. Bányai, H. Haug, Phys. Rev. B. **50** 1541 (1994).

[47] B. K. Ridley "*Quantum Processes in Semiconductors*" Clarendon Press, Oxford UK (1982).

[48] S.M. Goodnick, P. Lugli, Phys. Rev. B **37**, 2578 (1988).

[49] J.H. Collet, Phys. Rev. B **47**, 10279 (1993).

[50] V.L. Gurevich, M.I. Muradov, D.A. Parshin, Euro-phys. Lett. **12**, 375, (1990).

[51] For a review see S. Feneuille, Rep. Prog. Phys. **40**, 1257 (1977).

[52] A. Mysyrowicz, D. Hulin, A. Antonetti, A. Migus, W.T. Masselink, H. Morkoc, Phys. Rev. Lett. **56**, 2748 (1986).

[53] A. von Lehmen, J. E. Zucker, J.P. Heritage, D.S. Chemla, Opt. Lett. **11**, 609, (1986).

[54] K. Tai, J. Hegarty, W.T. Tsang, Appl. Phys. Lett. **51**, 152, (1987).

[55] M. Joffre, D. Hulin, and A. Antonetti, J. Phys. (Paris) **348**, C5-537 (1987), and M. Joffre, D. Hulin, A. Migus, and M. Combescot, Phys. Rev. Lett. **362**, 74 (1989).

[56] W. H. Knox, D. S. Chemla, D. A. B. Miller, J. B. Stark, and S. Schmitt-Rink, Phys. Rev. Lett. **62**, 1189 (1989).

[57] D. S. Chemla, W. H. Knox, D. A. B. Miller, S. Schmitt-Rink, J. B. Stark, and, R. Zimmermann J. Lum. **44** 233 (1989).

[58] S. Schmitt-Rink, and D.S. Chemla, Phys. Rev. Lett. **57**, 2752 (1986).

[59] S. Schmitt-Rink, D.S. Chemla, H. Haug, Phys. Rev. B **37**, 941 (1988).

[60] M. Lindberg, S. W. Koch Phys. Rev. B. **38**, 3342 (1988-I).

[61] I. E. Perakis, and D.S. Chemla, Phys. Rev. Lett. **72**, 3202 (1994).

[62] See for example J.R. Schrieffer, "Theory of Superconductivity" Addison-Wesley Pub. Co. New York (1988).

[63] L. V. Keldysh A.N. Kozlov, Zh. Eksper. Teor. Fiz. **54**, 978 (1968).

[64] C. Comte, Ph. Nozieres, J. Physique **43**, 1069 (1982) and Ph. Nozieres, C. Comte, J. Physique **43**, 1083 (1982).

[65] M. Combescot, R. Combescot, Phys. Rev. Lett. **61**, 117 (1988).

[66] M. Combescot, Phys. Rep. **221**, 167 (1992).

[67] R. Zimmermann, Phys. Stat. Sol. B **146**, 371 (1988).

[68] R. Zimmermann and M. Hartmann, Phys. Stat. Sol. B **150**, 365 (1988).

[69] R. Zimmermann, Phys. Stat. Sol. B **146**, 545 (1988).

[70] R. Zimmermann, Proc. 19th Int. Conf. Phys. Semicond., Warsaw (1988).

[71] W. Schäfer, K. H. Schuldt, and R. Binder, Phys. Stat. Sol. B 3150, 407 (1988).

[72] W. Schäfer, Adv. Solid State Phys. **28**, 63 (1988).

[73] C. Ell, J. F. Mueller, K. El Sayed, L. Bányai, and H. Haug, Phys. Stat. Sol. B **3150**, 393 (1988).

[74] C. Ell, J. F. Mueller, K. El Sayed, and H. Haug, Phys. Rev. Lett. **362** 304 (1989).

[75] J.-P. Likforman, M. Joffre, D. Hulin Phys. Rev. Lett. **79**, 3716 (1997).

[76] I. E. Perakis, Chem. Phys. **210**, 259 (1996).

[77] I. E. Perakis, I. Brener, W. H. Knox, and D. S. Chemla, J. Opt. Soc. Am. B **13**, (1996).

[78] G. W. Fehrenbach, W. Schäfer, J. Treusch, R. G. Ulbrich, Phys. Rev. Lett. **49**, 1281 (1982).

[79] G. W. Fehrenbach, W. Schäfer, R. G. Ulbrich, J. Lumin. **30**, 154 (1985).

[80] N Peygahmbarian, H. M. Gibbs, J.L. Jewell, A. Antonetti, A. Migus, D. Hulin, A. Mysyrowicz, Phys. Rev. Lett. **53**, 2433 (1984).

[81] W.H. Knox, C. Hirlimann, D.A.B. Miller, J. Shah, D. Chemla C.V Shank Phys. Rev. Lett. **56**, 1191 (1986).

[82] D. Hulin, A. Mysyrowicz, A. Antonetti, A. Migus, W.T. Masselink, H. Morkoc, H. M.

Gibbs, N Peygahmbarian, Phys. Rev. B **33**, 4389 (1986).

[83] D.S Chemla, S. Schmitt-Rink, D.A.B. Miller, in *Optical Nonlinearities and Instabilities in Semiconductors,* H. Haug Ed., Academic Press, New York (1988).

[84] S. Schmitt-Rink, D.S Chemla, D.A.B. Miller, Phys. Rev. B **32**, 6601 (1985).

[85] H. Haug, S. Schmitt-Rink, Prog. Quant. Electron. **9**, 1, (1984).

[86] J.-P. Foing, D. Hulin, M. Joffre, M.K. Jackson, J.-L. Oudar, C. Tanguy, and M. Combescot, Phys. Rev. Lett. **68**, 110 (1992).

[87] M.-A. Mycek, J.-Y. Bigot, I. E. Perakis and D.S. Chemla, J. Nonlin. Opt. Phys. Mater. **4**, 497 (1995), and JOSA B (1996).

[88] C. Tanguy, and M. Combescot, Phys. Rev. Lett. **68**, 1935 (1992).

[89] P.C. Becker, H.L. Fragnito, C.H. Brito Cruz, R.L. Fork, J.E. Cunningham, J.E. Henry, and C.V. Shank Phys. Rev. Lett **61**, 1647 (1988).

[90] J.-Y. Bigot, M.T. Portella, R.W. Schoenlein, J.E. Cunningham and C.V. Shank Phys. Rev. Lett. **67**, 636 (1991).

[91] L. Schultheis, J. Kuhl, A. Honold, C.W. Tu, Phys. Rev. Lett. **57**, 1797 (1986).

[92] A. Honold, L. Schultheis, J. Kuhl, C.W. Tu, Phys. Rev. B **40**, 6442 (1989).

[93] A. Honold, L. Schultheis, J. Kuhl, C.W. Tu, in *Ultrafast Phenomena VI* T. Yajima, K. Yoshihara, C. B. Harris S. Shionoya Eds. Springer, Berlin (1989).

[94] K. Leo, M. Wegener, J. Shah, D.S. Chemla, E.O. Göbel, T.C. Damen, S. Schmitt-Rink, and W. Schäfer, Phys. Rev. Lett. **65**, 1340 (1990).

[95] M. Wegener, D.S. Chemla, S. Schmitt-Rink, and W. Schäfer, Phys. Rev. A **42**, 5675 (1990).

[96] For a recent review see: W. Schäfer, "*Manybody Effects in Nonlinear Optics of Semi-*

conductor Structures" in "*Optics of Semiconductor Nanostructures,*". F. Henneberger, S. Schmitt-Rink, E.O. Göbel, Eds. Akademie Verlag, Berlin (1993).

[97] A. Stahl, I. Balslev, *Electrodynamics of the Semiconductor Band edge* Springer Tracts in Modern Physics, Springer-Verlag, Berlin, (1987).

[98] I, Balslev, R. Zimmermann, A. Stahl, Phys. Rev. B **40** 4095 (1989).

[99] S. Glutsch, U. Siegner, D. S. Chemla, Phys. Rev. B **52**, 4941 (1995-I).

[100] M.-A. Mycek, S. Weiss, J.-Y. Bigot, S. Schmitt-Rink, D.S. Chemla, Appl. Phys. Lett. **60**, 2666 (1992).

[101] S. Weiss, M.-A. Mycek, J.-Y. Bigot, S. Schmitt-Rink, and D.S. Chemla, Phys. Rev. Lett. **69**, 2685 (1992).

[102] D.S. Kim, J. Shah, T.C. Damen, W. Schäfer, F. Jahnke, S. Schmitt-Rink, and K. Köhler, Phys. Rev. Lett. **69** 2725 (1992).

[103] S. Schmitt-Rink, S. Mukamel, K. Leo, J. Shah, and D.S. Chemla, Phys. Rev. A **44**, 2124 (1991).

[104] B. F. Feuerbacher, J. Kuhl, R. Eccleston, K. Ploog Sol State Comm. **74** 1279 (1990).

[105] K. Leo, T.C. Damen, J. Shah, E. O. Göbel, K. Köhler, Appl. Phys. Lett. **57**, 19 (1990).

[106] K. Leo, E. O. Göbel, T.C. Damen, J. Shah, S. Schmitt-Rink, W. Schäfer, J.F. Muller, K. Köhler, P. Ganser, Phys. Rev. B **44**, 5726 (1991).

[107] M. Koch, G. von Plessen, J. Feldmann, E.O. Göbel, Chem. Phys. **120**, 367 (1996).

[108] S. Schmitt-Rink, D. Bennhardt, V. Heuckeroth, P. Thomas, P. Haring, G. Maidorn, H.J. Bakker, K. Leo, D.S. Kim, J. Shah, K. Kohler, Phys. Rev. B **46**, 10460 (1992).

[109] G. Bartels and A. Stahl *Private communication.*

[110] M. Koch, J. Feldmann, G. von Plessen, E.O. Göbel, P. Thomas, K. Kohler, Phys. Rev.

Lett. **69**, 3631 (1992).

[111] V.G. Lyssenko, J. Erland, I. Balslev, K.-H. Pantke, B.S. Razbirin, J.M. Hvam, Phys. Rev. B **48**, 5720 (1993).

[112] J.-Y. Bigot, M.-A. Mycek, S. Weiss, R.G. Ulbrich, and D.S. Chemla, Phys. Rev. Lett. **70**, 3307 (1993).

[113] D.S. Chemla, J.-Y. Bigot, M.-A. Mycek, S. Weiss, W. Schäfer, Phys. Rev. **50**, 8439 (1994-II).

[114] D.S. Chemla, J.Y. Bigot, Chem. Phys. **210**, 135 (1995).

[115] S. Bar-Ad, I. Bar-Joseph, Phys. Rev. Lett. **66**, 2491 (1991).

[116] H. Wang, M. Jiang, R. Merlin, D.G. Steel, Phys. Rev. Lett. **69**, 804 (1992).

[117] E.O. Göbel, K. Leo, T.C. damen, J. Shah, S. Schmitt-Rink, W. Schäfer, J.F. Muller, K. Köhler, Phys. Rev. Lett. **64**, 1801 (1990).

[118] M. Joschko, M. Woerner, T. Elsässer, E. Binder, T. Kuhn, R. Hey, H. Kostial, and K. Ploog, Phys. Rev. Lett. **78**, 737 (1997).

[119] K. Leo, J. Shah, E. O. Göbel, T.C. Damen, S. Schmitt-Rink, W. Schäfer, K. Köhler, Phys. Rev. Lett. **66**, 201 (1991).

[120] G. Bastard, C. Delalande, R. Ferriera, H.U. Liu, J. Lumin. **44**, 247 (1989), and R. Ferriera, C. Delalande, H.U. Liu, G. Bastard, B. Etienne, J. F. Palmier, Phys. Rev. B **42** 9170 (1990).

[121] A.M. Fox, D.A.B. Miller, G. Livescu, J.E. Cunningham, J.E. Hemry, W.Y. Jan, Phys. Rev. B **42**, 1841 (1990) and Phys. Rev. B **44**, 6231 (1991).

[122] F. Bloch, Z. Physik **52**, 555 (1928).

[123] C. Zener., Proc. R. Soc. London Ser. A **145**, 523 (1932).

[124] E. E. Mendez, F. Agullo-Rueda, J. M. Homg, Phys. Rev. Lett. **60**, 2426 (1988).

[125] P. Voisin, J. Bleuse, C. Bouche, S. Gaillard C. Alibert, A. Regreny, Phys. Rev. Lett. **61**, 1639 (1988).

[126] M. M. Dignam, J.E. Sipe, Phys. Rev. Lett. **64**, 1797 (1990).

[127] G. Bastard, R. Ferreira, in *Spectroscopy of Semiconductor Microstructures* NATA ASI Series, Plenum Press, NY (1989).

[128] J. Feldmann, K. Leo, J. Shah, D.A.B. Miller, J.E. Cunningham, T. Meier, G. von Plessen, A. Schulze, P. Thomas, S. Schmitt-Rink, Phys. Rev. B **46**, 7252 (1992).

[129] K. Leo, P. Haring Bolivar, F. Brüggemann, R. Schwedler, K. Köhler, Sol. State Comm. **84**, 943 (1992).

[130] K. Leo, J. Feldmann, J. Shah, G. von Plessen, S. Schmitt-Rink, J.E. Cunningham, Superlattices and Microstructures **13**, 55 (1993).

[131] P. Leisching P. Haring Bolivar, W. Beck, Y. Dhaibi F. Brüggemann, R. Schwedler, H. Kurz, K. Leo, K. Köhler, Phys. Rev. B **50**, 14389 (1994).

[132] V. G. Lyssenko, G. Valusis, F. Löser, T. Hasche, K. Leo, K. Köhler, Phys. Rev. Lett. **79**, 301 (1997).

[133] R.C. Miller, D.A. Kleinman, J. Lummin. **30** 520 (1985).

[134] S. Barad, I. Bar-Joseph, Phys. Rev. Lett. **68**, 349 (1992).

[135] D.J. Lovering, R.T. Phillips, G.J. Denton, G.W. Smith, Phys. Rev. Lett. **68** 1880 (1992).

[136] G. Finkelstein, S. Barad, O. Carmel, I. Bar-Joseph, Y. Levinson, Phys. Rev. B **47**, 12964 (1993).

[137] E.J. Mayer, G.O. Smith, V. Heuckeroth, J. Kuhl, K. Bott, A. Schulze, T. Meier, D.

Benhardt, S.W. Koch, P. Thomas, R. Hey, K. Ploog, Phys. Rev. B **50**, 1470 (1994).

[138] D. S. Kim, J. Shah, T. C. Damen, L. N. Pfeiffer, W. Schäfer, Phys. Rev. B, **50**, 5775 (1995).

[139] E.J. Mayer, G.O. Smith, V. Heuckeroth, J. Kuhl, K. Bott, A. Schulze, T. Meier, S.W. Koch, P. Thomas, R. Hey, K. Ploog, Phys. Rev. B **5**, 10909 (1995).

[140] G.J. Denton, R.T. Phillips, G.W. Smith, Appl. Phys. Lett. **67** 238 (1995).

[141] F. C. Spano and S. Mukamel, Phys. Rev. A **40**, 5783 (1989).

[142] F. C. Spano and S. Mukamel, Phys. Rev. Lett. **66**, 1197 (1991).

[143] O. Dubovsky and S. Mukamel, J. Chem Phys. **95**, 7828 (1991).

[144] J. A. Leegwater and S. Mukamel, Phys. Rev. A **46**, 452 (1992).

[145] S. Mukamel *"Manybody Effects in Nonlinear Susceptibilities; Beyond the Local-field Approximation,"* in *"Molecular Nonlinear Optics,"* J. Zyss, Ed., Academic Press, New York, (1994).

[146] V.M. Axt, A. Stahl, Z. Phys. **B93**, 195 (1994) and **B93** 205 (1994).

[147] K. Victor, V. M. Axt, and A. Stahl; Phys. Rev. B, **51**, 14164 (1995).

[148] M.Z. Maialle, L.J. Sham, Phys. Rev. Lett. **73**, 3310 (1994).

[149] T. Östreich, K. Schönhammer, L.J. Sham, Phys. Rev. Lett. **74**, 4698 (1995).

[150] V.M. Axt, A. Stahl, E. J. Mayer, P. Haring-Bolivar, S. Nüsse, K. Ploog, K. Köhler Phys. Stat. Sol. **(b) 188**, 447 (1995)

[151] W. Schäfer, D. S. Kim, J. Shah, T. C. Damen, J. E. Cunningham, K. W. Goossen, L. N. Pfeiffer, and K. Köhler; Phys. Rev. B, **53**, 1 (1996).

[152] H. Wang, K. Ferio, D. G. Steel, Y.Z. Hu, R. Binder S.W. Koch, Phys. Rev. Lett. **71**

1261 (1993).

[153] H. Wang, K. Ferio, D. G. Steel, P.R. Berman, Y.Z. Hu, R. Binder S.W. Koch, Phys. Rev. A **49** R1552 (1994).

[154] Y.Z. Hu, R. Binder S.W. Koch, S.T. Cundiff, H. Wang, D. G. Steel, Phys. Rev. B **49** 14382 (1994).

[155] M. U. Wehner, D. Steinbach, M. Wegener, Phys. Rev. B **54** R5211 (1996).

[156] P. Kner, S. Bar-Ad, M.V. Marquezini, D. S. Chemla W. Schäfer, Phys. Rev. Lett. **78** 1319, (1997).

[157] P. Kner, S. Bar-Ad, M.V. Marquezini, D. S. Chemla W. Schäfer, Phys. Stat. Sol. (a) **164** 579, (1997).

[158] R. Lövenich, W. Schäfer, P. Kner, D. S. Chemla Phys. Stat. Sol. (a) **164** , (1997).

[159] I.V. Lerner and Yu. E. Lozovik, Zh. Eksp. Teor. Fiz. **80**, 1488 (1981) [Sov. Phys. JEPT 53, 763 (1981)]

[160] C. Stafford, S. Schmitt-Rink, W. Schäfer, Phys. Rev. B **41**, 10,000 (1990-I).

[161] A. V. Korolev and M. A. Liberman, Phys. Rev. Lett. **72**, 270 (1994); A. V. Korolev and M. A. Liberman, Phys. Rev. A **45**, 1762 (1992).

[162] F.H. Pollak and M. Cardona, Phys. Rev. **172**, 816 (1968).

[163] M. U. Wehner, J. Hetzler, M. Wegener, Phys. Rev. B **55**, 4031 (1997).

[164] S. Bar-Ad, P. Kner, M.V. Marquezini, K. El Sayed and D.S. Chemla, Phys. Rev. Lett. **77**, 3177 (1996).

[165] F. X. Camescasse, A. Alexandrou, D. Hulin, L. Bányai, D. B. Tran Thoai, and H. Haug. Phys. Rev. Lett. **77**, 5429 (1996).

[166] P. Roussignol, D. Richard, C. Flytzanis, N. Neuroth, Phys. Rev. Lett. **62**, 312, (1989).

[167] R.W. Schoenlein, D. M. Mittleman, J.J. Shiang, A. P. Alivisatos, C.V. Shank, Phys. Rev. Lett. **70**, 1014, (1993).

[168] D. M. Mittleman, R.W. Schoenlein, J.J. Shiang, V.L. Colvin, A. P. Alivisatos, C.V. Shank, Phys. Rev. B **49**, 14435, (1994).

[169] L. Bányai, D.B. Tran Thoai, E. Reitsamer, H. Haug, D. Steinbach, M.U. Wehner, M. Wegener, T. Marschner and W. Stolz, Phys. Rev. Lett. **75**, 2188 (1995).

[170] D. Steinbach, M.U. Wehner, M. Wegener, Bányai, E. Reitsamer, H. Haug, Chem. Phys. **210**, 49 (1996).

[171] H. Haug, Phys. Status Solidi B **173**, 139 (1992).

[172] L. Bányai, D.B. Tran Thoai, C. Remling, H. Haug, Phys. Status Solidi B **173**, 149 (1992).

[173] W.Z. Lin, L.G. Fujimoto, E.P. Ippen, R.A. Logan, Appl. Phys. Lett. **50**, 124 (1987).

[174] R.W. Schoenlein, W.Z. Lin, E.P. Ippen, J.G. Fujimoto, Appl. Phys. Lett. **51**, 1442 (1987).

[175] A. Leitenstorfer, C. Furst, A. Laubereau, W. Kaiser, G. Trankle, G. Weimann, Phys. Rev. Lett. **76**, 1545 (1996).

[176] C. Fürst, A. Leitenstorfer, A. Laubereau, and R. Zimmermann, Phys. Rev. Lett. **78**, 3733 (1997).

[177] V. Meden, C. Wöhler, J. Fricke, K. Schönhammer, Z. Phys. B **99**, 357, (1996).

[178] M. U. Wehner, M. U. Ulm, D. S. Chemla, M. Wegener. Phys. Rev. Lett. **80**, 1992 (1998).

[179] A.V. Nurmikko and R.L. Gunshor: "Physics and Device Science in II-VI Semiconductor Visible Light Emitters" in *Solid State Physics* **48**, H. Ehrenreich and F. Spaepen

Eds., Academic Press (1995) and references therein.

[180] "*II-VI Blue/Green Light Emitters: Device Physics and Epitaxial Growth*", in *Semiconductors and Semimetals*, **44**, R.L. Gunshor and A.V. Nurmikko, Eds Academic Press (1996).

[181] A.V. Nurmikko "*Optical Gain and Excitonic Processes in Widegap Semiconductor Quantum Wells*" in *New Aspects in Optical Properties of Nanostructures*, T. Takagahara Ed. J. of Phase Transitions Gordon and Breach (1997).

[182] D.D. Awschalom and N. Samarth, "*Polaron Dynamics and Spin Scattering in Magnetic Quantum Structures*" in *Optics of Semiconductor Nanostructures*, F. Henneberger, S. Schmitt-Rink, and E.O. Göbel Eds. Akademie Verlag, Berlin, (1993).

[183] S. T. Cundiff, R. Hellmann, M. Koch, G. Mackh, E. Göbel, JOSA B, **13** , 1263 (1996).

[184] S.A. Crooker, D.D. Awschalom, J.J. Baumberg, F. Flack, and N. Samarth, Phys. Rev. B **56**, 7574 (1997).

[185] J.B. Stark, W. H. Knox, D. S. Chemla W. Schäfer, S. Schmitt-Rink, C. Stafford, Phys. Rev. Lett. **65**, 3033 (1990).

[186] S. Schmitt-Rink, J.B. Stark, W. H. Knox, D. S. Chemla, W. Schäfer, Appl. Phys. A **53**, 491 (1991).

[187] J.B. Stark, W. H. Knox, D. S. Chemla Phys. Rev. Lett. **68**, 3080 (1992).

[188] J.B. Stark, W. H. Knox, D. S. Chemla Phys. Rev. B **46**, 7919 (1992).

[189] J.B. Stark, W. H. Knox, D. S. Chemla in *Femtosecond Nonlinaer Optical Response of Magnetically Confined Quantum Well Excitons*" in "*Optics of Semiconductor Nanostructures,*". F. Henneberger, S. Schmitt-Rink, E.O. Göbel, Eds. Akademie Verlag, Berlin (1993) and references therein.

[190] U. Siegner, S. Barad, D. S. Chemla, Chem. Phys. **210**, 155 (1996) and references

therein.

[191] U. Siegner, S. Glutsch, S. Barad, M.-A. Mycek, P. Kner, D. S. Chemla, JOSA B **13**, 969 (1996) and References therein.

[192] M. C. Nuss, J. Orenstein, *Terahertz Time-Domain Spectroscopy* to appear in *"Millimeter and Submillimeter Spectroscopy of Solids"*, Topics in Applied Physics 74, G. Gruner Ed. Springer-Verlag, New York, NY, (1998) and references therein.

[193] G. Khitrova, H. M. Gibbs, F. Jahnke, M. Kira S. W. Koch to be published in Rev Mod. Phys (1998), and reference therein.

X. FIGURE CAPTIONS

Figure 1: Sketch of the energy levels and selection rules for optical transition near the band gap of Zinc Blende and Wurtzite direct band gap semiconductors.

Figure 2: Solid lines, experimental spectra of the absorption coefficient and refractive index of $GaAs$ at the fundamental absorption edge. The $1\mu m$ sample is at T=1.6K; it is glued on a sapphire substrate, and the thermally induced stress has shifted the heavy-hole/light-hole degeneracy. Dotted lines, fits to the analytical formulae discussed in the text.

Figure 3: Absorption of a $1\mu m$ $GaAs$ sample in a $B = 10T$ magnetic field for σ^+ and σ^- polarizations. Regular Lorentzian exciton resonances are seen at the lowest edge, at the higher Landau edges strong Fano resonances are observed.

Figure 4: Comparison of the absorption coefficient, of (a) a modulation doped (solid line) and (b) an undoped (dotted line) $GaAs$ quantum well structure at $T = 8K$. The Fermi Edge Singularity, at the edge of the modulation doped sample spectrum, is as pronounced as the regular excitons in the spectrum of the undoped sample.

Figure 5: Phonon scattering in and out rates calculated with non-Markovian and Boltzmann Kinetics theories according to Ref. ([39,40]). In the non-Markovian case, the region of phase-space accessibility is much broader than in the Boltzmann case.

Figure 6: Time-momentum evolution of a population of electrons generated in 20fs in the conduction band of $GaAs$ calculated with Quantum Kinetic theory. (Courtesy of Prof. K. El Sayed.)

Figure 7: Excitonic optical Stark effect observed in ultrafast time resolved pump probe experiment Ref. [52]. The pump pulse duration is $\approx$ 100fs and the sample is a 10nm $GaAs$

quantum well structure. The pump spectrum shows where, below the resonances, the sample is excited. The absorption spectra for $\Delta t = -2$ps, 0ps and $+1.2$ps are given by the solid line, the dotted line and the dashed line respectively.

Figure 8: At low excitation and large detuning the excitonic optical Stark effect corresponds to a pure shift without change of oscillator strength. This is shown by the comparison of the differential transmission spectrum, measured in a QW sample excited $50meV$ below the 1S *hh*-X for a pump intensity $\approx 30MWcm^{-2}$ (solid line), with the ω-derivative of the linear absorption spectrum (dashed line), Ref. [56].

Figure 9: Differential transmission spectra versus time delay measured on a *GaAs* quantum well structure at room temperature excited about 20meV above the exciton resonances, Ref. [81]. One sees clearly the Pauli blocking of the absorption by the nonthermal carrier population as it is created and thermalizes. The signal at the exciton resonances increases as the carriers fill up the bottom of the bands. Inset: Comparison of the pump spectrum with a differential transmission spectrum at $\Delta t = 0$, showing that the spectral hole is down-shifted as compared to the pump spectrum.

Figure 10: Pump/probe differential transmission spectrum measured for a set of time delays in a *GaAs* sample at low temperature (solid lines), as compared to the pump spectrum (dotted lines), Ref. [86]. The lineshape and the shift are due to excitonic effects at the two edges of the transient populations generated by the pump. The inset shows the laser spectrum and the sample absorption spectrum.

Figure 11: Time integrated self-diffracted four wave mixing signal from a homogeneously broadened exciton resonance in a 17nm *GaAs* quantum well structure Ref. [94]. The negative time delay signal is due entirely due to the Coulomb interaction. The rise time of the signal for $\Delta t < 0$ is exactly half the decay time for $\Delta t > 0$.

Figure 12: Time resolved self-diffracted four wave mixing signal from a 17nm *GaAs*

sample, showing that the emission due to the Coulomb interaction can be so much delayed that it appears as a separate pulse Ref. [102].

Figure 13: Ratio of the contribution of the bare Coulomb interaction and the Pauli blocking (phase space filling) nonlinearities as a function of the density of carrier excitations, Ref. [114].

Figure 14: Quantum beats between the heavy hole and light hole excitons, seen in the time integrated four wave mixing signal measured on a 15nm $GaAs$ quantum well structure when the two excitons are simultaneously excited, Ref. [106].

Figure 15: Distinction between quantum beats and polarization interference Ref. [110]. Top graphs, the amplitude of the time resolved four wave mixing signal is plotted as a function of the absolute time t for a series of time delays Δt in the case of (a) quantum beats and (b) polarization interference. Lower graphs, position of the signal maximum in the t-Δt plane in solid line for the two cases; the dashed lines show the $t = 2\Delta t$ and the $t = \Delta t$ slopes.

Figure 16: Time-energy picture of the four wave mixing signal, showing that the shift in emission frequency in a quantum beat is not instantaneous and satisfies the uncertainty principle, Ref. [113]. (a) spectra of the laser (dotted line) and four wave mixing signal (solid line), (b) interferomeric auto-correlation (AC) of the four wave mixing signal, (c) AC-fringe spacing relative to the reference laser showing the sudden π shift during the quantum beat, (d) detail of the interferomeric-AC at the center of the profile and near the first node.

Figure 17: Observation of by pump/probe spectroscopy of an electronic wave packet oscillation in an asymmetric coupled quantum well structure Ref. [119]. As the electrons oscillate between the two wells they modulate the transmission of the probe beam.

Figure 18: Observation of the Bloch oscillations in a superlattice structure by four wave

mixing for a set of applied electrostatic fields, Ref. [129]. The electron oscillations modulate the four wave mixing signal.

Figure 19: Measurement of the amplitude of the wave-packet center of mass motion during Bloch oscillations in a superlattice, Ref. [132]. The maximum amplitude is $\approx$ 14nm.

Figure 20: Exciton-Biexciton oscillation observed in a $GaAs$ quantum well sample by pump/probe technique, using a σ^- probe and a σ^+ pump, Ref. [134].

Figure 21: Differential transmission spectra showing the broadening of the exciton resonance due to dephasing induced by $n \approx 3 \times 10^{15} cm^{-3}$ photogenerated excitons, Ref. [152]. The DTS lineshape is very well described as the difference between two Lorentzians. Inset: Linear absorption spectrum of the sample.

Figure 22: Time integrated four wave mixing signal measure with σ^-/σ^- polarization, $GaAs$ sample as a function of the applied magnetic field, Ref. [156]. As the magnetic field is increased the $\Delta t < 0$ signal acquire a long and nonexponential profile that can be seen as far a $\approx$ 100 time the laser pulse duration. It signals 4-particle correlations not accounted for in the time dependent Hartree-Fock theory.

Figure 23: Calculation of the time integrated four wave mixing (TI-FWM) signal using the "effective" polarization and exciton-exciton correlation, showing the contrasted time dependence of the Pauli Blocking (PSF), the bare Coulomb interaction and the exciton-exciton correlation contributions Ref. [157].

Figure 24: Theoretical time integrated four wave mixing signal calculated for $GaAs$ at $B = 10T$ and low density using the "Density Controlled Truncation Scheme" formalism. The large $\Delta t < 0$ signal is due to the exciton-exciton correlation Ref. [157].

Figure 25: Dynamics of the coherent FWM emission vs. time delay Δt. Left curve:

logarithm of the time integrated FWM signal intensity vs. Δt. Central panel: FWM power spectrum for three time delays between -80fs and 160fs, as indicated by the arrows on the left curve. The solid curves are the experimental results and the dashed curves the theoretical results of the Semiconductor Bloch Equations. For comparison the laser spectrum is depicted as a dotted line in the $\Delta t = 0$ graph of the central panel. It is tuned slightly below the *hh*-exciton resonance. Right panels: corresponding phase difference with the reference laser. Ref. [114].

Figure 26: Comparison between the experimental δ(DTS), derivative of the differential transmission spectrum with respect of the time delay, and the best simulations using the Semiconductor Bloch Equation within the relaxation time approximation: (a) experimental results for 30fs pump and probe pulses on a $1\mu m$ $GaAs$ sample, (b) theory with $T_2 = 200$fs, and no population relaxation, (c) theory with $T_2 = 200$fs and a population relaxation, $\tilde{T}_1 \sim 36$fs, towards a Maxwell-Boltzmann distribution with the same instantaneous number of carriers and total energy as that generated by the pump pulse, Ref. [164].

Figure 27: Time integrated four wave mixing signal measured in a $GaAs$ sample at $T = 77K$ with $\approx$ 14fs pulses and for three carrier densities $n_{eh} \approx 1.2, 1.9, 6.3 \times 10^{16} cm^{-3}$. The dashed curve, marked AC, shows the laser autocorrelation. The dots show the results of the Quantum Kinetics theory, Ref. [169].

Figure 28: Coherent control of phonon scattering processes: Lineshape of the time integrated four wave mixing signal as a function of the time delay $t_{21'}$ between the pulses along $\vec{k}_2$ and $\vec{k}_1$ for a series of fixed time delay $\Delta t_{11'}$ between two phase-locked pulses. The range of $\Delta t_{11'}$, $t_{11'} = -43.64$ (top) $\rightarrow -41.11$ fs (bottom), corresponds approximately to one optical cycle. It was scanned in steps of 0.21 fs. The $GaAs$ sample is at $T = 77K$, the excited carrier density is $n_{e,h} \approx 3.6 \times 10^{15} cm^{-3}$. Inset: Laser (dotted line) and TI-FWM (solid line) spectra at zero time delay. The phonon oscillations are absent for $t_{11'} = -43.64$ fs and pronounced for $t_{11'} = -42.38$ fs Ref. [178].

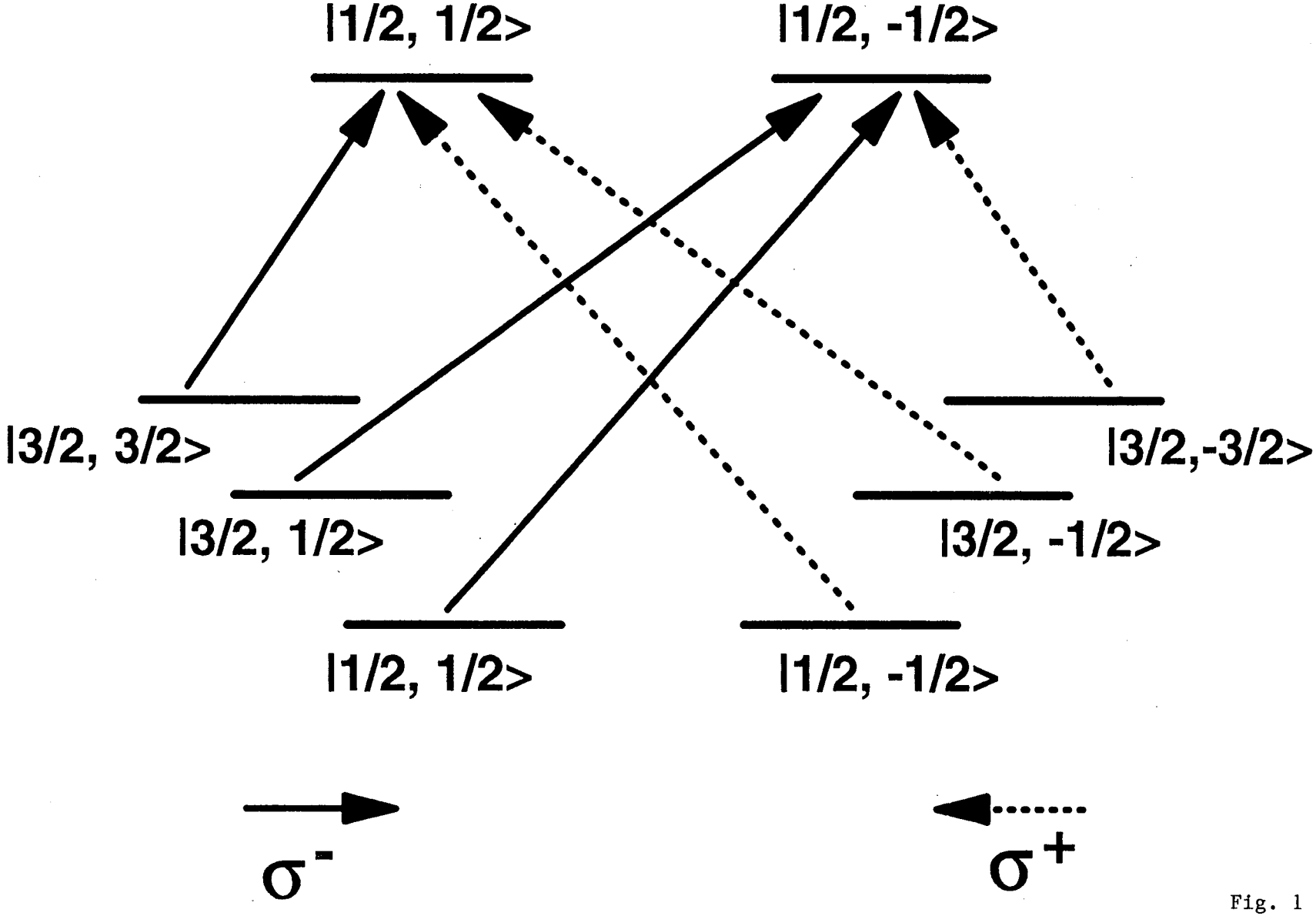

Fig. 1

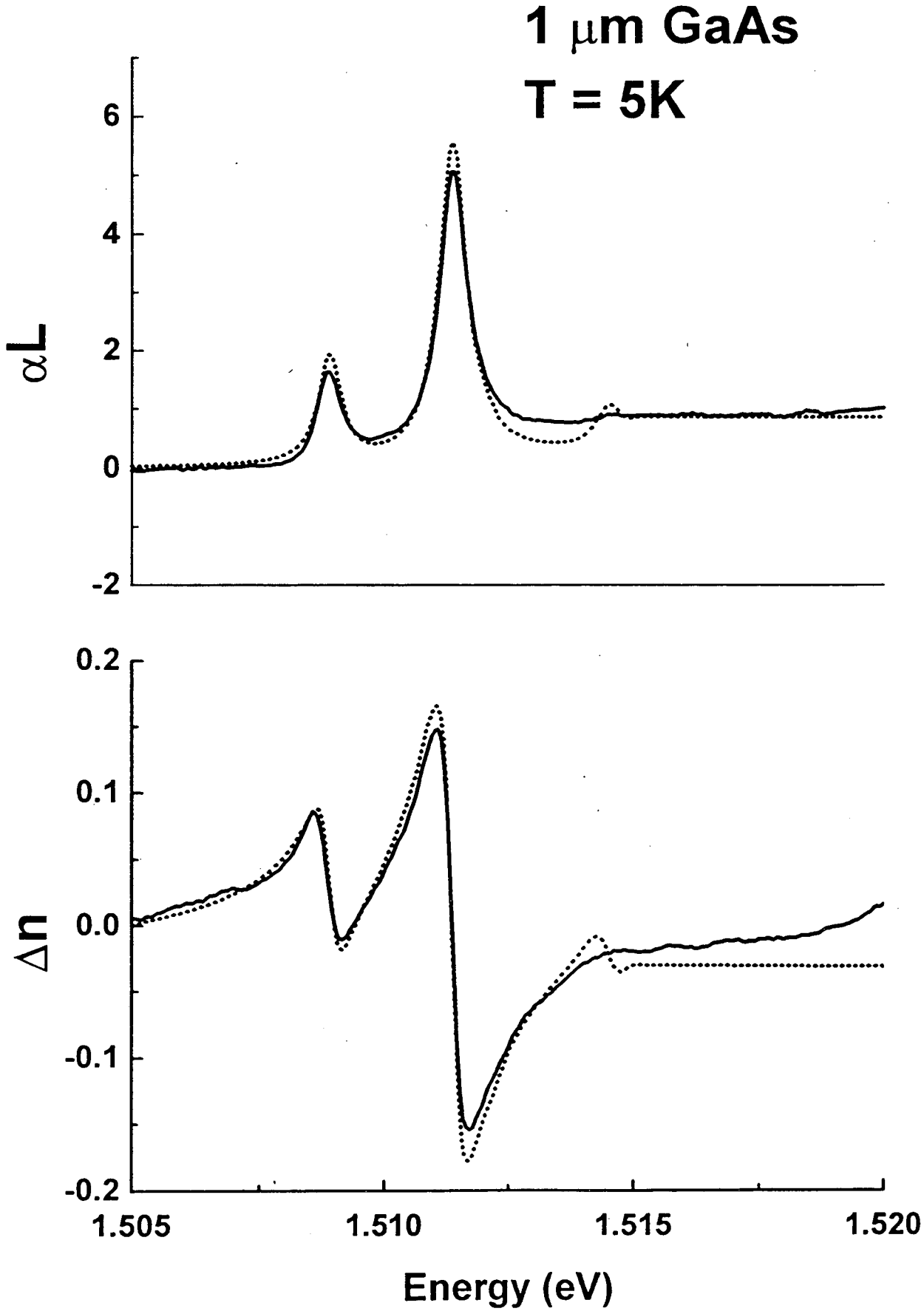
1 μm GaAs
T = 5K
αL
6
4
2
0
-2
Δn
0.2
0.1
0.0
-0.1
-0.2
1.505
1.510
1.515
1.520
Energy (eV)

Fig. 2

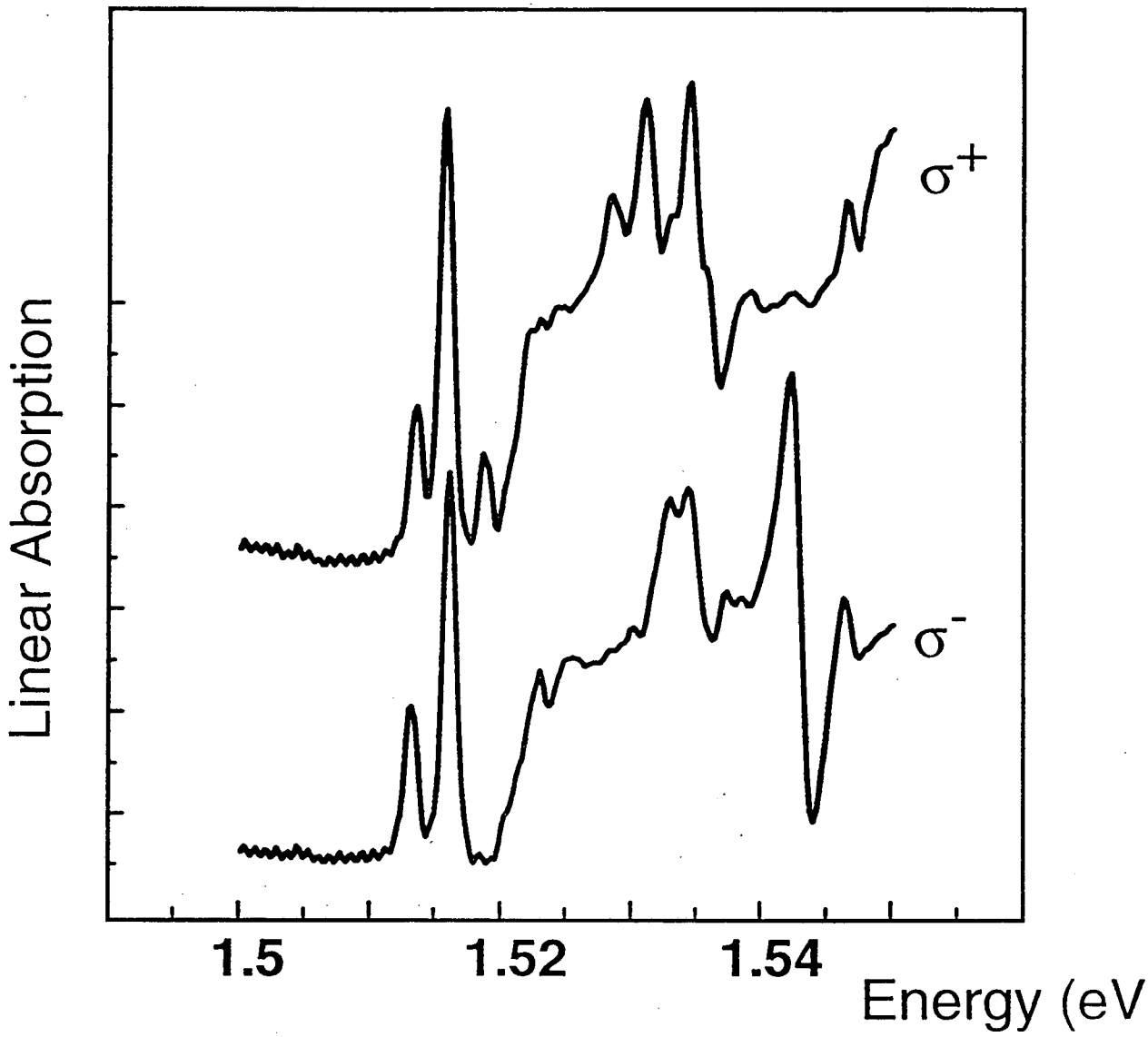

Fig. 3

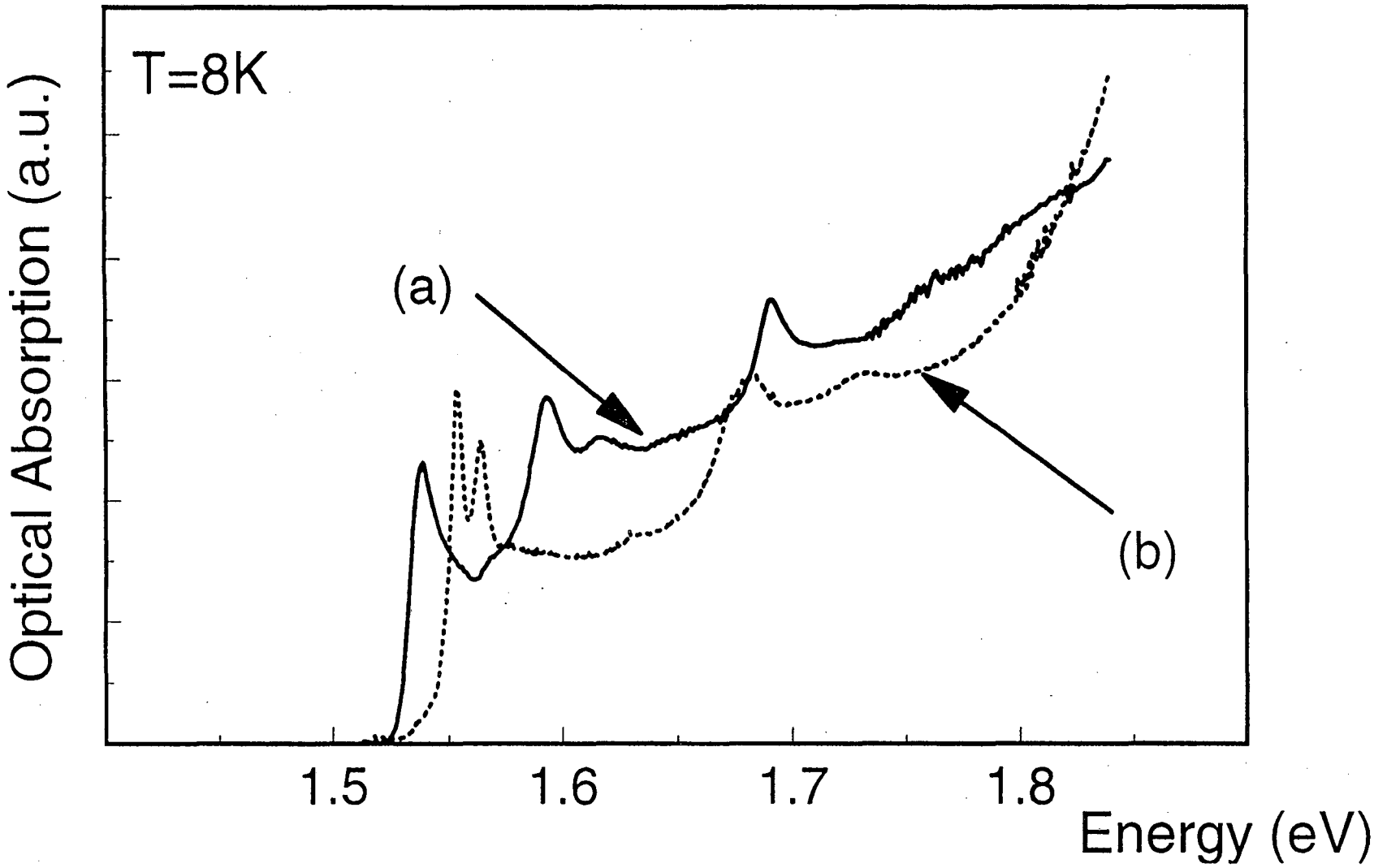

Fig. 4

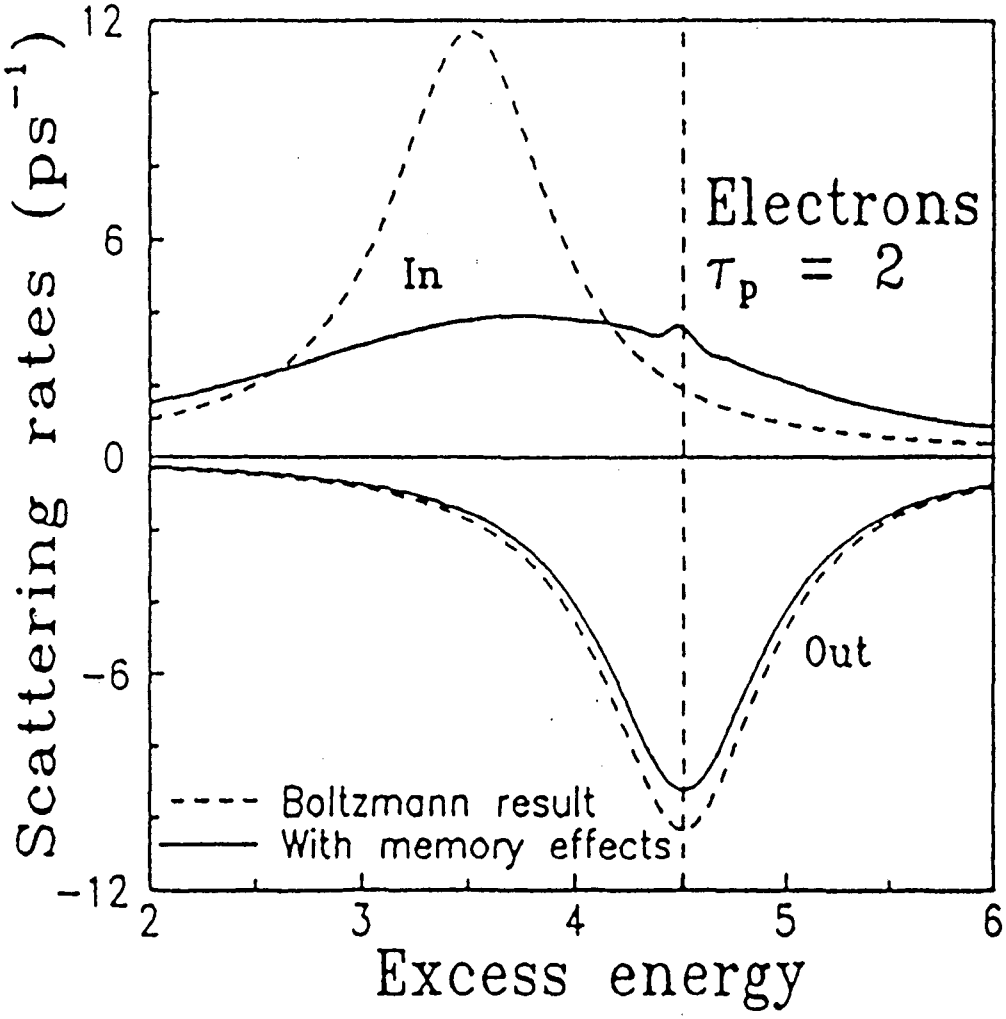
Scattering rates (ps^{-1})
12
6
0
-6
-12
2
3
4
5
6
Excess energy
In
Out
Electrons
τ_p = 2
Boltzmann result
With memory effects

Fig. 5

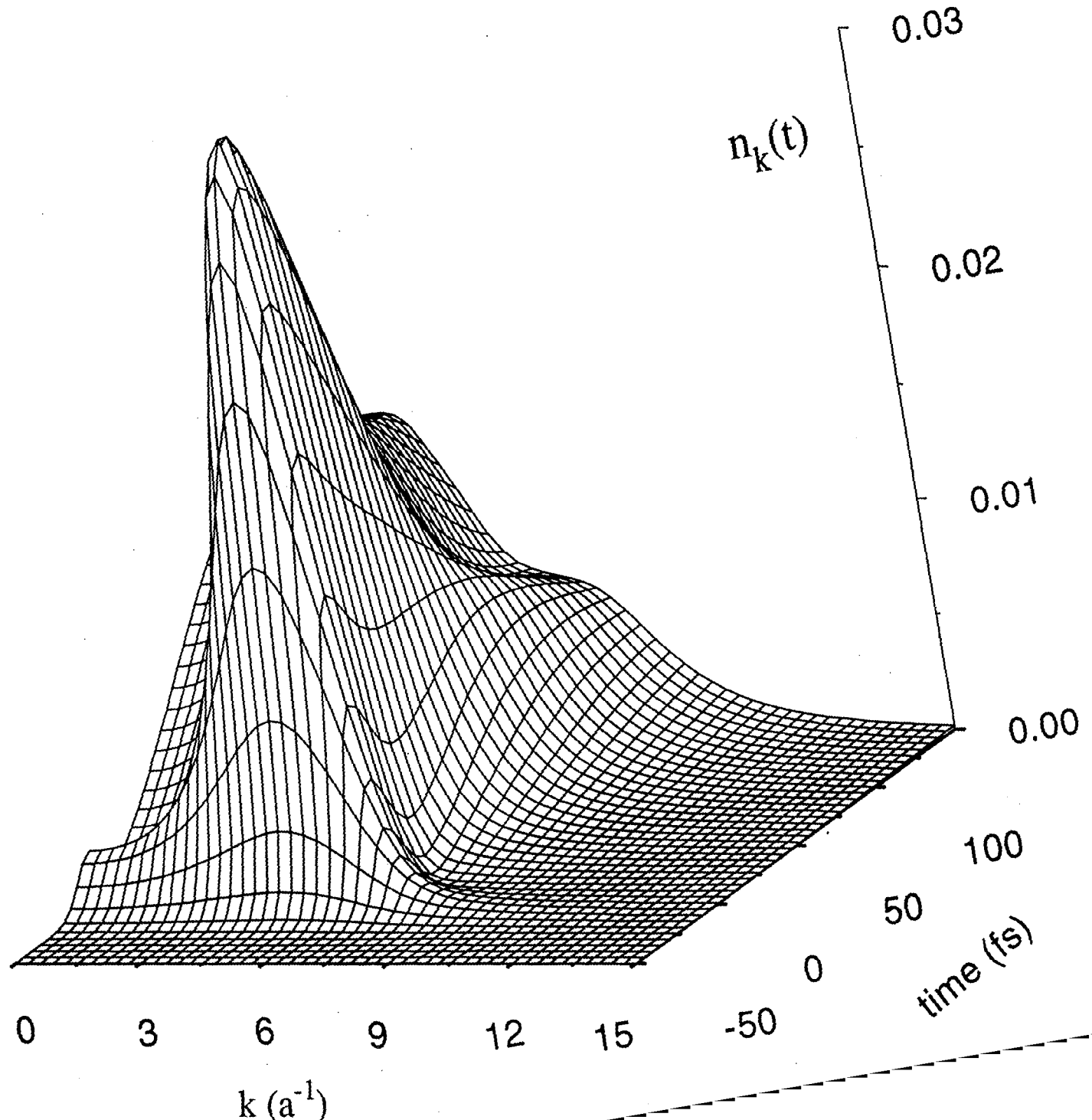

Fig. 6

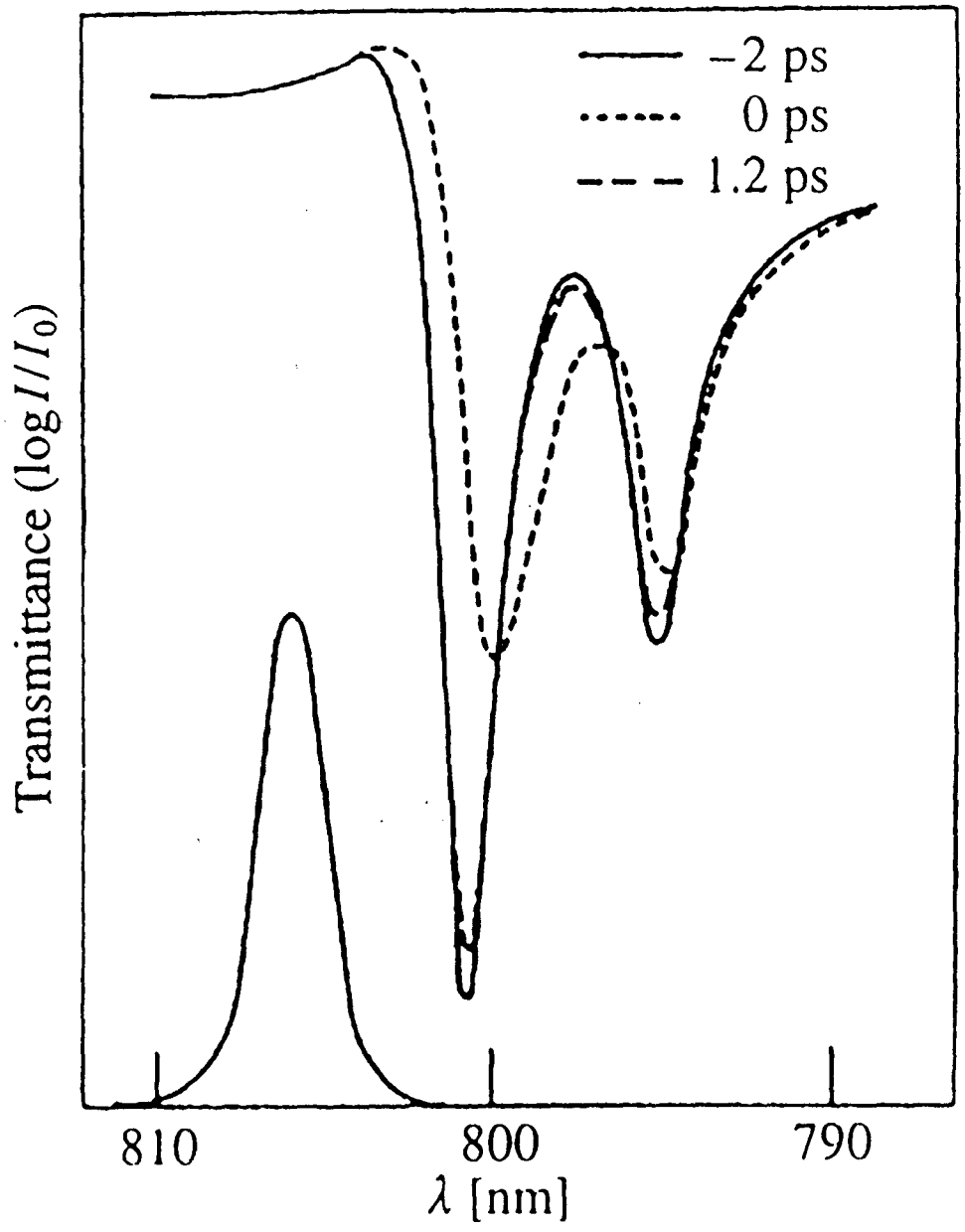

Fig. 7

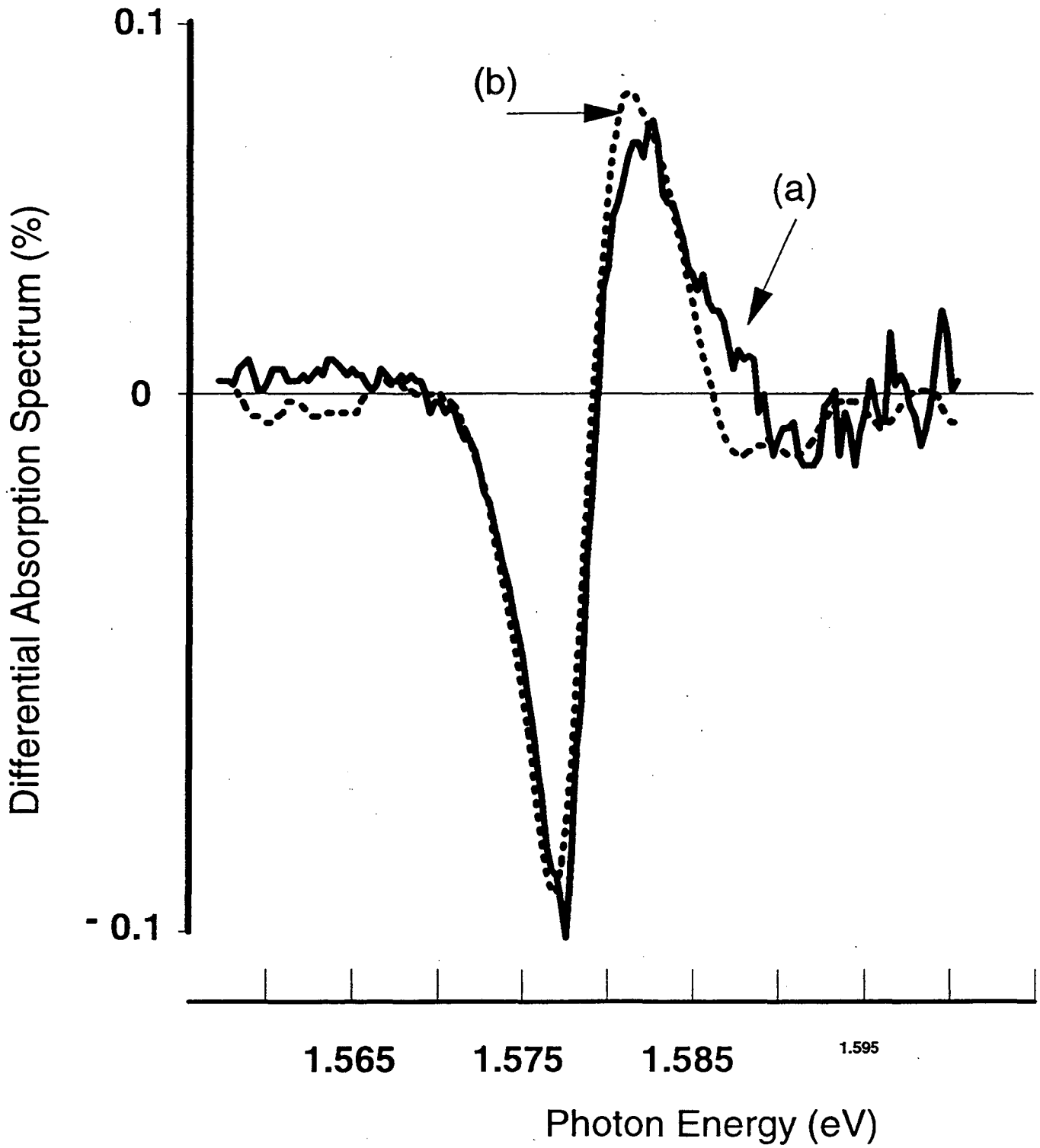
0.1
0
- 0.1
(b)
(a)
Differential Absorption Spectrum (%)
1.565
1.575
1.585
1.595
Photon Energy (eV)

Fig. 8

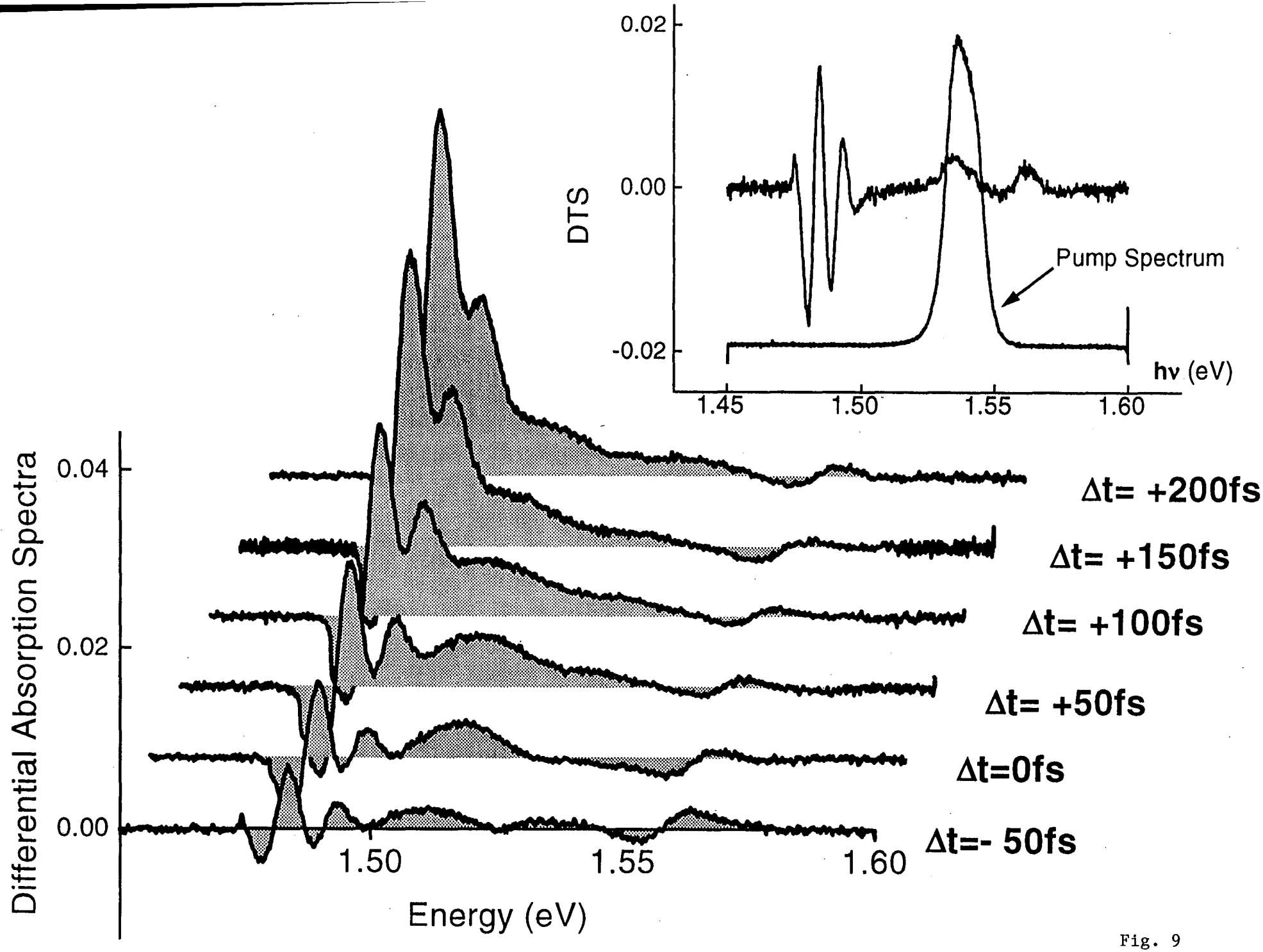
0.02
0.00
-0.02
DTS
Pump Spectrum
hν (eV)
1.45
1.50
1.55
1.60
Differential Absorption Spectra
0.04
0.02
0.00
Δt= +200fs
Δt= +150fs
Δt= +100fs
Δt= +50fs
Δt=0fs
Δt=- 50fs
1.50
1.55
1.60
Energy (eV)

Fig. 9

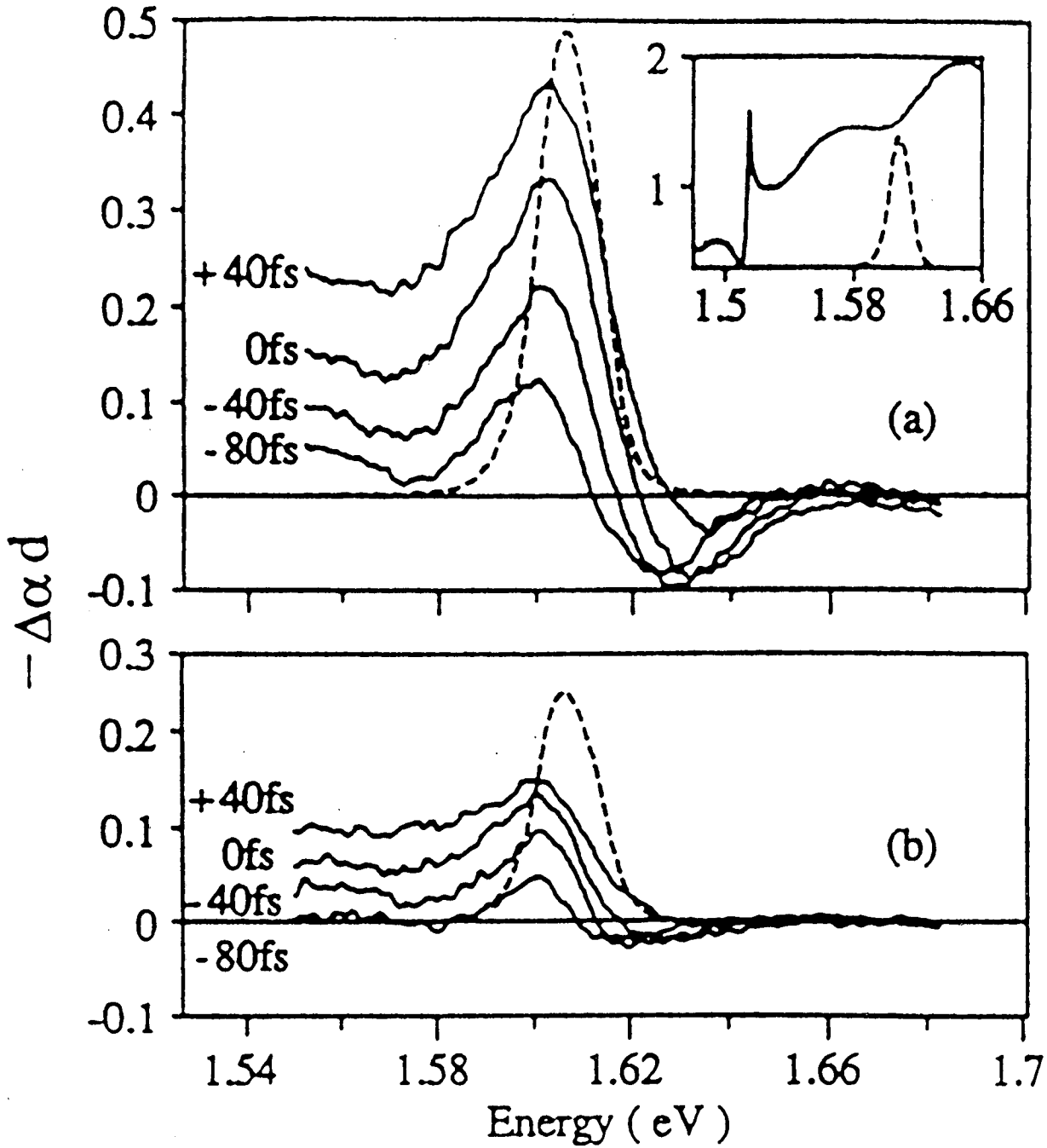
0.5
0.4
0.3
0.2
0.1
0
-0.1
+40fs
0fs
-40fs
-80fs
(a)
2
1
1.5
1.58
1.66
0.3
0.2
0.1
0
-0.1
+40fs
0fs
-40fs
-80fs
(b)
1.54
1.58
1.62
1.66
1.7
Energy (eV)
− Δα d

Fig. 10

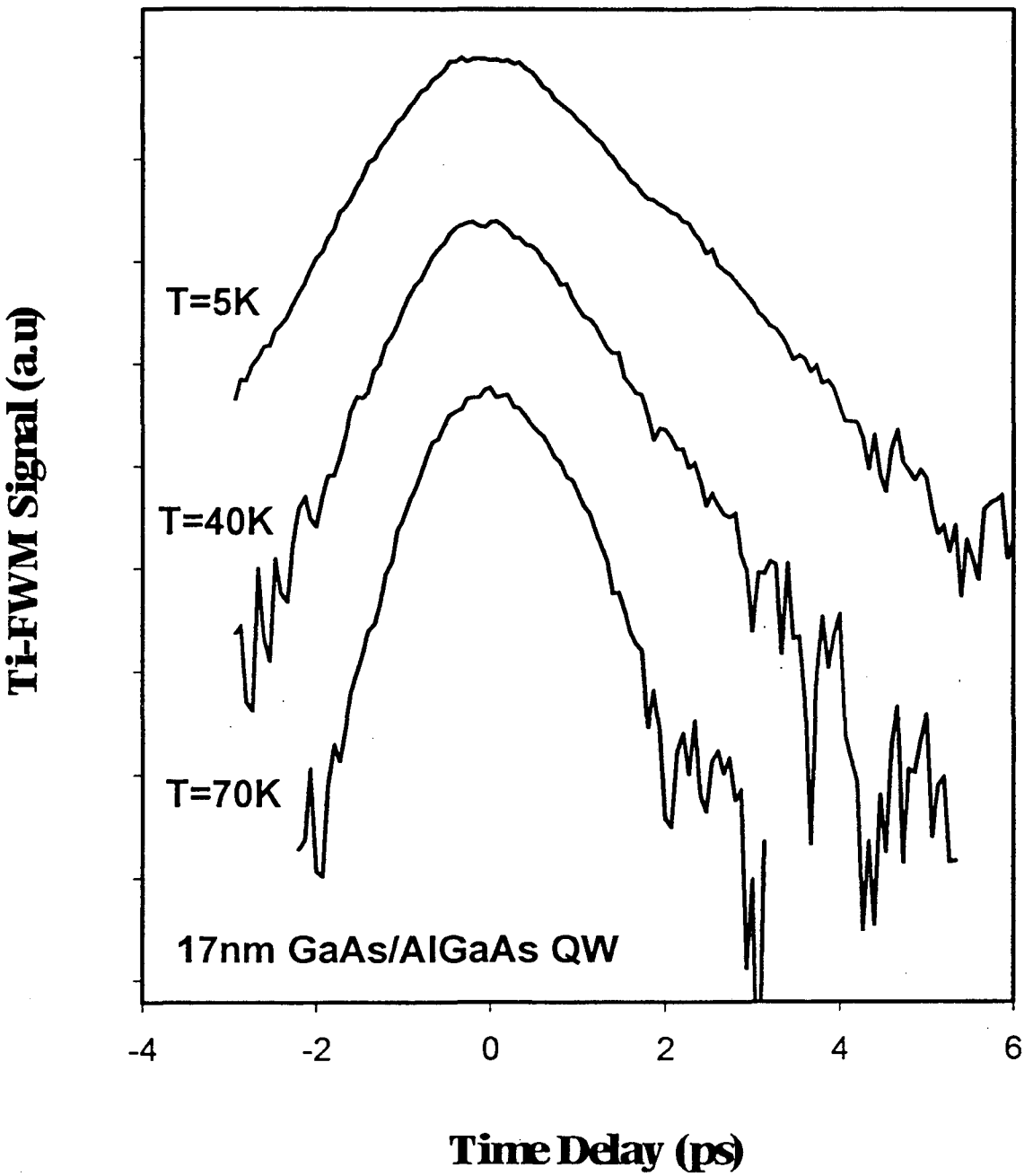
Ti-FWM Signal (a.u)
T=5K
T=40K
T=70K
17nm GaAs/AlGaAs QW
-4
-2
0
2
4
6
Time Delay (ps)

Fig. 11

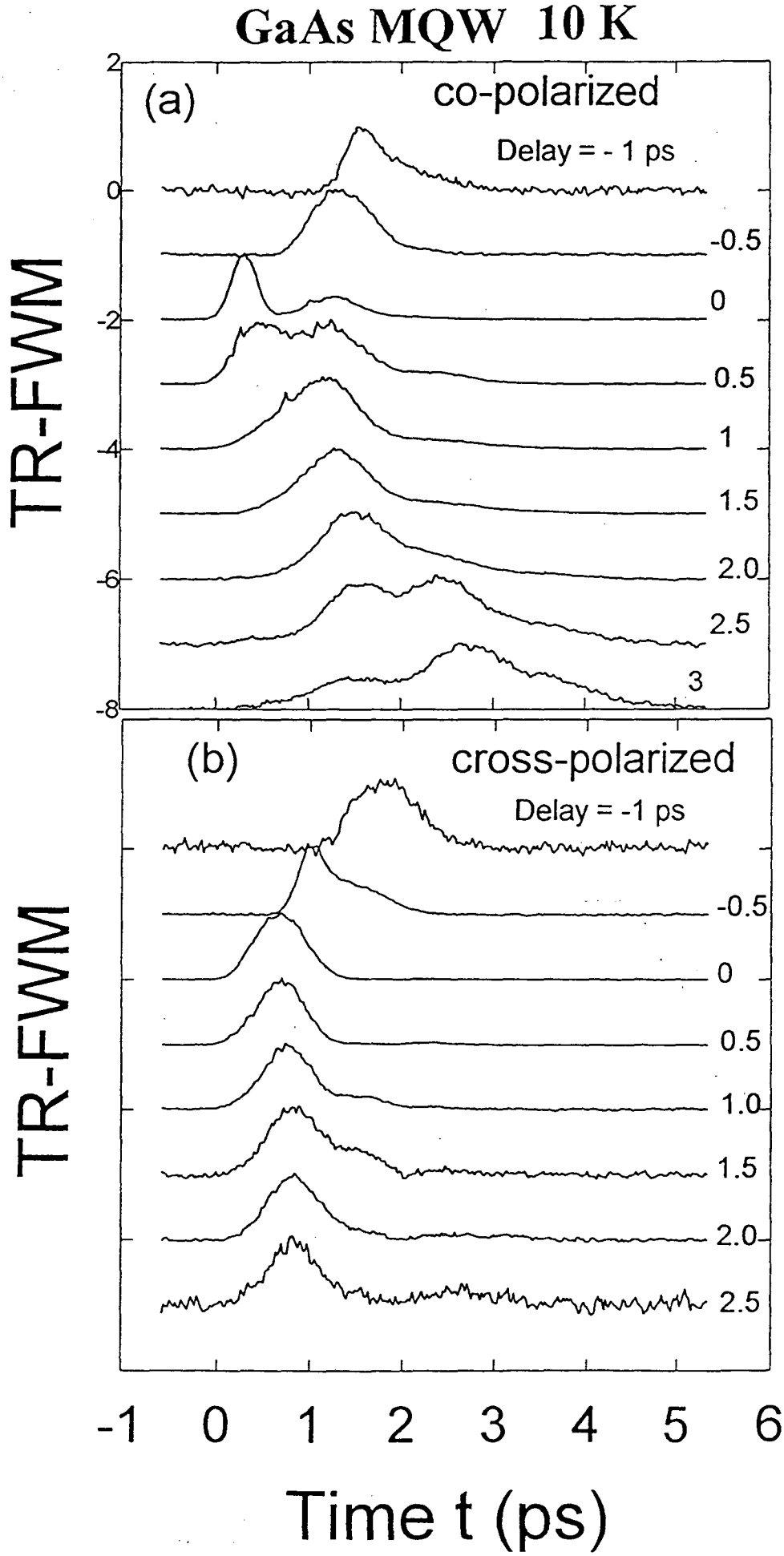
GaAs MQW 10 K
(a)
co-polarized
Delay = - 1 ps
-0.5
0
0.5
1
1.5
2.0
2.5
3
(b)
cross-polarized
Delay = -1 ps
-0.5
0
0.5
1.0
1.5
2.0
2.5
TR-FWM
TR-FWM
2
0
-2
-4
-6
-8
-1 0 1 2 3 4 5 6
Time t (ps)

Fig. 12

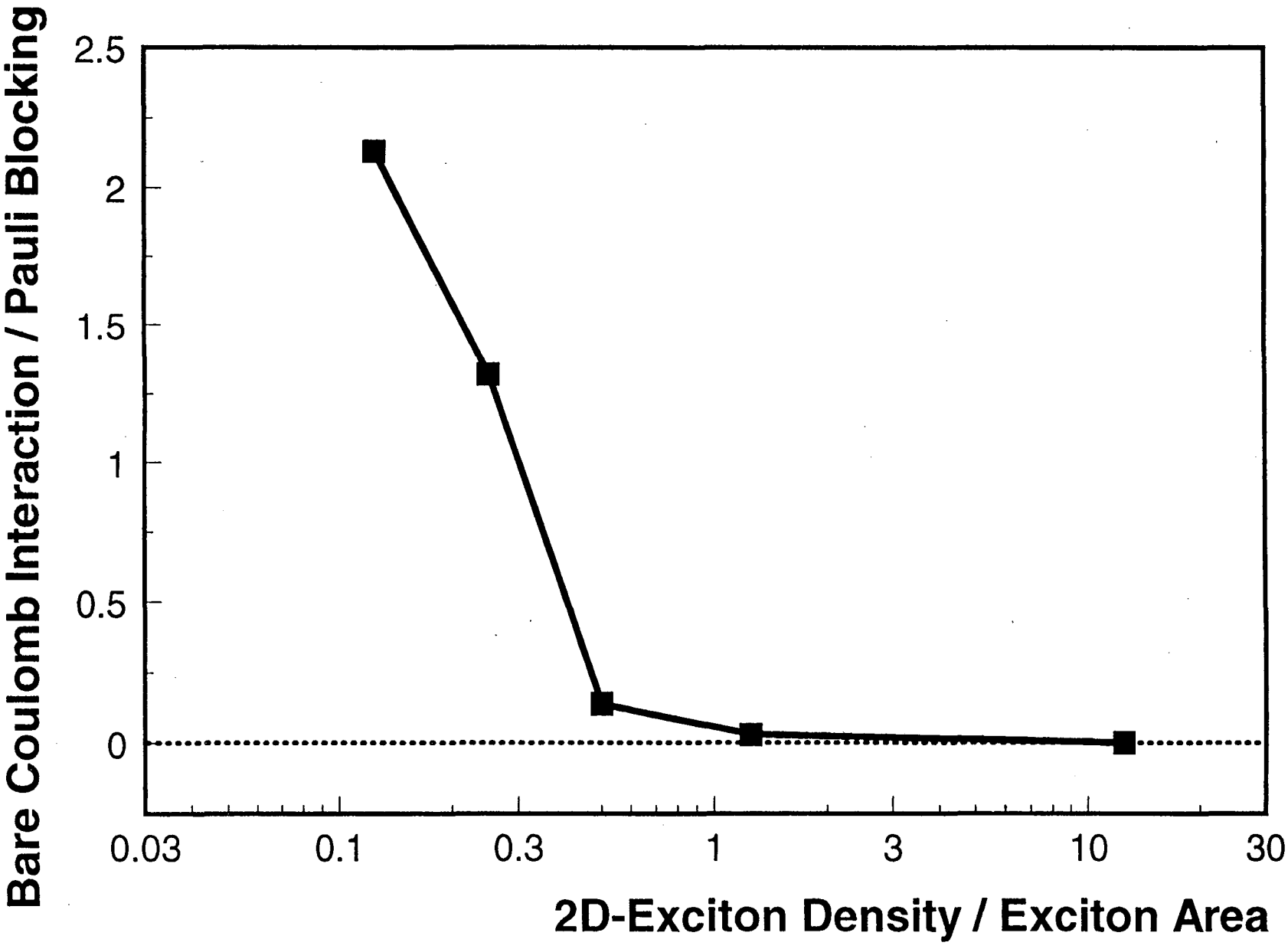
Bare Coulomb Interaction / Pauli Blocking
2.5
2
1.5
1
0.5
0
0.03
0.1
0.3
1
3
10
30
2D-Exciton Density / Exciton Area

Fig. 13

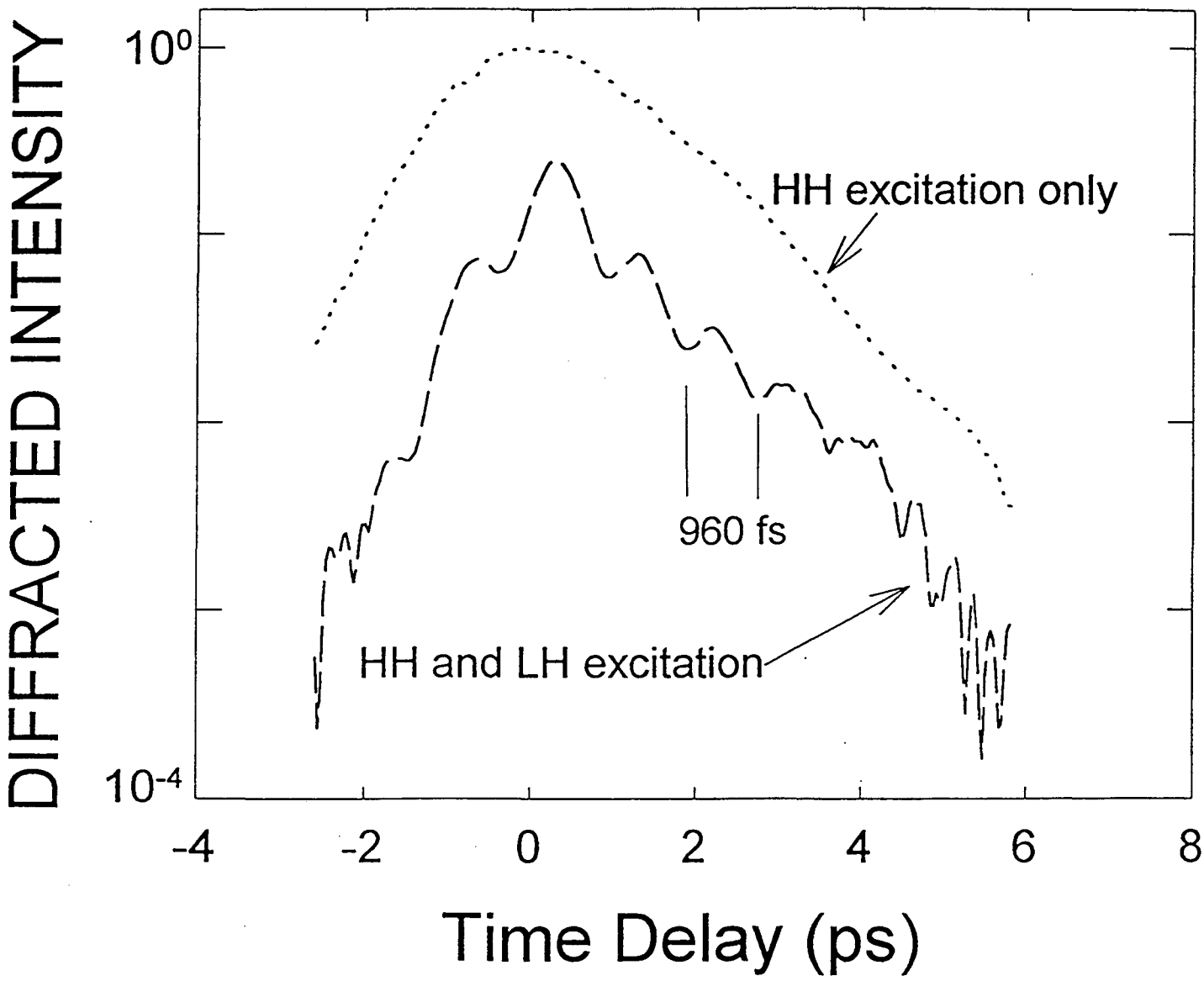
DIFFRACTED INTENSITY
10^0
10^-4
HH excitation only
960 fs
HH and LH excitation
-4
-2
0
2
4
6
8
Time Delay (ps)

Fig. 14

(a) Quantum beats

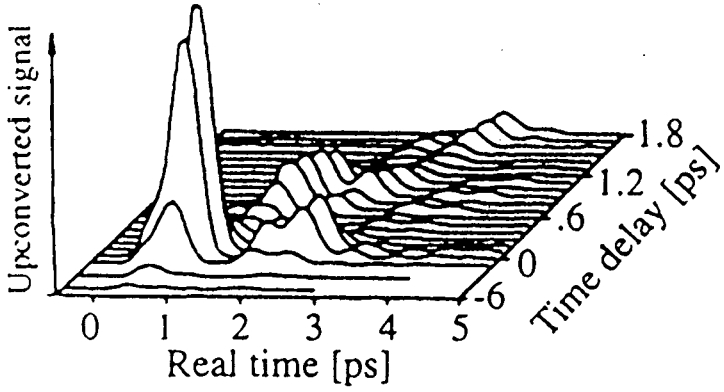

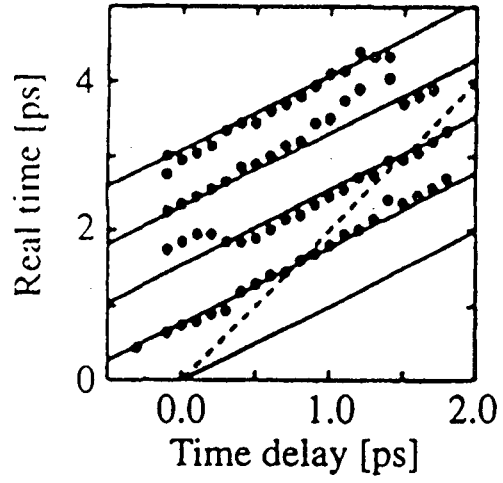

(b) Polarization beats

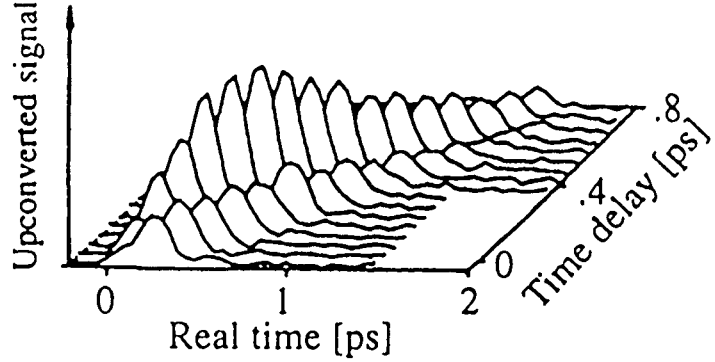

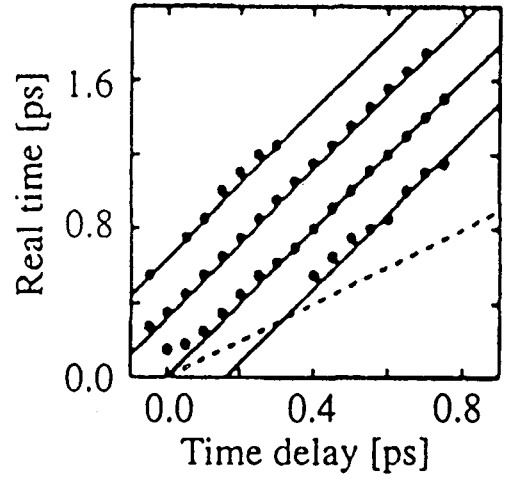

Fig. 15

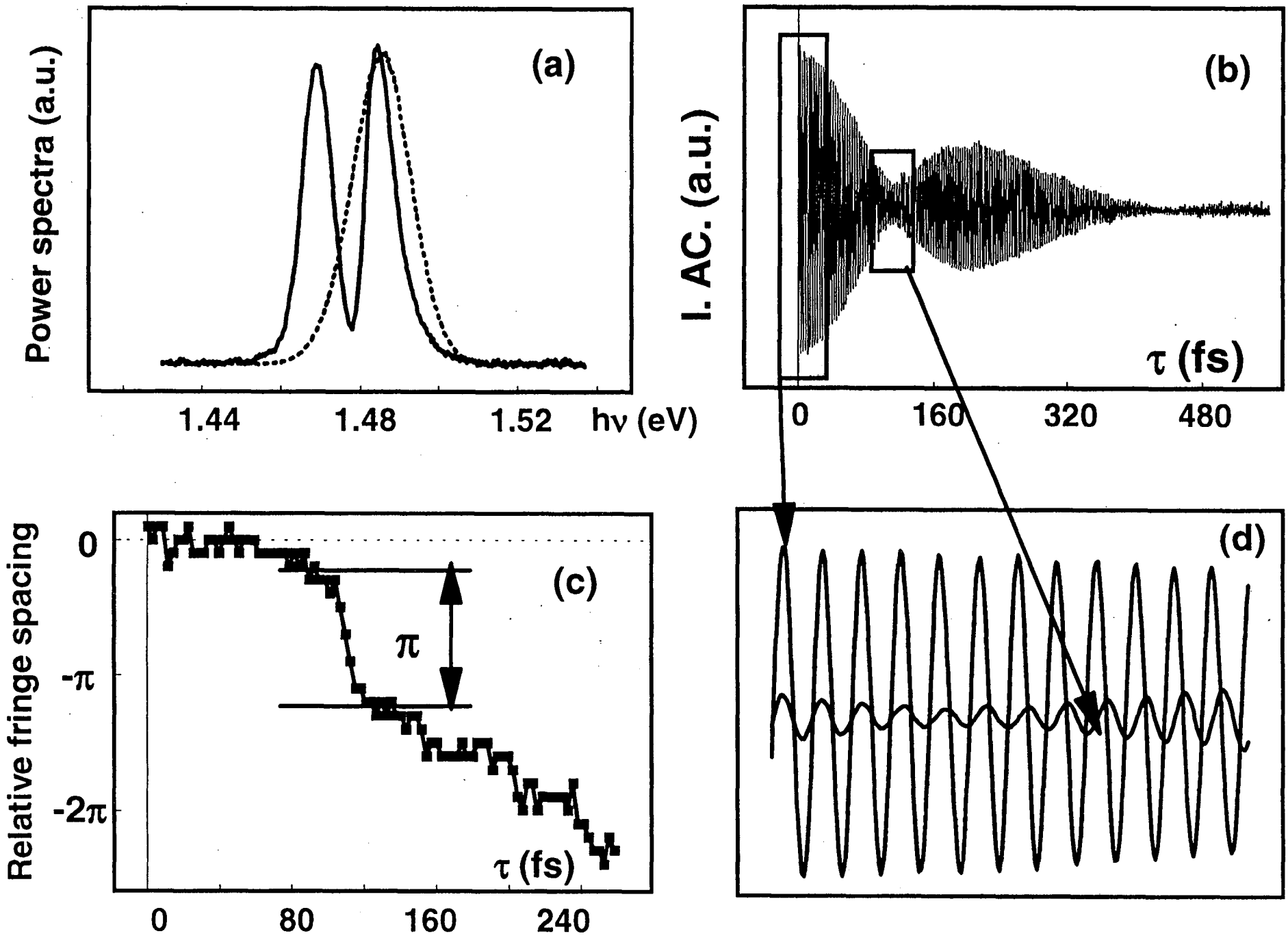
(a)
Power spectra (a.u.)
1.44
1.48
1.52
hν (eV)
(b)
I. AC. (a.u.)
τ (fs)
0
160
320
480
(c)
Relative fringe spacing
0
-π
-2π
π
τ (fs)
0
80
160
240
(d)

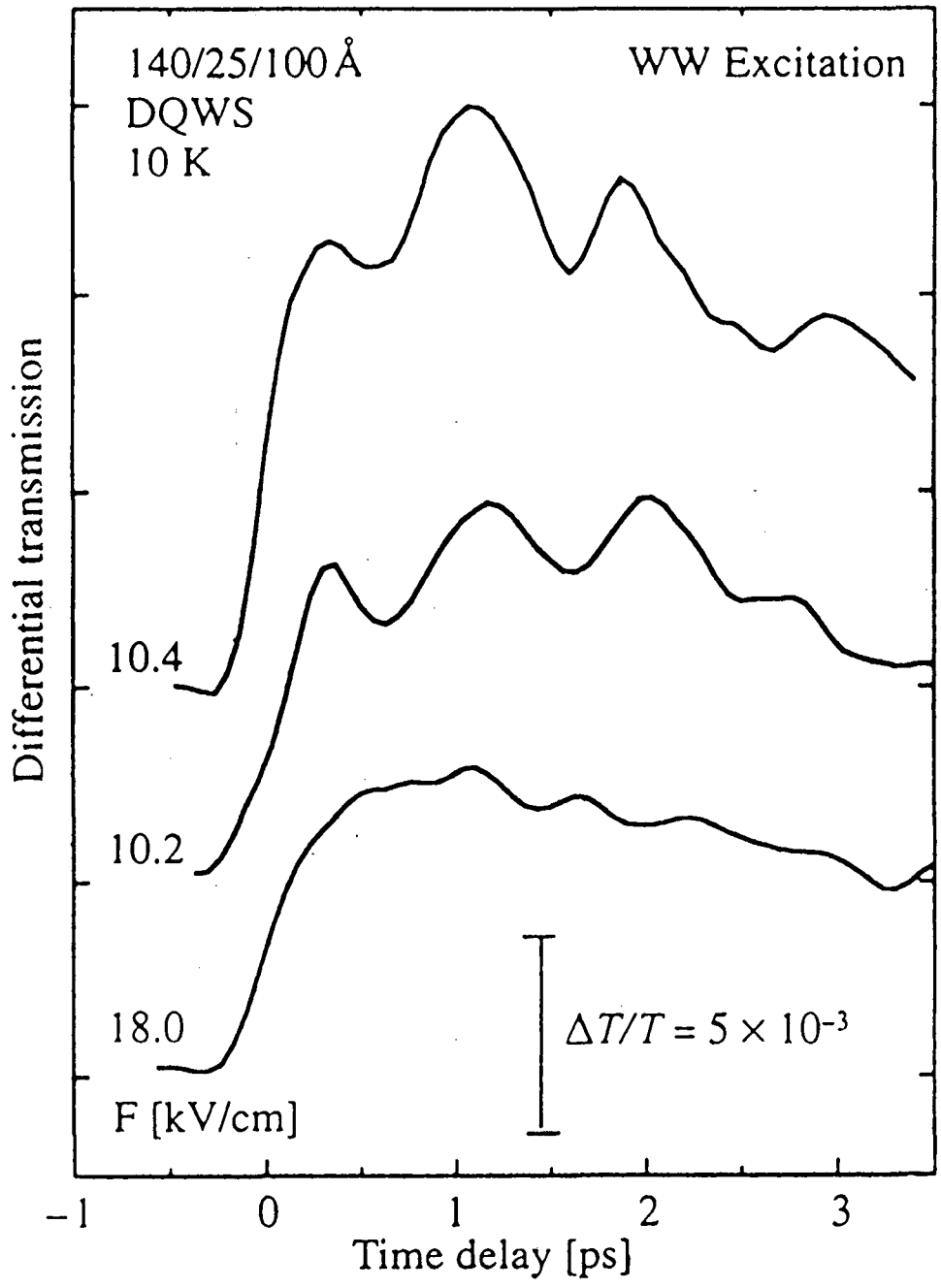
140/25/100 Å
DQWS
10 K
WW Excitation
Differential transmission
10.4
10.2
18.0
F [kV/cm]
$\Delta T/T = 5 \times 10^{-3}$
−1
0
1
2
3
Time delay [ps]

Fig. 17

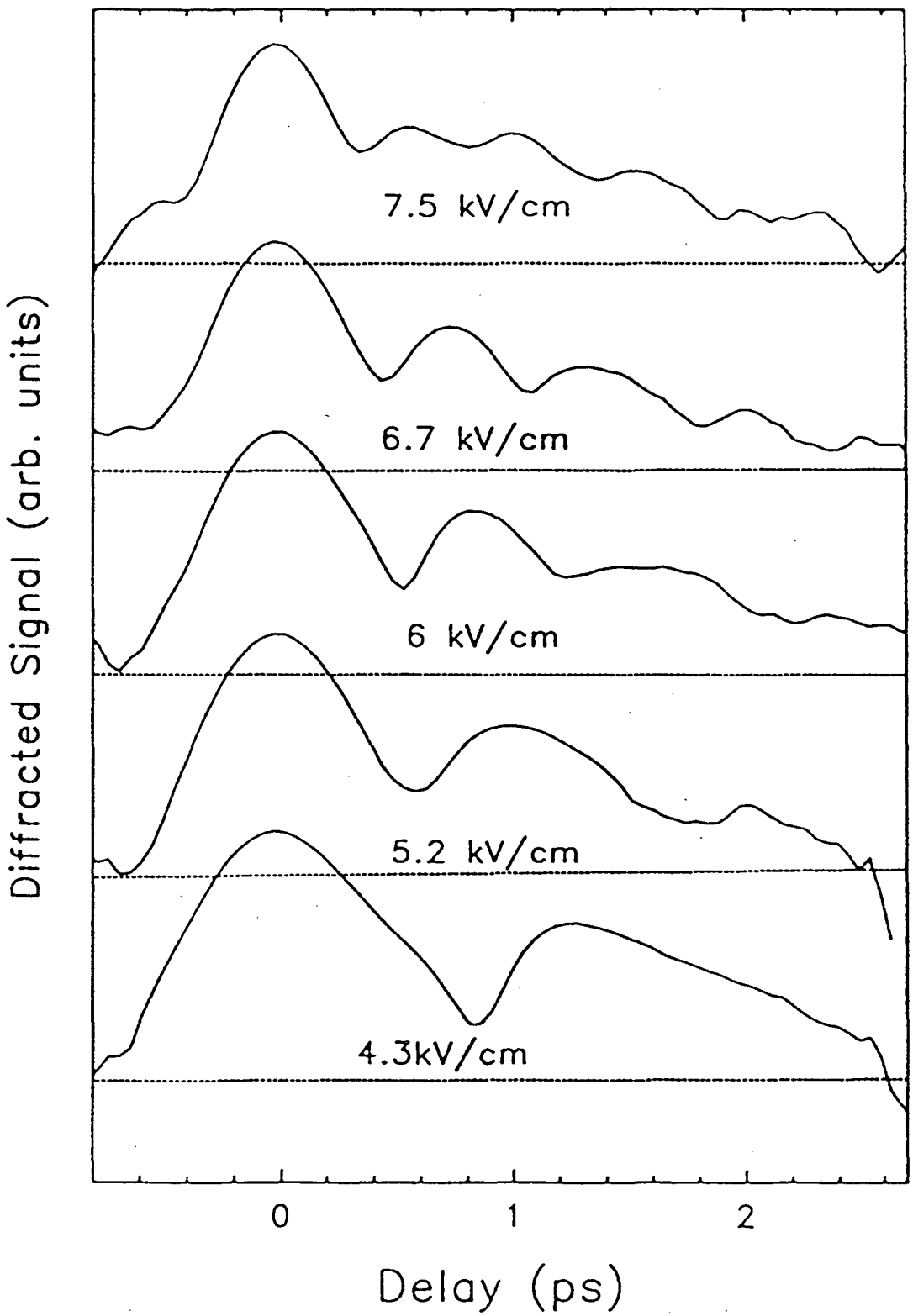
7.5 kV/cm
6.7 kV/cm
6 kV/cm
5.2 kV/cm
4.3kV/cm
Diffracted Signal (arb. units)
0
1
2
Delay (ps)

Fig. 18

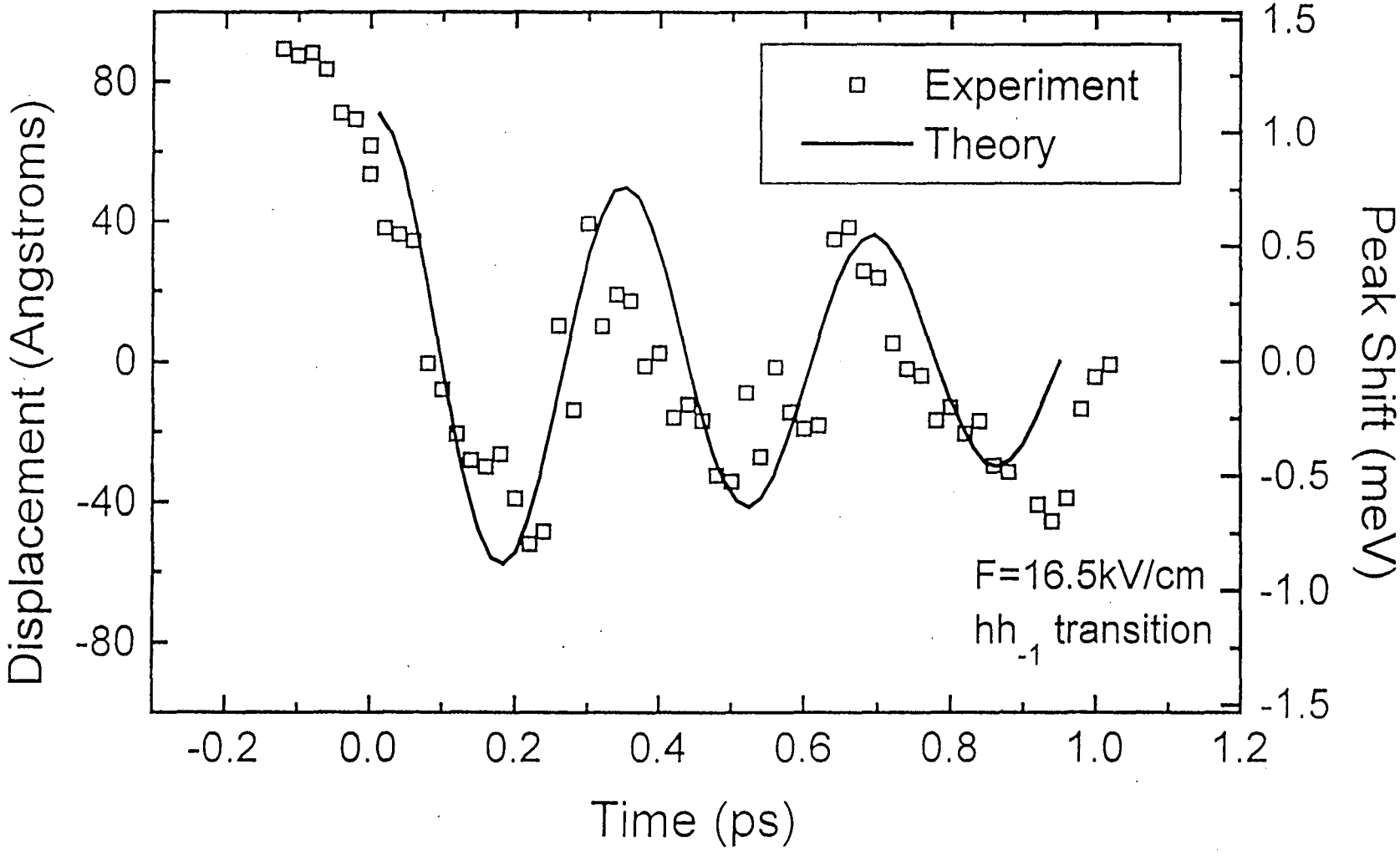
Displacement (Angstroms)
80
40
0
-40
-80
-0.2
0.0
0.2
0.4
0.6
0.8
1.0
1.2
Time (ps)
1.5
1.0
0.5
0.0
-0.5
-1.0
-1.5
Peak Shift (meV)
Experiment
Theory
F=16.5kV/cm
hh -1 transition

Fig. 19

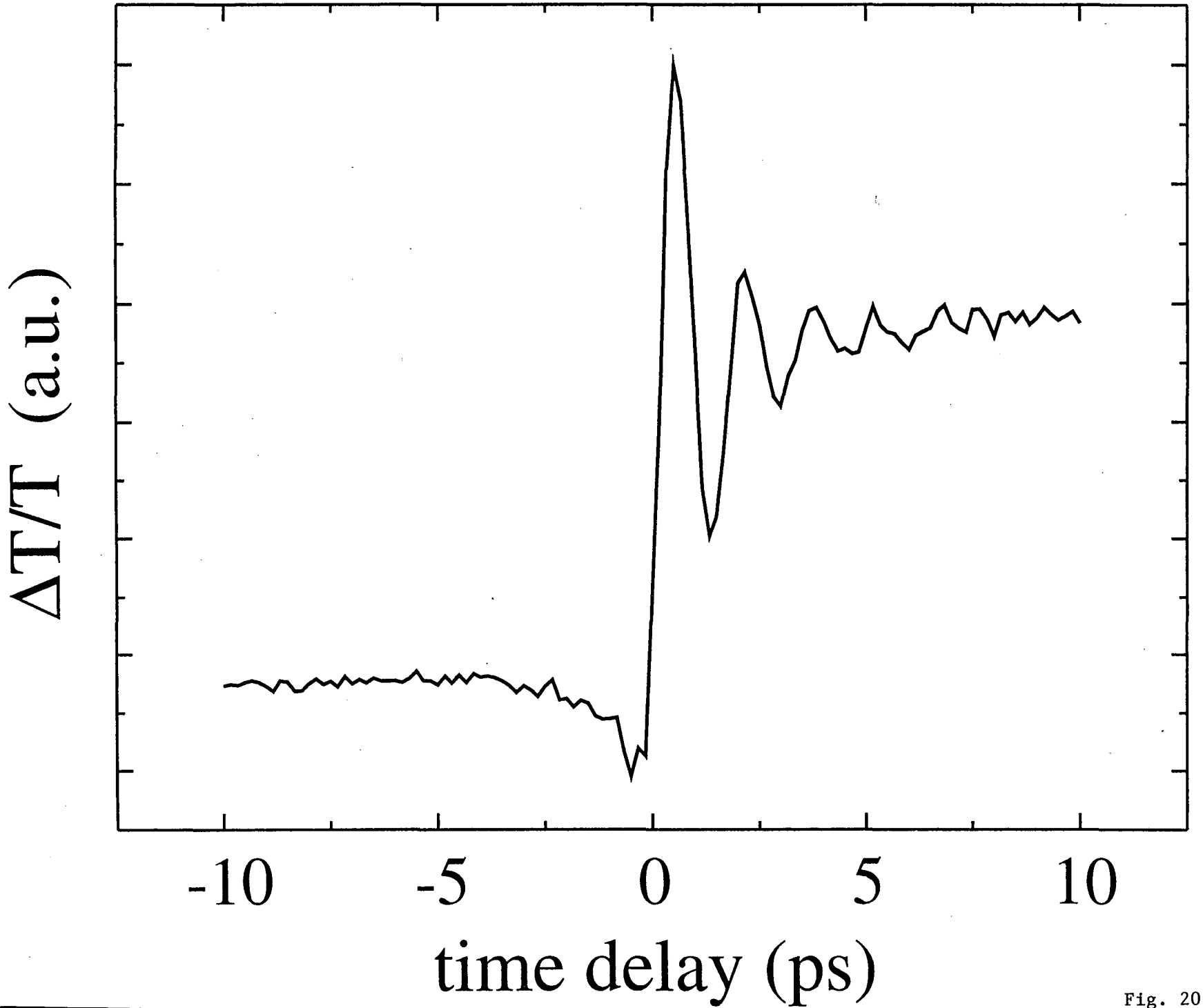

Fig. 20

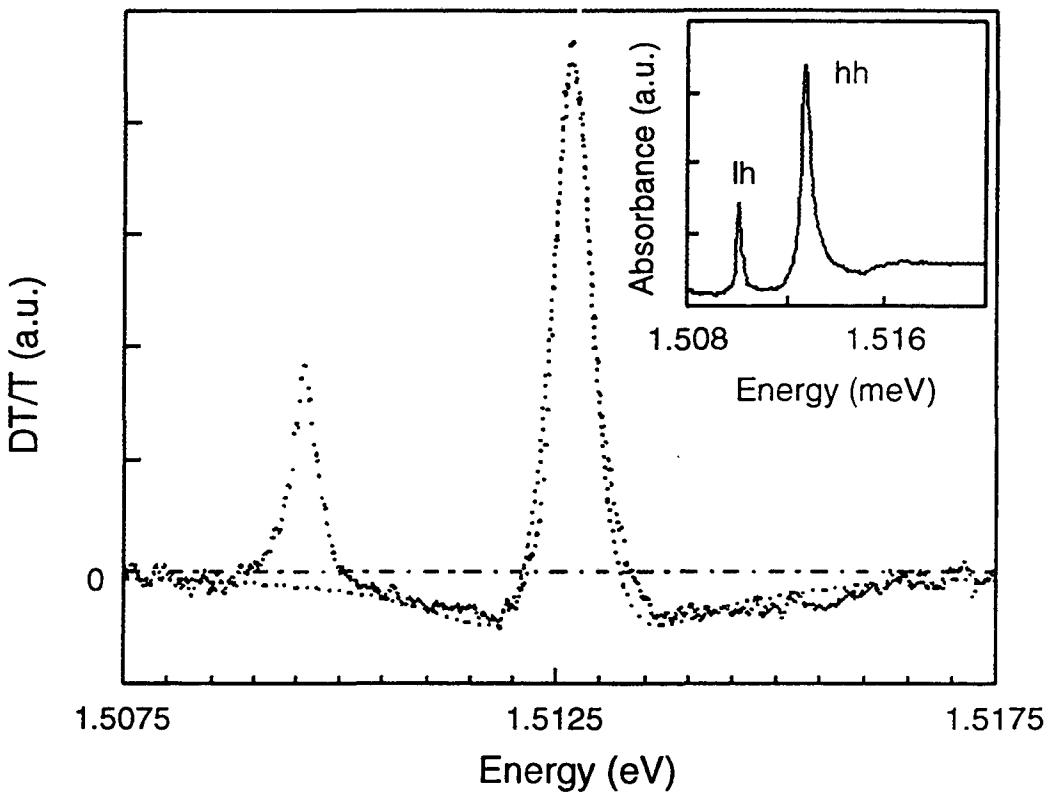
DT/T (a.u.)
0
1.5075
1.5125
1.5175
Energy (eV)
Absorbance (a.u.)
lh
hh
1.508
1.516
Energy (meV)

Fig. 21

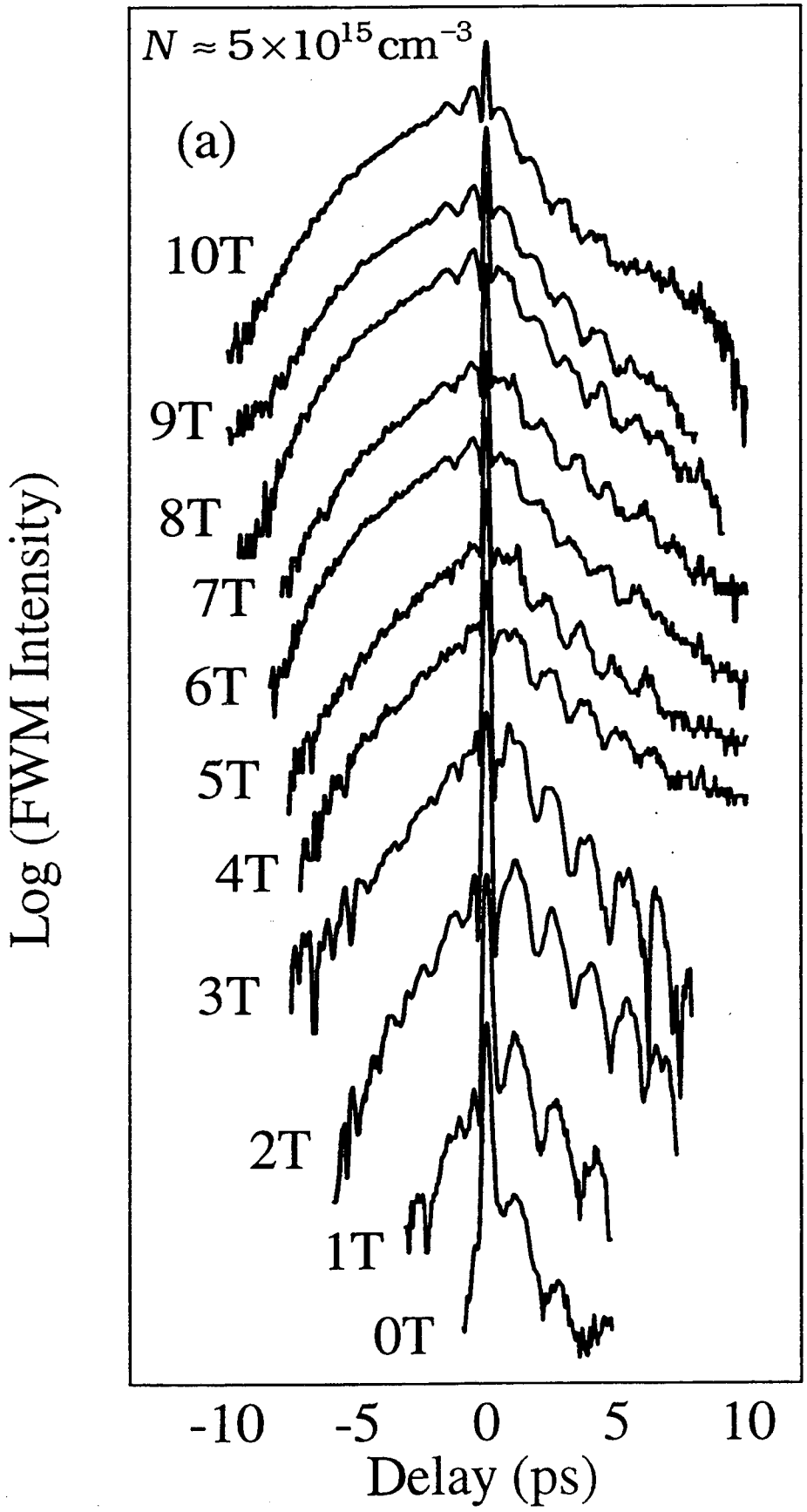
$N \approx 5\times10^{15}\text{cm}^{-3}$
(a)
10T
9T
8T
7T
6T
5T
4T
3T
2T
1T
0T
Log (FWM Intensity)
-10
-5
0
5
10
Delay (ps)

Fig. 22

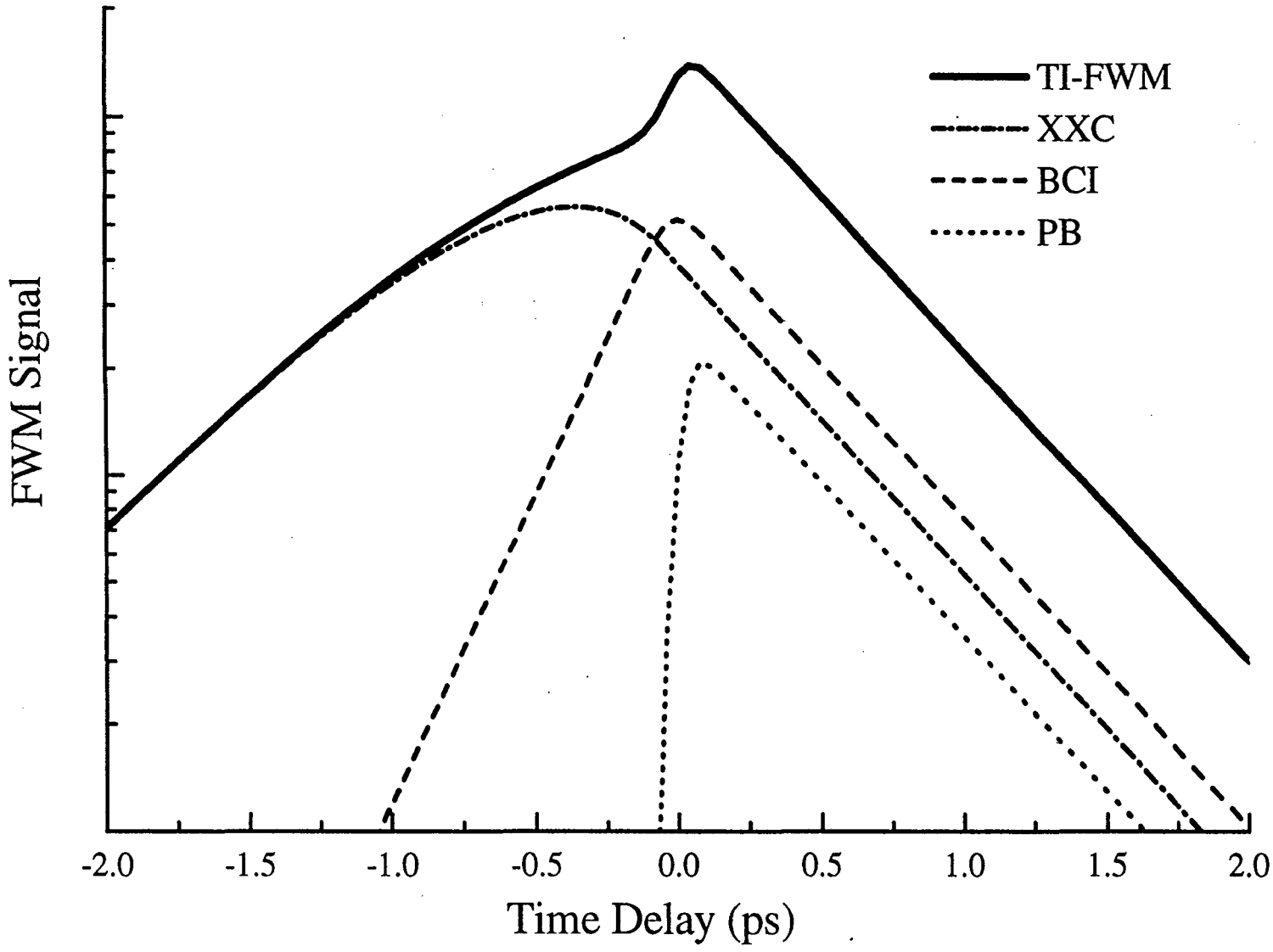
TI-FWM
XXC
BCI
PB
FWM Signal
-2.0
-1.5
-1.0
-0.5
0.0
0.5
1.0
1.5
2.0
Time Delay (ps)

Fig. 23

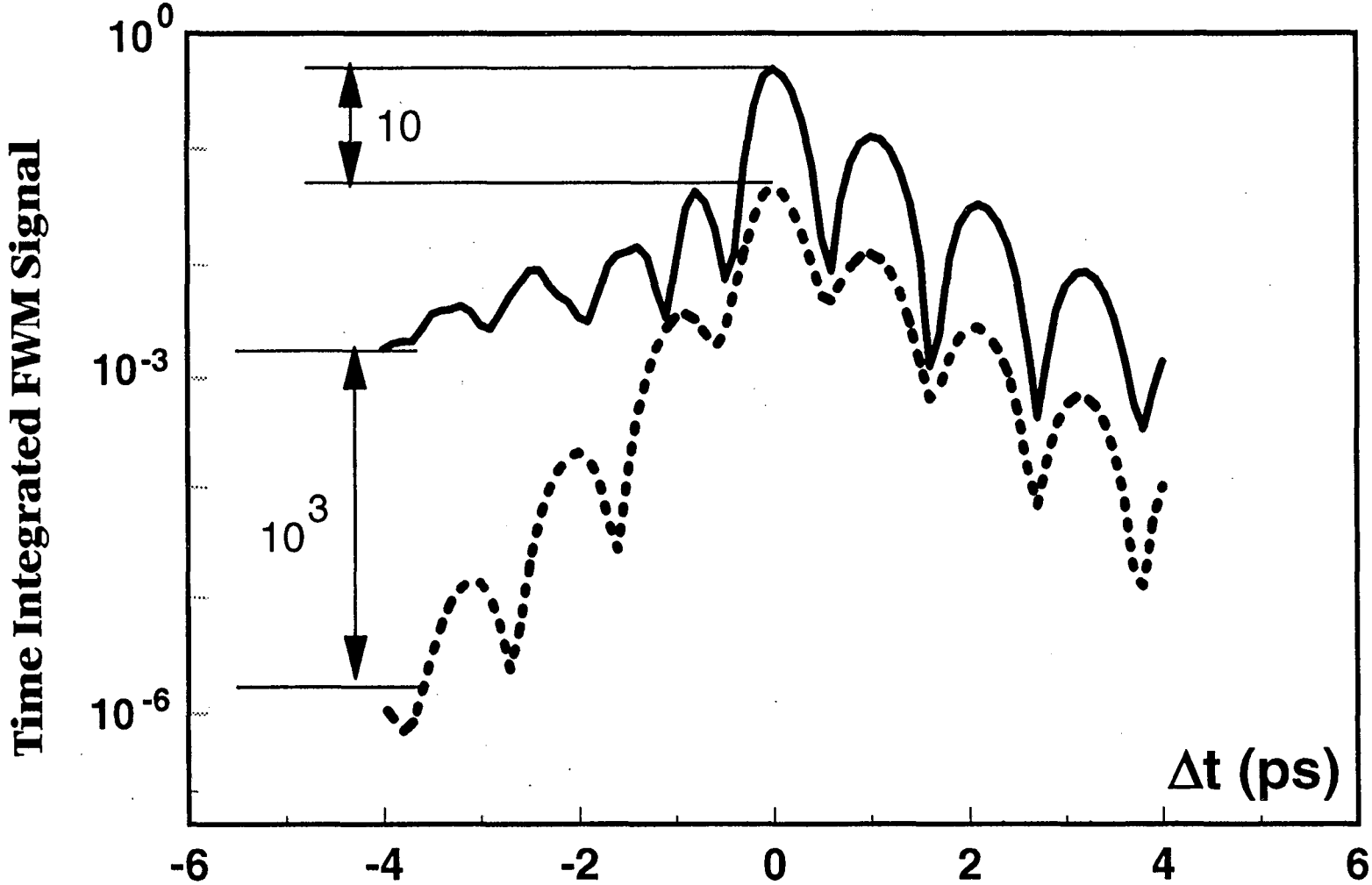

····· **Pauli Blocking + Bare Coulomb**

—— **Pauli Blocking + Bare Coulomb + Exciton-Exciton Correlation**

Fig. 24

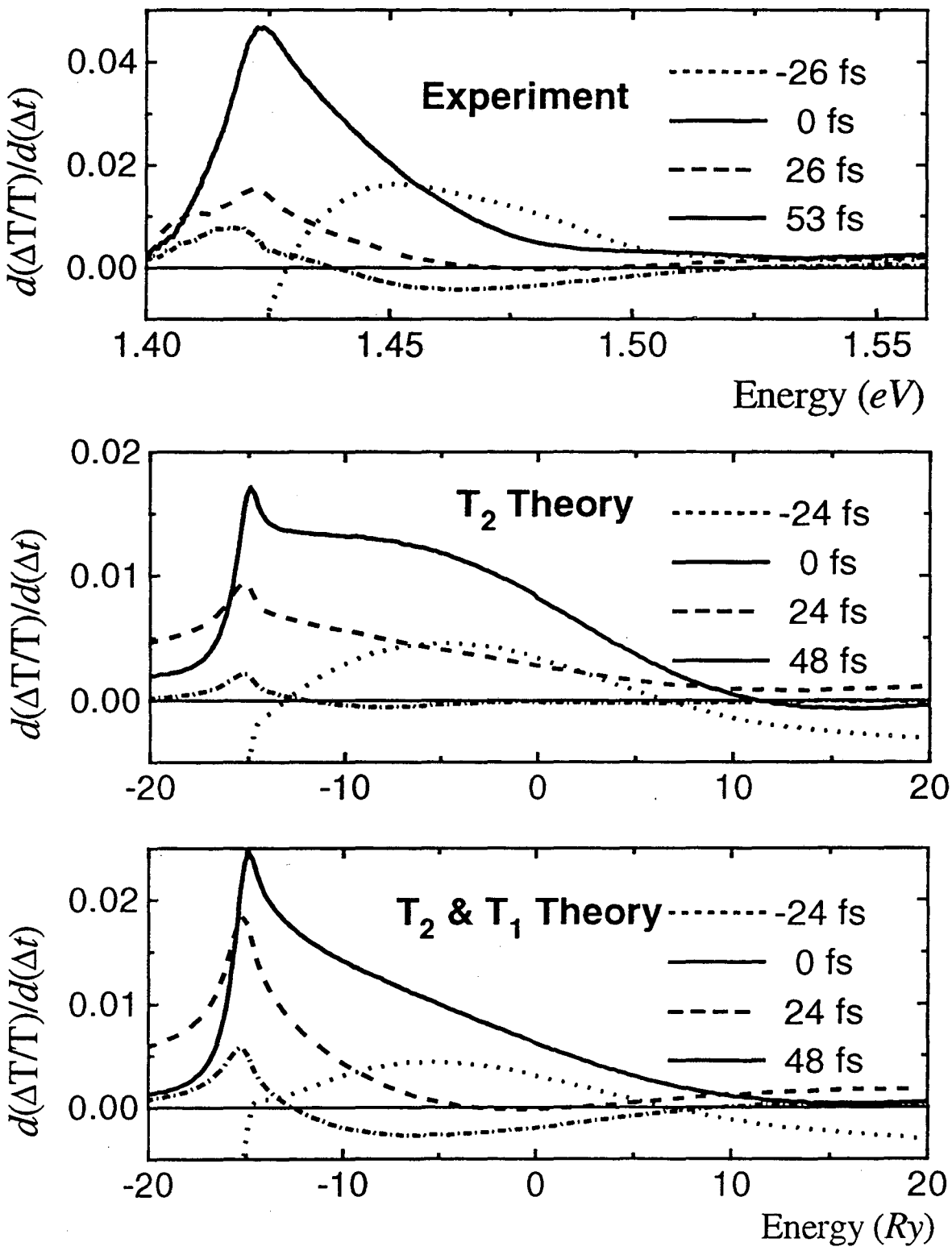
Experiment
-26 fs
0 fs
26 fs
53 fs
0.04
0.02
0.00
1.40
1.45
1.50
1.55
Energy (eV)
d(ΔT/T)/d(Δt)
T2 Theory
-24 fs
0 fs
24 fs
48 fs
0.02
0.01
0.00
-20
-10
0
10
20
T2 & T1 Theory
-24 fs
0 fs
24 fs
48 fs
0.02
0.01
0.00
-20
-10
0
10
20
Energy (Ry)

Fig. 25

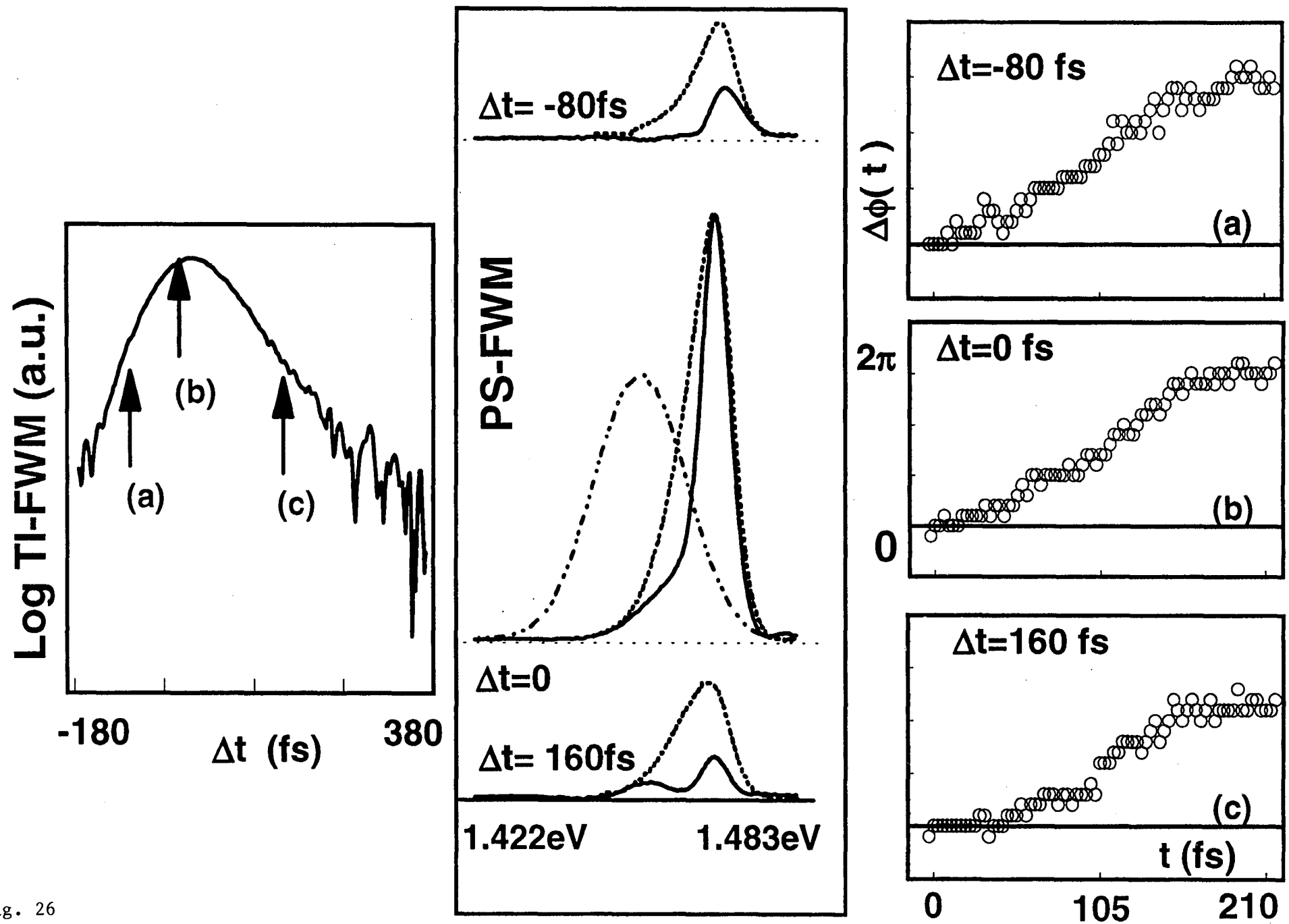
Log TI-FWM (a.u.)
(a)
(b)
(c)
-180
Δt (fs)
380
PS-FWM
Δt= -80fs
Δt=0
Δt= 160fs
1.422eV
1.483eV
Δφ(t)
2π
0
Δt=-80 fs
(a)
Δt=0 fs
(b)
Δt=160 fs
(c)
t (fs)
0
105
210

Fig. 26

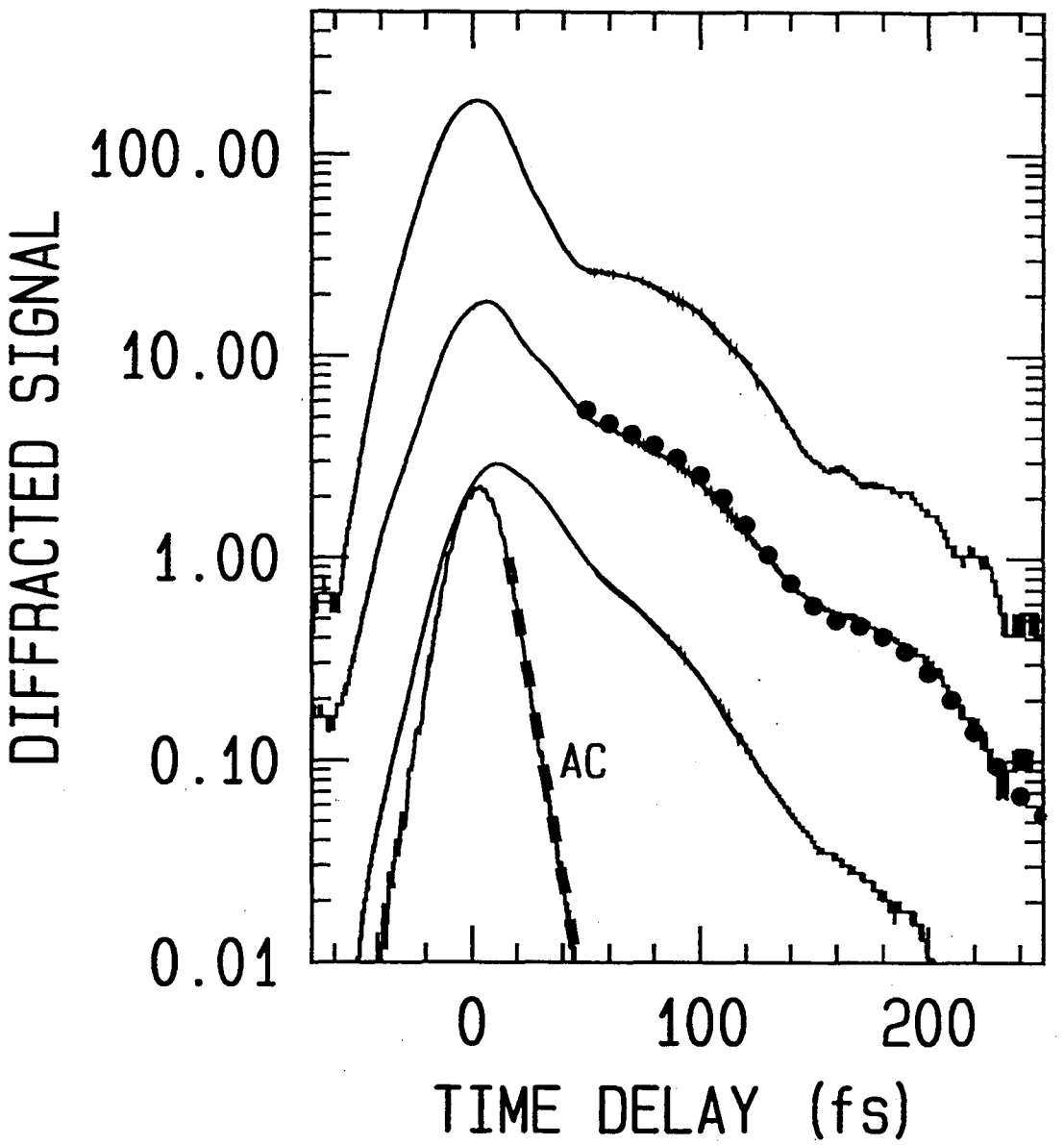
DIFFRACTED SIGNAL
100.00
10.00
1.00
0.10
0.01
AC
0
100
200
TIME DELAY (fs)

Fig. 27

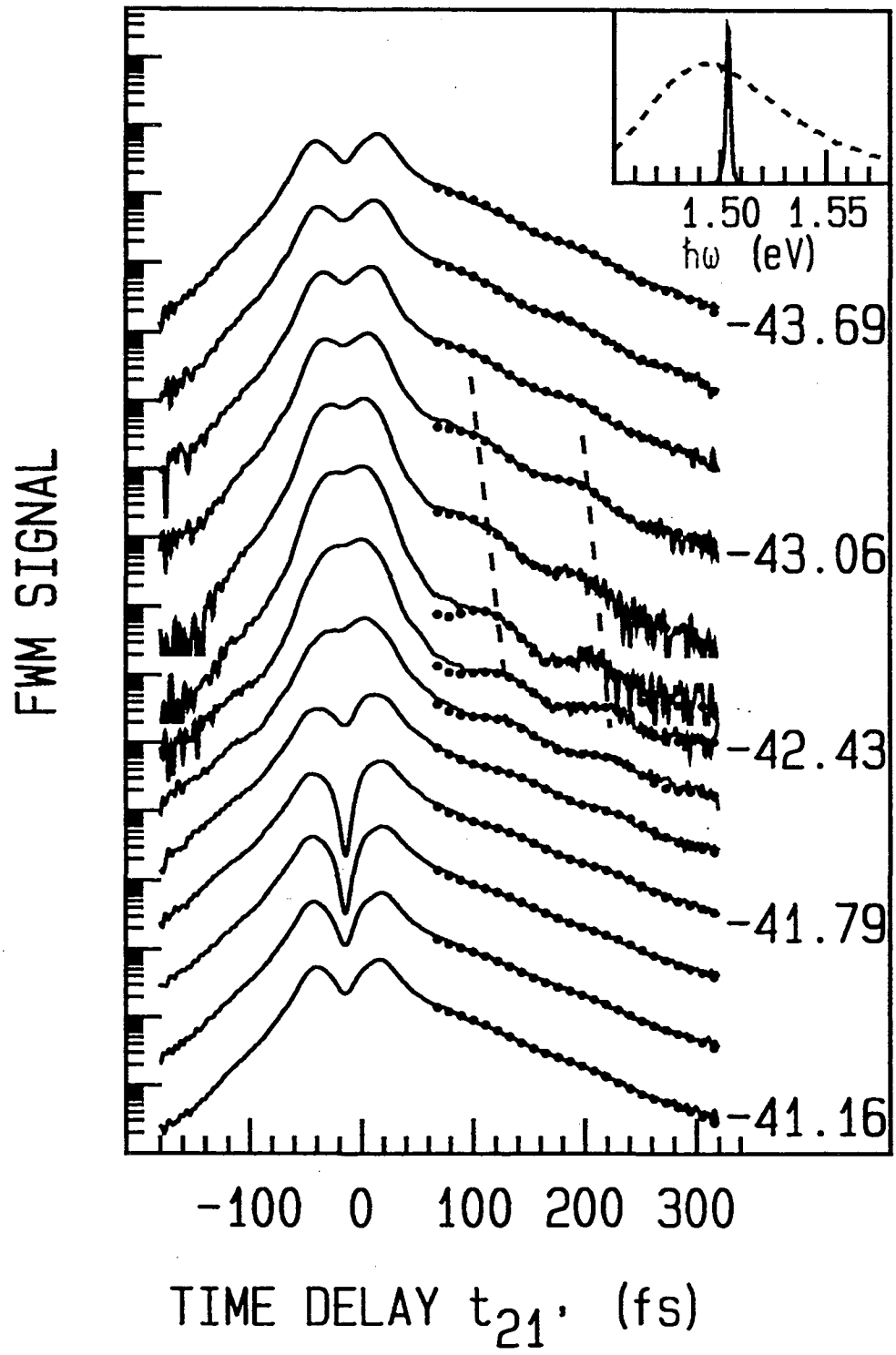
1.50 1.55
ħω (eV)
-43.69
-43.06
-42.43
-41.79
-41.16
FWM SIGNAL
$t_{11'}$ (fs)
-100 0 100 200 300
TIME DELAY $t_{21'}$ (fs)

Fig. 28

Ernest Orlando Lawrence Berkeley National Laboratory
One Cyclotron Road | Berkeley, California 94720

Prepared for the U.S. Department of Energy under Contract No. DE-AC03-76SF00098